CONTROL OF MICROSTRUCTURE EVOLUTION DURING SPUTTERDEPOSITION

Ivan Petrov
Materials Research Laboratory, University of Illinois at Urbana-Champaign, USA
Department of Physics, Chemistry, and Biology, Linköping University, Sweden

petrov@illinois.edu

RWTH Aachen University
February 11, 2025

Sputter deposition

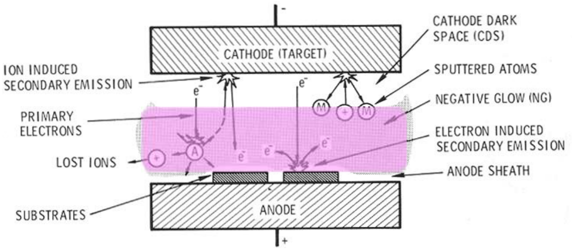

Important processes:
- Ion-solid interactions on the target.
- Plasma generation and discharge maintenance
- Collisions in the gas phase – ionization, scattering.
- **Nucleation and film growth on the substrate.**
- **Use of ion solid interactions to modify film growth**

Control of micro- and nanostructure in thin film

1. Nucleation and growth
   - Surface structure: terraces, steps, kinks, vacancies
   - Film growth processes-nucleation, coalescence, competitive grain growth, recrystallization
   - Zone diagrams
   - Epitaxial growth
   - Effects of reactive species.
2. Use of low-energy gas ion bombardment to control microstructure during low temperature film growth
   - Effects of sputtered atoms energy
   - Effects of gas-ion energy
   - Use of high fluxes of low-energy gas ions, low-temperature sputter epitaxy
3. Use of low-energy metal-ion bombardment to control microstructure during low temperature film growth
   - High Power Impulse Magnetron Sputtering (HiPIMS), source of energetic target atoms ions
   - Hybrid HiPIMS/DCMS processes
   - Light metal ions (Al$^+$, Si$^+$): synthesis of highly metastable Transition Metal Nitride (TMN) coatings
   - Heavy metal ions (Ta$^+$, W$^+$): low-T synthesis of dense, hard, low-stress TMN coatings
4. Kinetic roughing and surface facet formation
5. Texture inheritance
6. Metal-ion etch and adhesion control
7. Self-organized nanostructure formation
   - Thermal segregation and renucleation – random nanocomposites
   - Ion-assisted segregation – highly-oriented nanocomposites; equiaxed to columnar transition

8. Modeling TiN(001) film growth by classical molecular dynamics

Atomic-scale phenomena affecting N&G

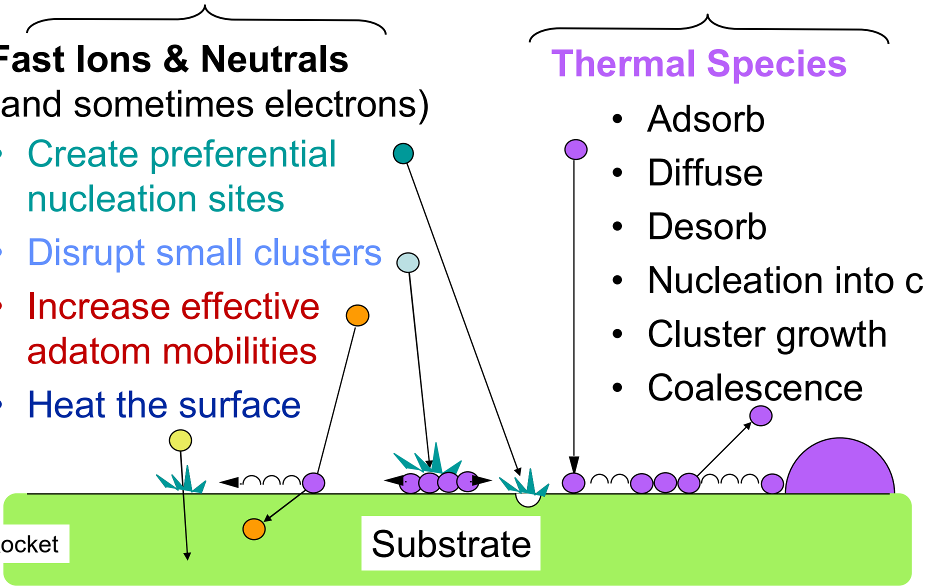

Fast Ions & Neutrals
(and sometimes electrons)

- Create preferential nucleation sites
- Disrupt small clusters
- Increase effective adatom mobilities
- Heat the surface

Thermal Species

- Adsorb
- Diffuse
- Desorb
- Nucleation into clusters
- Cluster growth
- Coalescence

Prof. Angus Rocket

Thermodynamics of Nucleation

Energy cost to form a new surface (spherical particle): $4\pi r^2\gamma$

Energy gain to form a stable phase: $4/3\ (\pi\ r^3)\ \Delta\ G_V$

(1) $\Delta\ G_{Tot.} = 4pr^2\ \gamma - 4/3\ (\pi\ r^3)\ \Delta G_V$

Where: γ = surface energy per unit area
$\Delta\ G_V$ = free energy of nuclei per unit volume
$\Delta\ G_{Tot.}$ = the total change in free energy

Set $d(\Delta\ G_V)/dr = 0$ and solve for critical cluster size:

(2) $\mathbf{r^* = 2\ \gamma / \Delta\ G_V}$ ⟶ *The critical cluster size*

(3) $\Delta\ \mathbf{G^*_{Tot.} = 16\ \pi\ \gamma^3 / 3\ (\Delta\ G_V)^2}$ ⟶ *Homogeneous nucleation barrier*

(4) $\Delta\ \mathbf{G^*_{Het.} = \Delta\ G^*_{Tot.}\ S(\Theta)}$ ⟶ *Heterogeneous nucl. Barrier*

(5) $S(\Theta) = (2 + \cos\Theta)(1 - \cos\Theta)^2/4$

$\Theta = 10° \Rightarrow S(\Theta) \approx 10^{-4}$

Prof. Angus Rocket

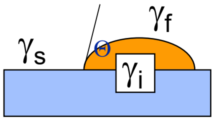

γ: surface and interfacial energies

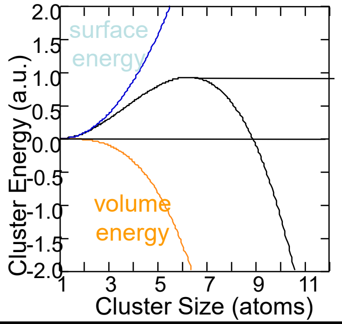

Nucleation and Growth

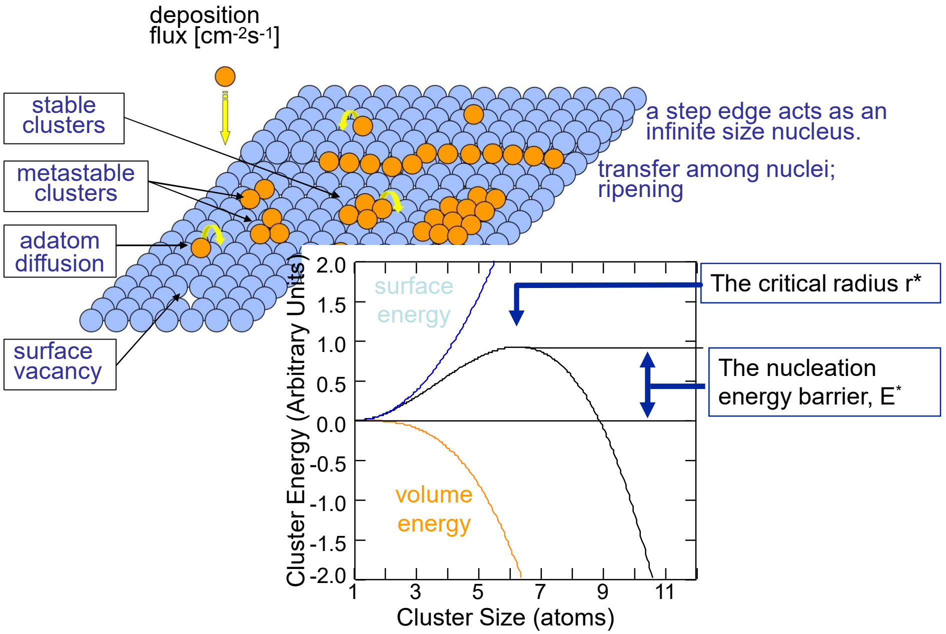

deposition flux [cm^{-2}s^{-1}]

stable clusters

metastable clusters

adatom diffusion

surface vacancy

a step edge acts as an infinite size nucleus.

transfer among nuclei; ripening

The critical radius r*

The nucleation energy barrier, E*

Modeling TiN(001) Film Growth by Classical Molecular Dynamics

Termal fluxes at 1200 K, N/Ti = 1

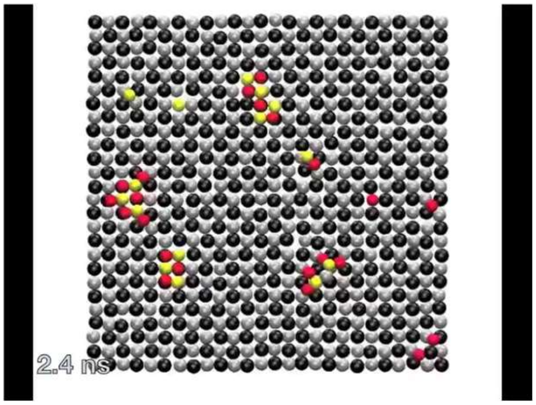

The understoichiometric island I 111 oriented

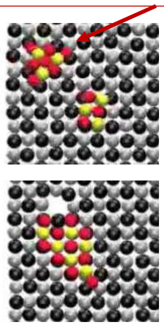

After coalescence the island is epitaxial

- coalescence is a key step in formation of preferred orientation and epitaxy;
- if complete leads to minimization of the interface and surface energies

Courtesy to Davide Sangiovanni davide.sangiovanni@liu.se unpublished

Growth modes

2-D Layer-by-Layer Growth(Frank-van der Merwe), e.g., Si/Si, TiN/MgO

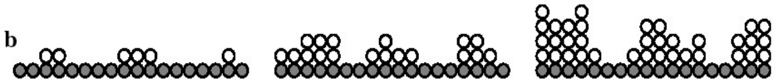

3-D Island Growth (Volmer-Weber), e.g., Metals on SiO_2

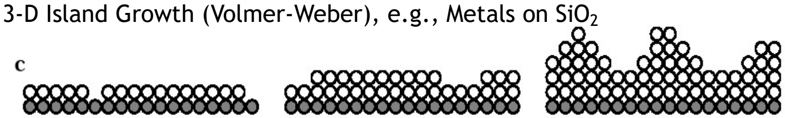

Stranski-Krastanov, e.g., In/Si, Ag/Si, Ge/Si

F.C.Frank

Jan H van der Merwe

Max Volmer

Iwan Stranski

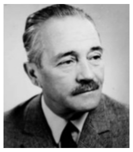

Lyubomir Krastanov

Ivan Markov, Crystal Growth for Beginners **https://www.worldscientific.com/worldscibooks/10.1142/10127**

Growth processes controlling microstructure evolution

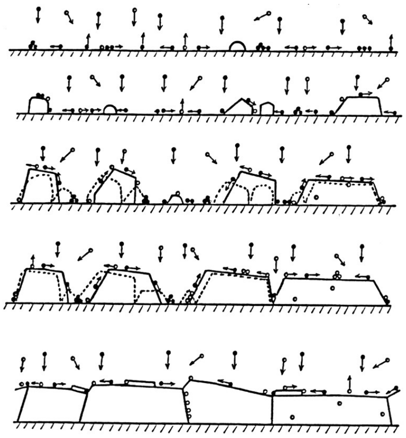

- •condensation of atom, surface diffusion
- •nucleation of isolated islands
- • island growth
- • impingement and coalescence of islands
- • formation of polycrystalline islands and channels
- • development of continuous film
- •local epitaxy on grains&columns
- •competitive colunm growth and grain coarsening
- • (Renucleation)

Case of pure elemental materials

P. Barna: In-situ TEM: indium evaporation on amorphous carbon

T_s = 90 °C
T_s/T_m = 0.85
R = 5 Å/s
p = 5.10^{-7} Torr

J.F. Pócza, Á. Barna and P.B. Barna J Vac Sci Technol 6, (1969) 472

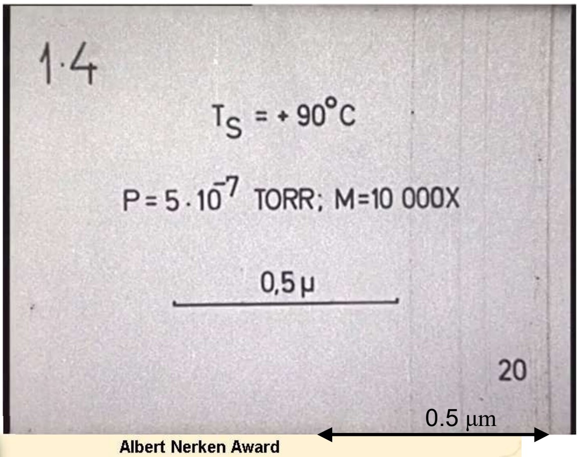

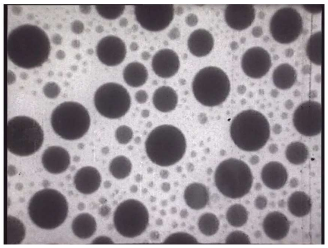

Close to the melting point small island are liquid;
Condensation is similar to water vapor condensing on a cold surface

Albert Nerken Award

AVS 2003

The Albert Nerken Award was established in 1984 by Veeco Instruments, Inc. in recognition of its founder, Albert Nerken, a founding member of AVS, and his early work in the field of high vacuum and leak detection, and contributions to the commercial development of that instrumentation. It is presented to recognize outstanding contributions to the solution of technological problems in areas of interest to AVS. The award consists of a cash prize and a certificate.

Dr. Peter B. Barna, Hungarian Academy of Sciences, "for seminal contributions in the use of in situ electron microscopy for the characterization and understanding of microstructural evolution and texture development during thin film growth."

P. Barna: In-situ TEM: indium evaporation on amorphous carbon

T_s = 75 °C
T_s/T_m = 0.81
R = 5 Å/s
p = 5.10^{-7} Torr

J.F. Pócza, Á. Barna
P.B. Barna J Vac Sci
Technol 6, (1969) 472

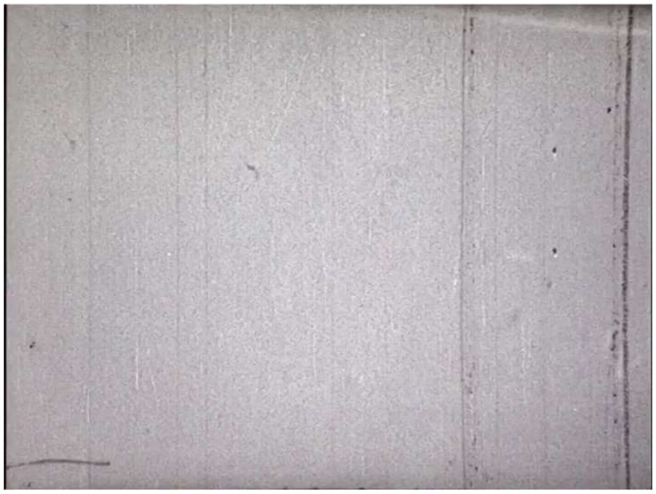

0.5 µm

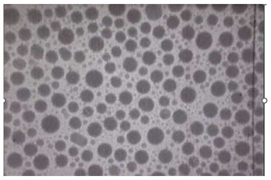

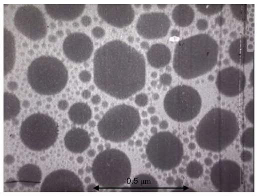

- Liquid-like coalescence - minimization of the interface and surface energies
- Size-dependent of the melting point

P. Barna: In-situ TEM: indium evaporation on amorphous carbon

T_s = -150 °C
T_s/T_m = 0.29
R = 2.5 Å/s
p = 2.10^{-7} Torr

J.F. Pócza, Á. Barna
P.B. Barna J Vac Sci
Technol 6, (1969) 472

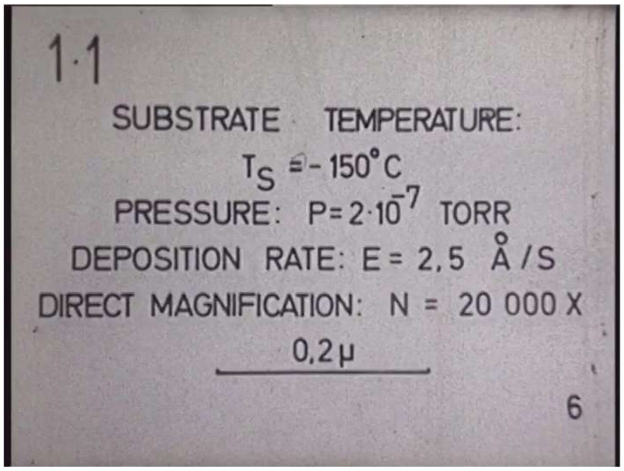

1·1

SUBSTRATE TEMPERATURE:
$T_S \cong -150°C$
PRESSURE: $P = 2 \cdot 10^{-7}$ TORR
DEPOSITION RATE: E = 2,5 Å/S
DIRECT MAGNIFICATION: N = 20 000 X
0,2 µ

6

0.2 µm

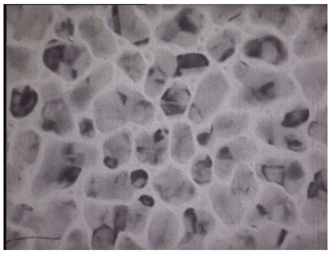

Grain boundaries form during coalescence, followed by grain coarsening

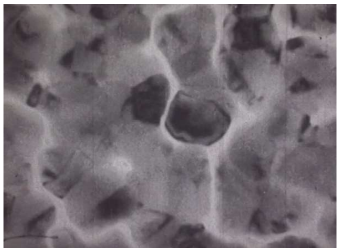

formation of polycrystalline islands and channels; Tensile stain upon channel "zipping"

Growth processes controlling microstructure evolution

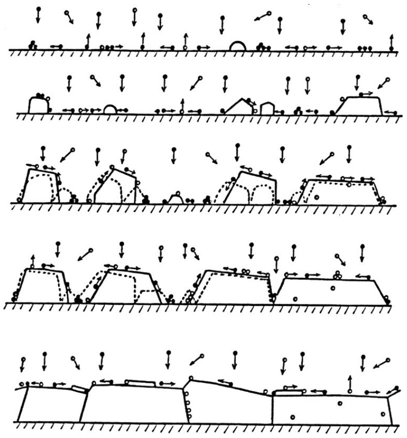

- condensation of atom, surface diffusion
- nucleation of isolated islands
- island growth
- impingement and coalescence of islands
- formation of polycrystalline islands and channels
- development of continuous film
- local epitaxy on grains&columns
- competitive colunm growth and grain coarsening
- (Renucleation)

Case of pure elemental materials

Zone Structure Models

Concept of *Homologuous* Temperature: $T_{substrate}/T_{melting}$

(to account for differences in activation barriers for different materials)

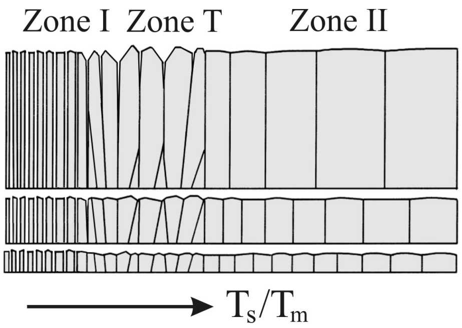

Zone I: *Random Aggregation*

Zone T: *Competitive Texture*

Zone II: *Recrystallization Texture*

SZMs systematically categorize self-organized structural evolution during PVD *(similar or related diagrams can be formulated for CVD and electrodeposition)* as a function of deposition parameters.

From an understanding of film formation follows the possibility for microstructural and nanostructural engineering in order to design a material for specific technological applications.

B.A. Movchan, A.V. Demchishin, Fiz. Met. Metalloved 28 /1969) 83
J.A. Thornton, Ann. Rev. Mater. Sci. 7 (1977) 239
P.B. Barna and M. Adamik, Thin Solid Films 317 (1998) 27

R.Messier, A.P.Giri, A.R. Roy, J.Vac.Sci.Technol.A2(1984)500
C.R.M.Grovenor,H.T.G.Hentzell,D.A.Smith, Acta Metall.32(1984)773
R.A. Roy, R.Messier, Mat. Res. Soc. Symp. Proc. 38 (1985) 363
J.A. Thornton, J. Vac. Sci. Technol. A4 (1986) 3059

J. Vac. Sci. Technol. A 21(5), Sep/Oct 2003

Microstructural evolution during film growth

I. Petrov, P.B. Barna, L. Hultman, J.E. Greene

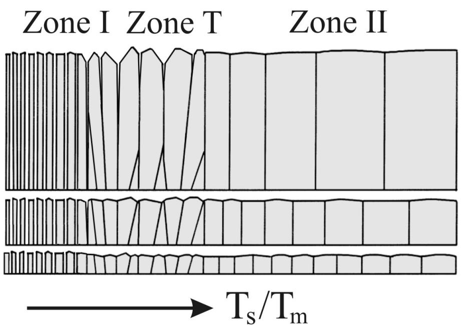

Zone I: *Random Aggregation*

Zone T: *Competitive Texture*

Zone II: *Recrystallization Texture*

Knobs to turn:

- Film growth processes; nucleation, coalescence, competitive growth (temperature, growth rate, epitaxy/strain)
- Phase separation (reactive species, immiscible systems)
- Ion bombardment
  - Gas ions: energy vs flux
  - Gas vs metal ions (DCMS vs HIPIMS)
  - Metal ion mass/type (light vs heavy)
- Nitrides and Borides
- Classical MD film growth

Recent advances

NaCl-structure transition-metal (TM) nitrides

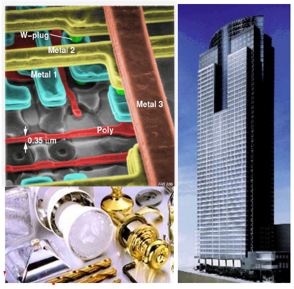

Materials physics interest stems from:

- TM Nitrides are anisotropic
  - preferred orientation is important
- all major uses require $T_s \leq 450$ °C ($T_s/T_m \approx 0.2$)
  - adatom mobilities are *relatively* low
- highly kinetically limited; underdense rough films with 111 PO

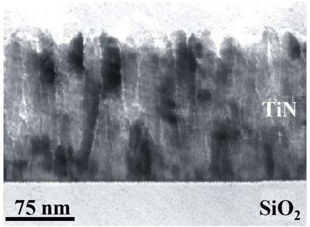

TiN & TaN: Model systems for low-temperature ion-assisted growth

TiN, $Ti_{1-x}Al_xN$, $Ti_{1-x}W_xN$, TiN/VN SL, CrN, $Cr_{1-x}Ti_xN$, δ-TaN, VN, ScN, $Sc_{1-x}Ti_xN$, CeN, $Ti_{1-x}Ce_xN$, YN

TiN/SiO$_2$, T$_s$ = 350 ^{o}C, E$_i$ = 20eV

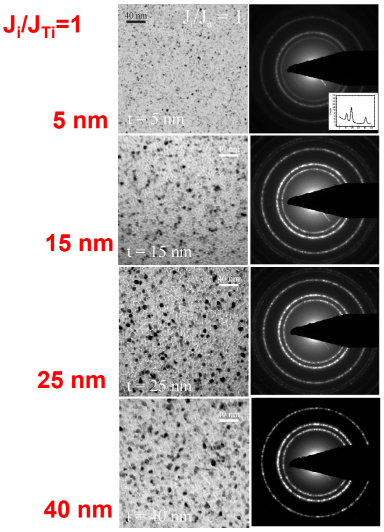

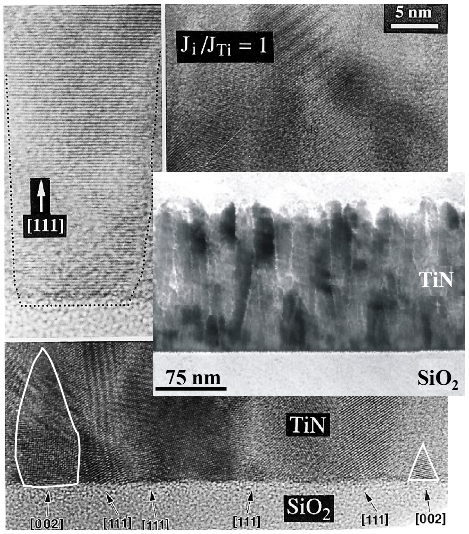

Random Nucleation; 111 texture dominates in a kinetically limited competitive column growth; properties function of thickness

2D mean-field kinetic MC “SOS” simulation

BC: $E_s^{111} > E_s^{001}$; $E_b^{111} > E_b^{001}$

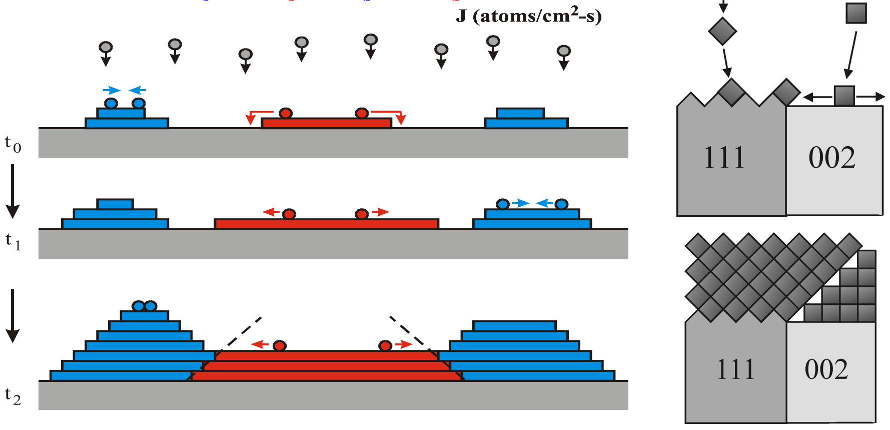

The lower surface adatom mobility on polar 111-surfaces (with three backbonds) results in a higher adatom incorporation probability on 111-grains which finally overgrow the non-polar 002-grains

3D kinetic MC simulation of low-T_s competitive 111 TiN texture evolution

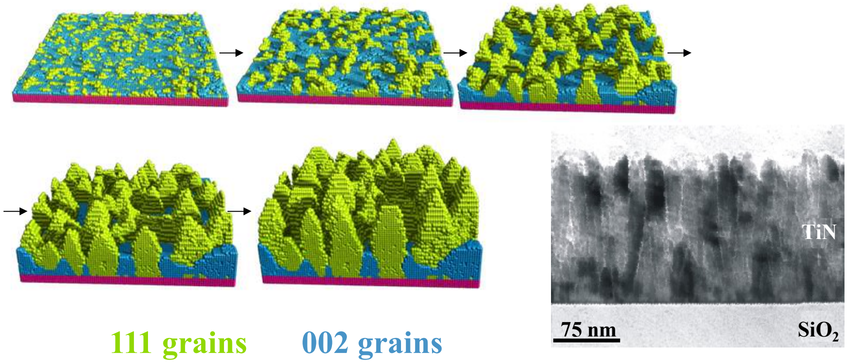

F. H. Baumann, D. L. Chopp, T. Díaz de la Rubia, G. H. Gilmer, J. E. Greene, H. Huang, S. Kodambaka, P. O’Sullivan, and I. Petrov, *MRS Bulletin,* **26** 182 (2001)

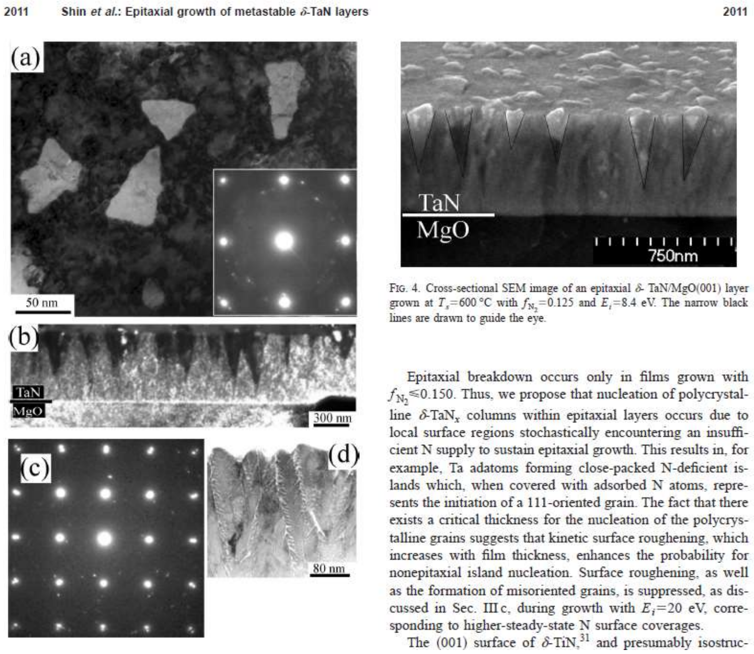

2011 Shin *et al.*: Epitaxial growth of metastable δ-TaN layers 2011

FIG. 4. Cross-sectional SEM image of an epitaxial δ- TaN/MgO(001) layer grown at T_s=600 °C with f_{N_2}=0.125 and E_i=8.4 eV. The narrow black lines are drawn to guide the eye.

Epitaxial breakdown occurs only in films grown with $f_{N_2} \leqslant 0.150$. Thus, we propose that nucleation of polycrystalline δ-TaN_x columns within epitaxial layers occurs due to local surface regions stochastically encountering an insufficient N supply to sustain epitaxial growth. This results in, for example, Ta adatoms forming close-packed N-deficient islands which, when covered with adsorbed N atoms, represents the initiation of a 111-oriented grain. The fact that there exists a critical thickness for the nucleation of the polycrystalline grains suggests that kinetic surface roughening, which increases with film thickness, enhances the probability for nonepitaxial island nucleation. Surface roughening, as well as the formation of misoriented grains, is suppressed, as discussed in Sec. III c, during growth with E_i=20 eV, corresponding to higher-steady-state N surface coverages.

The (001) surface of δ-TiN,[31] and presumably isostruc-

Structure-zone diagrams

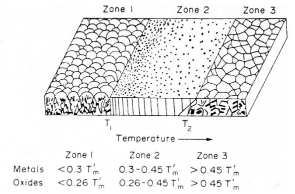

Movchan: evaporation

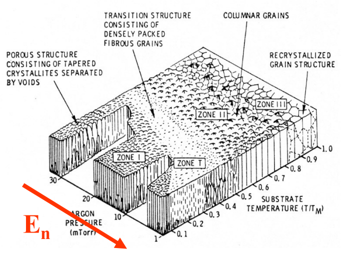

Thornton: sputtering

J_n, $E_n \sim 0.2$ eV

J_n, $E_n \sim 2\text{-}20$ eV

J_i, $E_i \sim e(U_{plasma}-U_{bias})$ eV

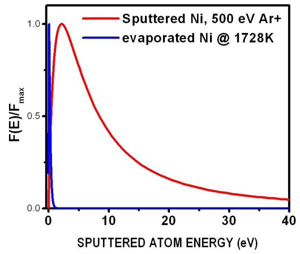

$J_i/J_n \sim 1$, $E_i \sim 100\text{-}500$ eV

$J_i/J_n \sim 5\text{-}20$, $E_i \sim 20$ eV

Effect of sputtered atom energy

Zone I

$E_i = 100$ eV, $J_{ion}/J_{Ti} = 0.5$, $T_s = 500$ °C

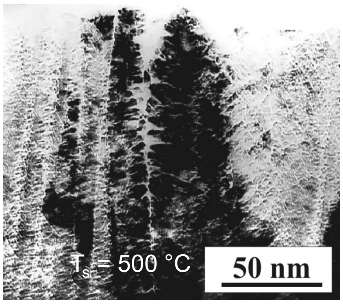

$P_{tot} = 38$ mTorr

$d_{target\text{-}substrate} = 5\ dt_{hermalization}$

Pressure is high enough to **thermalize energetic fluxes** from the sputtering target.

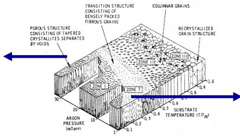

Zone T

$E_i = 20$ eV, $J_{ion}/J_{Ti} = 1$, $T_s = 350$ °C

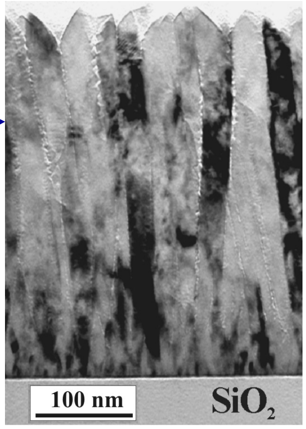

$P_{tot} = 5$ mTorr

$d_{target\text{-}substrate} < 5\ d_{thermalization}$

The grain size, initially small, increases with thickness while column boundaries become increasing more open. The Zone T structure forms through random nucleation, limited coarsening during coalescence, and competitive column growth. The column tops are faceted due to kinetic roughening, which in combination with atomic shadowing results in deep cusps between columns and open column boundaries The individual columns, however, are dense indicating sufficient adatom surface mobility to sustain local crystal growth.

Effects of Increasing E_i with $J_i/J_{Me} \leq 1$

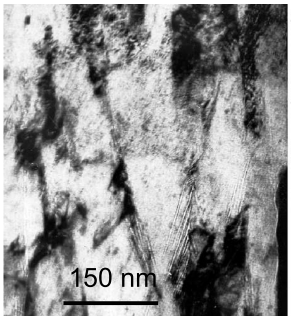

160 eV — Local disruption of epitaxial growth on columns and renucleation events

120 eV — Fully dense film & Incorporation of lattice damage

80 eV

Porous column boundaries

40 eV

XTEM image from the middle portion of a TiN layer grown by reactive magnetron sputter deposition at **300 °C** with a total pressure **P_t = 5.6 mTorr**. The ion-to-Ti flux ratio J_i/J_{Ti} incident at the film surface was < 1 while the ion energy E_i was varied in steps of 40 eV.

I. Petrov et al. Thin Solid Films 169 (1989) 299

Mechanisms of Ion-Irradiation Induced Densification;

100 eV Ar^+ on Ni

The impact of energetic ions on a surface collapses protruding areas and shrinks trapped void volume.

Shown are results of a ***molecular dynamics simulation*** of an ion impact on a surface.

- Forward sputtering
- Recoil Events
- Lattice relaxation

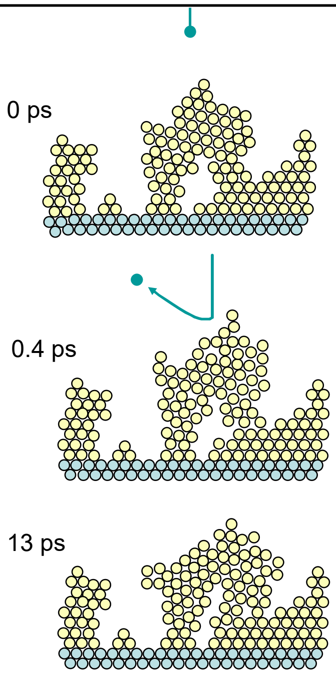

Figure from Karl-Heinz Müller, Surf. Sci. Lett. (1987)

Effects of gas ion energy

E_i > 100 eV, J_i/J_{Me} = 0.5

TiN/SiO_2
T_s= 350 °C

XTEM

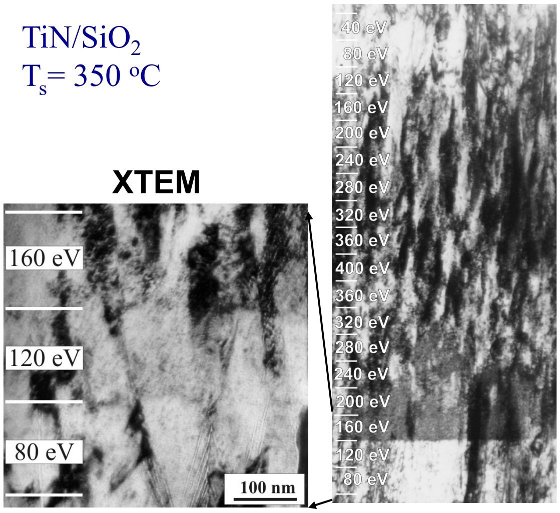

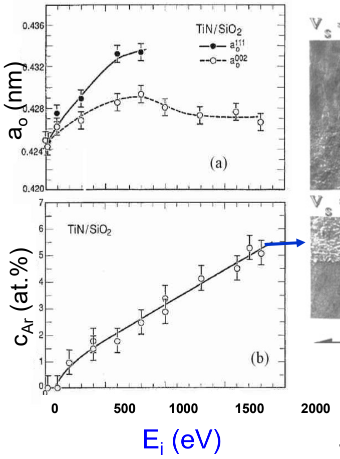

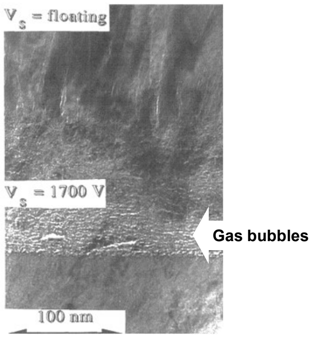

I. Petrov, L. Hultman, U. Helmersson, J.-E. Sundgren, J. E. Greene, *Thin Solid Films*, 169 299 (1989)

J.-E. Sundgren L Hultman,
G Håkansson, J Birch, I Petrov,
MRS Proc 168 (1992)71

Effects of gas ion energy

E_i > 100 eV, J_i/J_{Me} = 0.5

Prof. Lars Hultman

TiN/SiO_2
T_s= 350 °C

XTEM

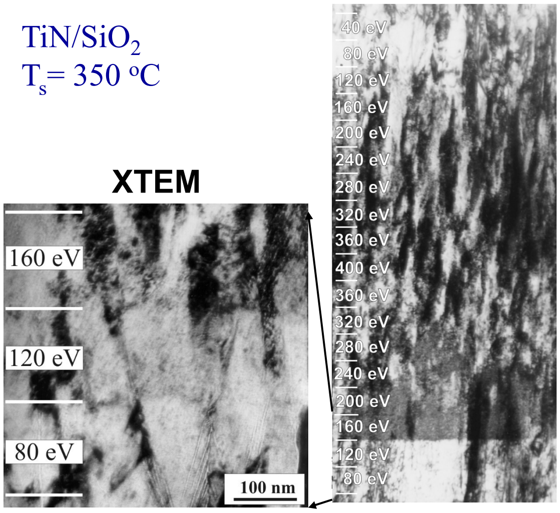

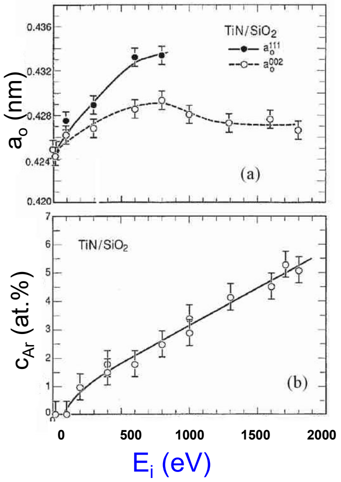

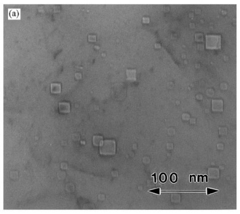

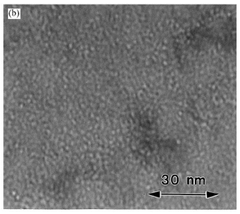

I. Petrov et al, *Thin Solid Films*, **169** 299 (1989)

And though the holes were rather small
They had to count them all
Now they know how many holes it takes to fill the Albert Hall

Control of microstructure

effect of ion energy

hyperthermal deposition

E_i = 20 eV, J_{ion}/J_{Ti} = 1, T_s = 350 °C

thermalized dep. flux

E_i = 100 eV, J_{ion}/J_{Ti} = 0.5, T_s = 500 °C

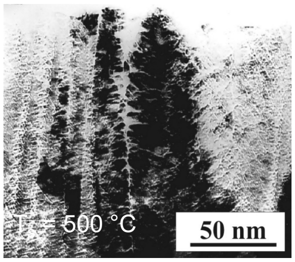

P_{tot} = 38 mTorr

$d_{target\text{-}substrate}$ = 5 $dt_{hermalization}$

Pressure is high enough to **thermalize energetic fluxes** from the sputtering target.

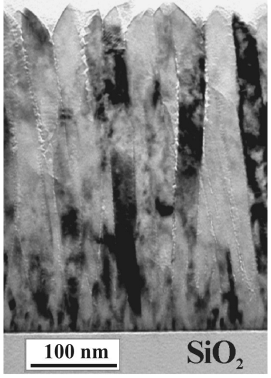

P_{tot} = 5 mTorr

$d_{target\text{-}substrate}$ < 5 $d_{thermalization}$

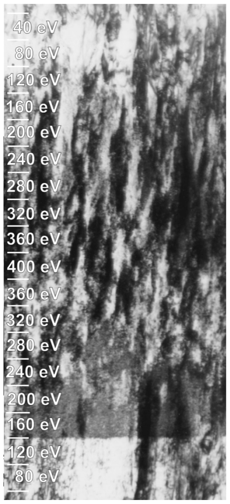

Independent control of ion flux and ion energy

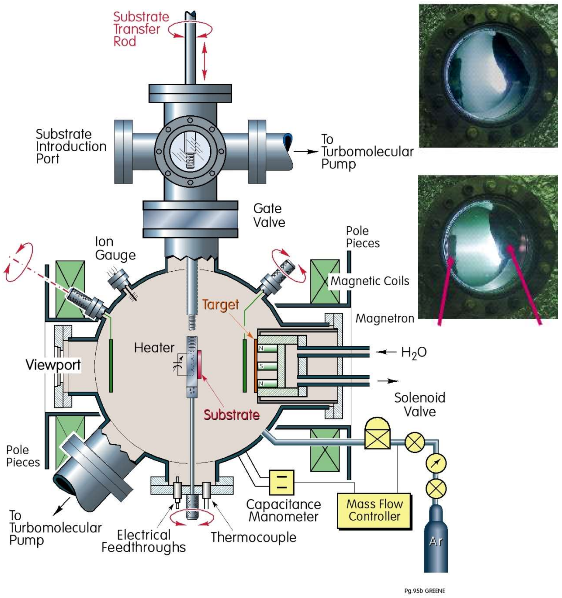

$$E_i = e(V_{plasma} - V_{bias})$$

$$J_i = f(B_{ext})$$

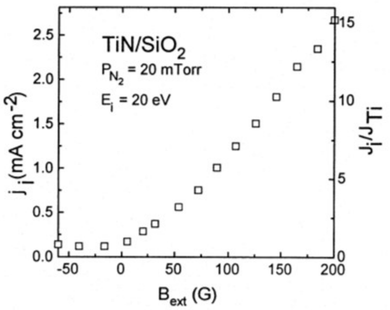

I. Petrov, F. Adibi, J.E. Greene, W.D. Sproul, and W.-D. Münz, *JVST* A10, 3283 (1992).

Average energy deposited per atom: A universal parameter for describing ion-assisted film growth?

Appl. Phys. Lett. 63, 36, 1993

I. Petrov, F. Adibi, and J. E. Greene
Department of Materials Science, the Coordinated Science Laboratory, and the Materials Research Laboratory, University of Illinois, Urbana, Illinois 61801

L. Hultman and J.-E. Sundgren
Thin Film Division, Physics Department, Linköping University, S-581 83 Linköping, Sweden

$Ti_{0.5}Al_{0.5}N/SiO_2$
$T_s = 350\ ^oC$

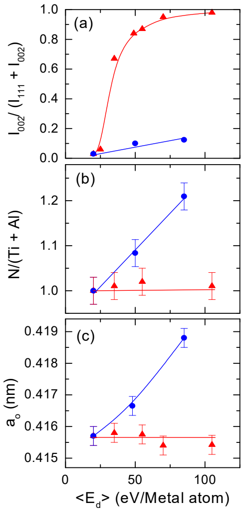

➡ $E_i = 20$ eV, J_i/J_{Me} varied
➡ $J_i/J_{Me} = 1$, E_i varied

At low energies, E_i ~ 10-20 eV, ***below the bulk lattice displacement threshold,*** there are distinctly different mechanistic pathways leading to microstructural evolution and texture development depending upon whether in E_i is varied at constant J_i/J_{Me} or J_i/J_{Me} is varied at constant E_i.

Under high fluxes of low-energy ions texture develops in the nucleation and coalescence stage

J_i/J_{Ti}=1

5 nm

15 nm

25 nm

40 nm

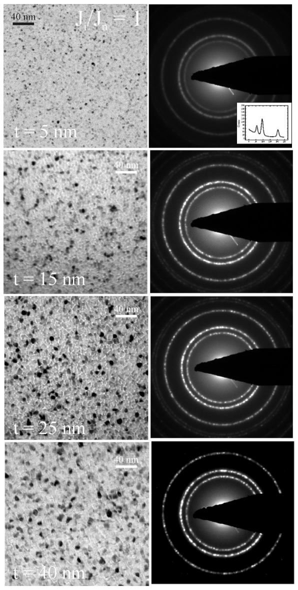

J_i/J_{Ti}=14

5 nm

15 nm

25 nm

40 nm

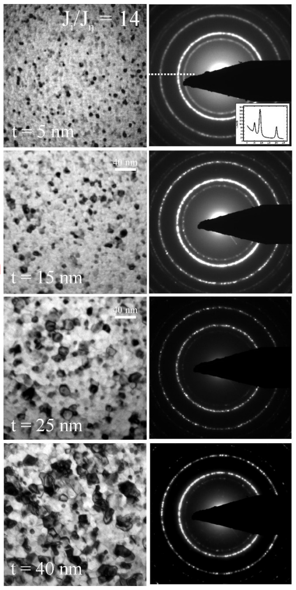

TiN/SiO_2,
$T_s = 350\ ^oC$, $E_i = 20eV$

Under high fluxes of low-energy ions texture develops in the nucleation and coalescence stage

TiN/SiO_2
$J_i/J_{Ti} = 14$
$E_i = 20$ eV
$T_s = 350$ °C

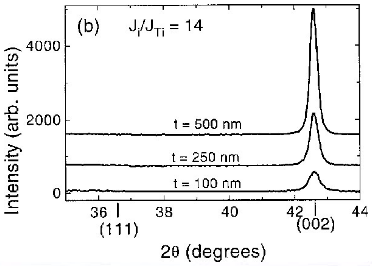

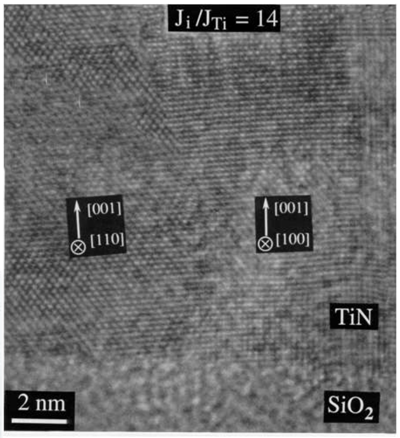

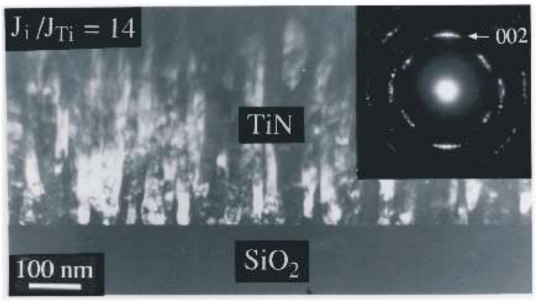

002 texture dominates from the earlier stages of growth

L. Hultman, J.-E. Sundgren, J.E. Greene, D.B. Bergstrom, and I. Petrov, *J. Appl. Phys.* 78, 5395 (1995)

Surface roughening and facet formation

Low temperature (T_S = 350 °C)

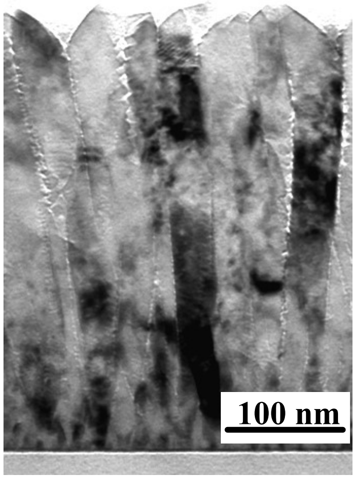

TiN/SiO_2

Intermediate temp. (T_S = 520 °C)

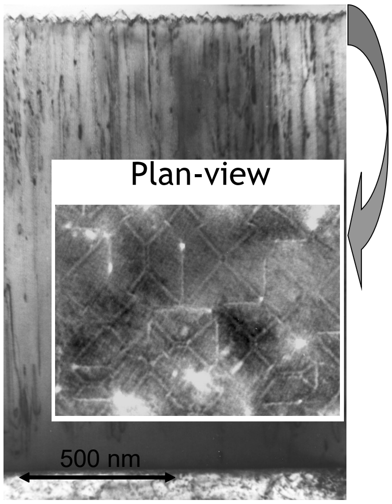

$Ti_{0.5}Al_{0.5}N$/MgO(001),
J_i/J_{Me} = 10, E_i= 20 eV

TiN/MgO(001) at high temperature (T_S = 750 °C)

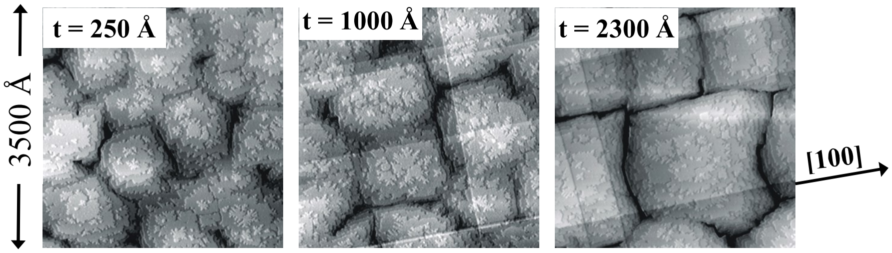

*Note: T_s = 750 °C → T_s/T_m ⍰ 30%

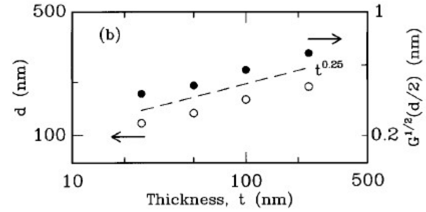

- In-situ STM study.
  In-plane length scale (d)
  with varying thickness (t)

*B. W. Karr, D. G. Cahill, I. Petrov, and J. E. Greene, *Phys. Rev. B* **61** 16137 (2000).

Ehrlich Barrier

Adatoms diffusing on an upper terrace require an additional energy (the Ehrlich barrier, **E_b**) to cross descending step edges. **E_s** is the surface diffusion activation barrier. Note that adatoms that cross descending edges move into a deep trap (**E_f**) due to higher bond coordination.

The barrier asymmetry at step edges leads to a tendency for up-hill flux resulting in kinetic roughening

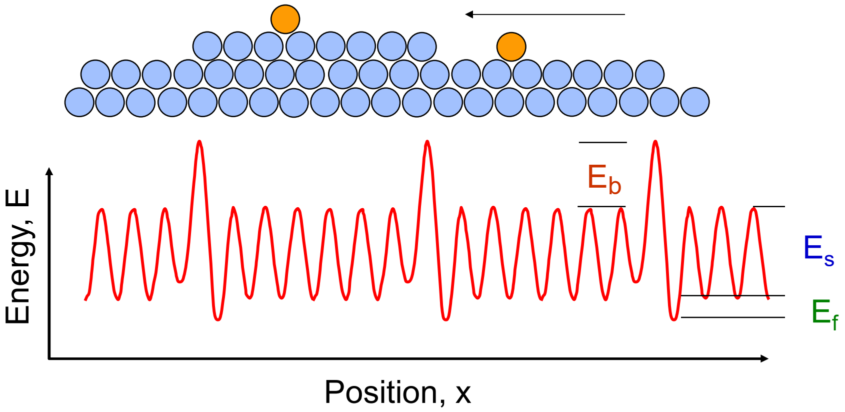

Gert Ehrlich
1926-2012
University of Illinois

Self-organized nano-pipes, mounds, ridges and pyramids

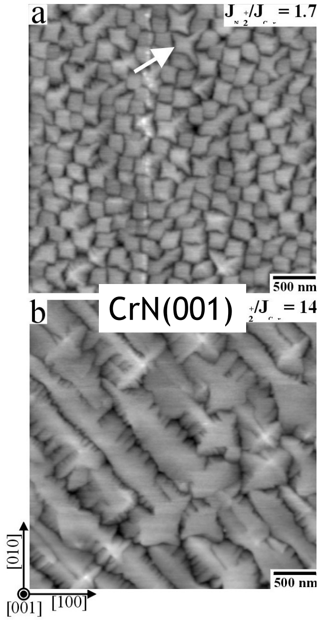

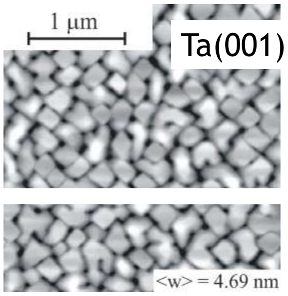

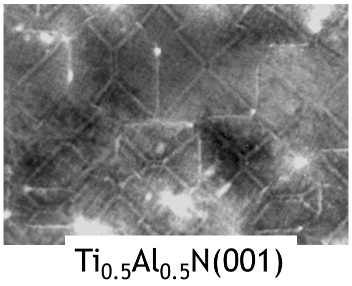

$J_i/J_n = 1$
Low mobility

Patterned MgO(001)
substrate by FIB

$J_i/J_n = 14$
High mobility

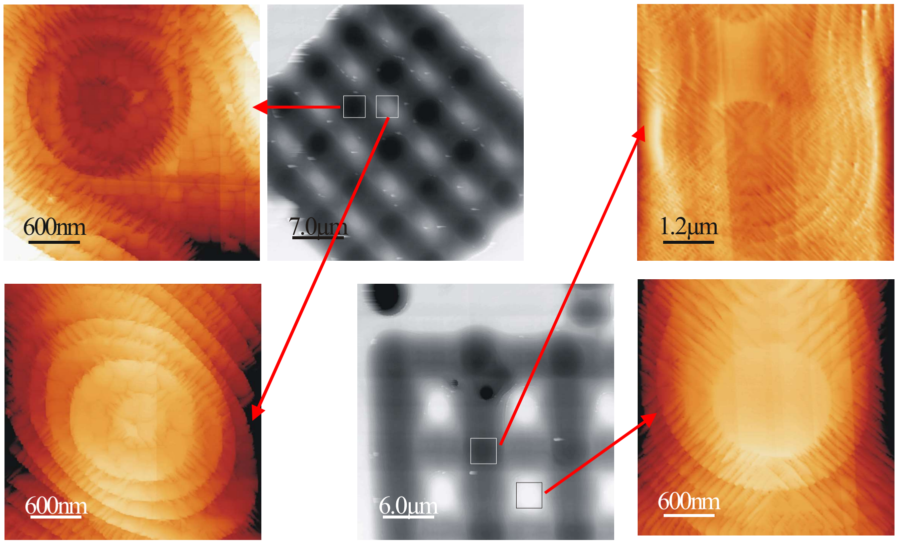

37

Low-temperature ($T_s/T_m \sim 0.3$) layer-by-layer TiN epitaxy

TiN/MgO(001), T_s = 750 °C J_i/J_{Me} = 14

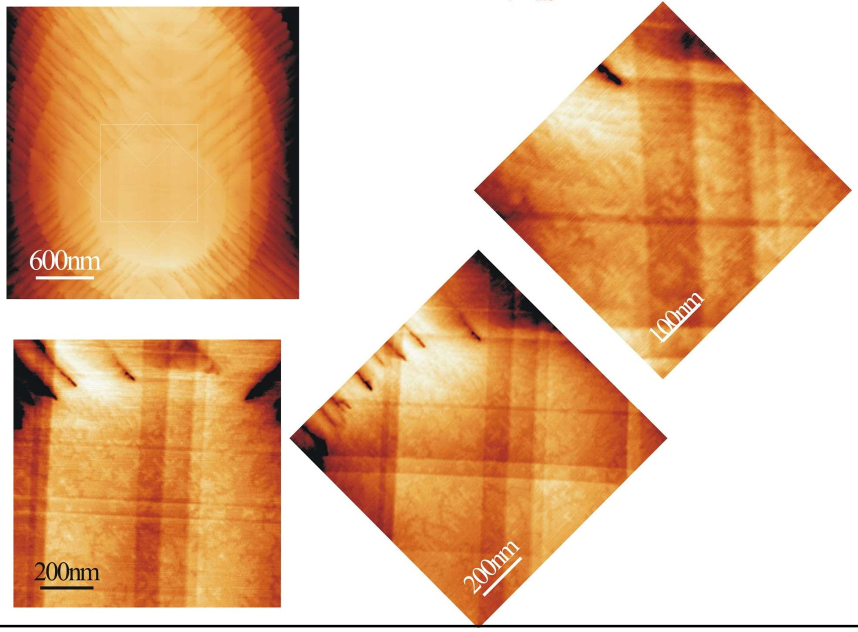

38

Low-temperature (T_s/T_m ~ 0.3) layer-by-layer TiN epitaxy

TiN/MgO(001), T_s = 750 °C J_i/J_{Me} = 14

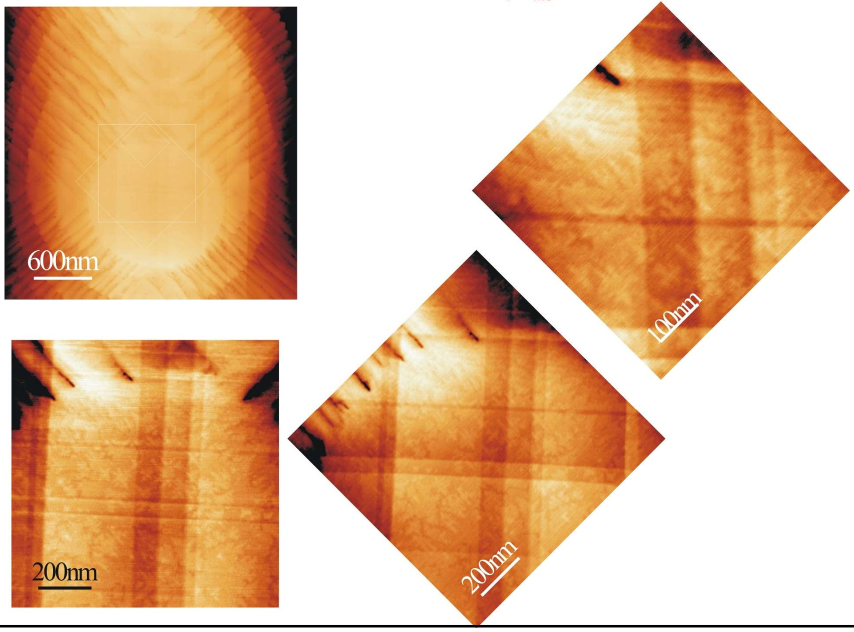

Bales & Zangwill growth instability

G. S. Bales, and A. Zangwill, Phys. Rev. B, **41**, 5500 (1990).

J_i/J_n = 14
High mobility

J_i/J_n = 1
Low mobility

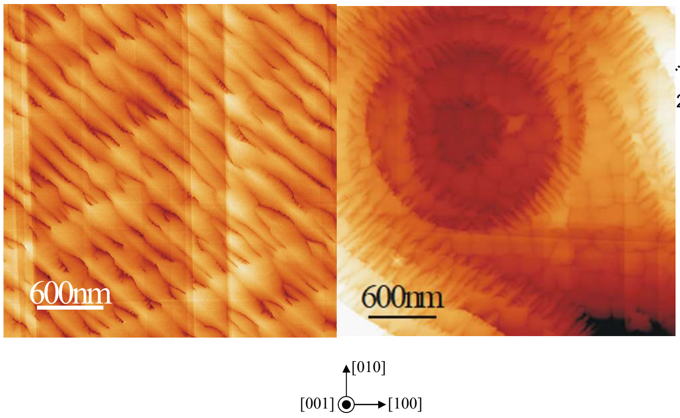

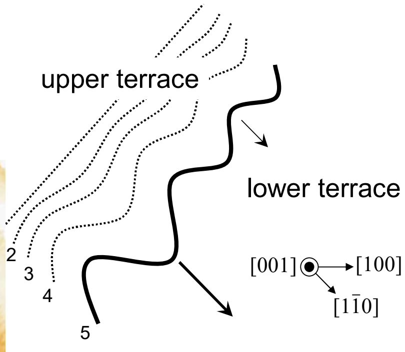

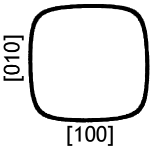

TiN Equilibrium
Island shape*

* S. Kodambaka, S. V. Khare, V. Petrova, A. Vailionis, I. Petrov and J. E. Greene, Surf. Sci. **513**, 468 (2002).

Low-temperature (T_s/T_m ~ 0.3) layer-by-layer TiN epitaxy

Mound formation; faceted pyramids; voids

J_i/J_{Me} = 1 E_i = 20 eV J_i/J_{Me} = 14

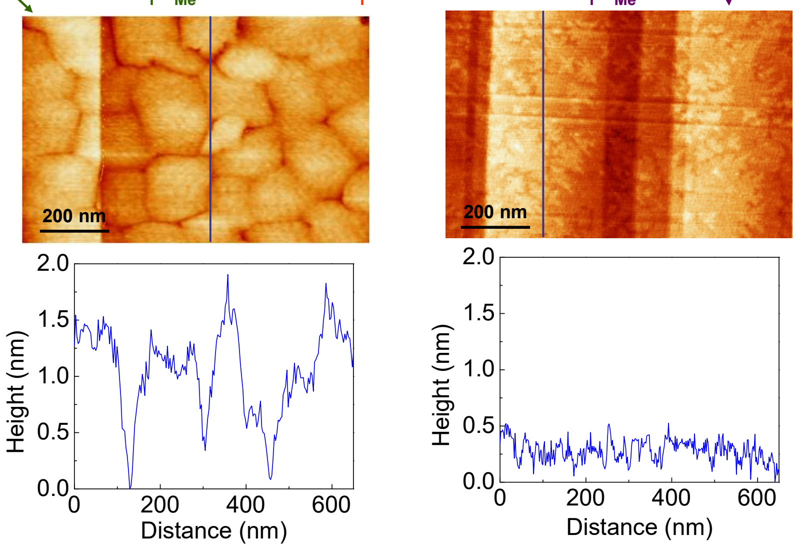

TiN/SiO$_2$, T_S=350°C, P_{N_2}=20 mTorr

J_i/J_{Me} = 7 E_i = 20 eV J_i/J_{Me} = 14

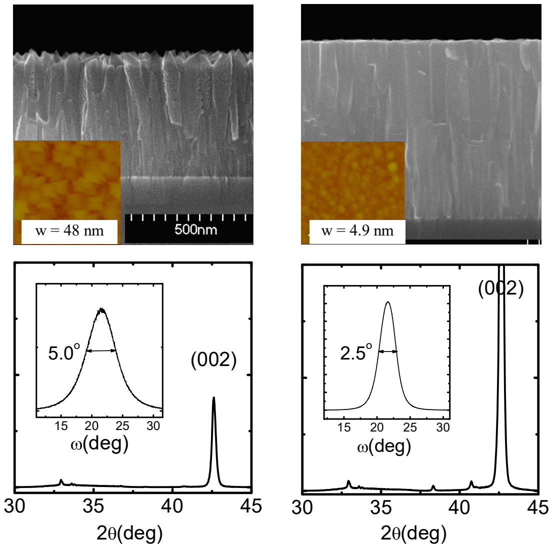

High Fluxes of Low Energy Ions

E_i ~ 20 eV, J_i/J_{Me} >10

control roughening
low temperature sputter epitaxy

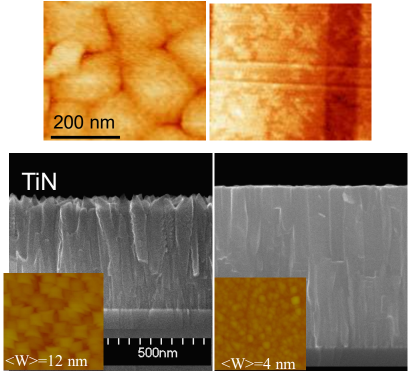

control nucleation

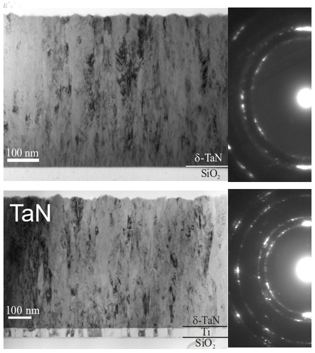

Shin et al, TSF, 402 (2002)172

control renucleation

Lee et al, APL, 84 (2003)

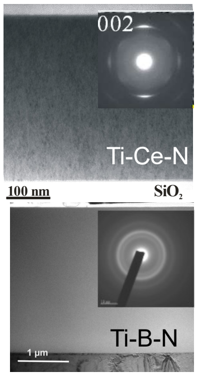

Mayrhofer, P JAP 100 (2006) 04430

Low Temperature Sputter Epitaxy of Transition Metal (TM) Nitrides

TM nitride	Group	a_o [nm]	m*	T_m [°C]	T_s/T_m	$\xi_\perp$ [nm]	$\xi_{\|}$ [nm]	E [GPa]	H [GPa]	ρ_{300K} [µΩ-cm]	RRR
ScN(1)	III	0.4501	0.069	2735	0.34	57	15	356	21±1.1	2000	--
TiN(2)	IVB	0.4240	0.007	2930	0.30	142	86	445±38	20±0.8	12.4	12
ZrN(3)	IVB	0.4573	0.086	2980	0.18	161	18	450±25	22.7±1.7	12.0	15
HfN(4)	IVB	0.4524	0.074	3250	0.26	182	22	450±9	25.2±0.7	14.2	4
CeN(5)	IV	0.5043	0.198	2830	0.34	26	7	330±16	15.0±0.9	68.5	2.3
VN(6)	VB	0.4130	0.009	2323	0.30	159	57	356±12	14.3±1.0	35.0	16
δ-TaN(7)	VB	0.4351	0.028	3090	0.26	104	21	445±12	31.5±1.0	185	--
CrN(8)	VIB	0.4162	0.008	1770	0.41	172	43	405±15	28.5±1.0	7700	--

(1) D. Gall, I. Petrov, N. Hellgren, L. Hultman, J. E. Sundgren, and J. E. Greene, JAP 84, 6034 (1998).
(2) C.-S. Shin, D. Gall, N. Hellgren, J. Patscheider, I. Petrov, and J. E. Greene, JAP **93**, 6025 (2003).
(3) A. B. Mei, B., M. Sardela, J. N. Eckstein, L. Hultman, A. Rockett, I. Petrov, and J. E. Greene, JVSTA **31**, 061516 (2013).
(4) H.-S. Seo, T.-Y. Lee, I. Petrov, J. E. Greene, and D. Gall, JAP **97**, 083521 (2005).
(5) T.-Y. Lee, D. Gall, C.-S. Shin, N. Hellgren, I. Petrov, and J. E. Greene, JAP **94**, 921 (2003).
(6) A. B. Mei, A. Rockett, L. Hultman, J.E. Greene, and I. Petrov, JAP **115**, 214908 (2014);
(7) C.-S. Shin, Y.-W. Kim, N. Hellgren, D. Gall, I. Petrov, and J. E. Greene, JVSTA **20**, 2007 (2002).
(8) D. Gall, C.-S. Shin, T. Spila, M. Odén, M. J. H. Senna, J. E. Greene, and I. Petrov, JAP **91**, 3589 (2002).

TiN_x, VN_x, ZrN_x, VN_x
$Ti_{1-x}Al_xN$, $Hf_{1-x}Al_xN$, $Ti_{1-x}W_xN$, $Sc_{1-x}Ti_xN$, $Ti_{1-x}Ce_xN$, $V_{1-x}Mo_xN$, $V_{1-x}W_xN$
Superlatticies TiN/VN, $Hf_{1-x}Al_xN$/HfN

Blueprint for work on diborides

Texture inheritance

Texture inheritance at low ion energies

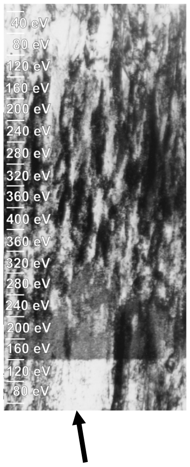

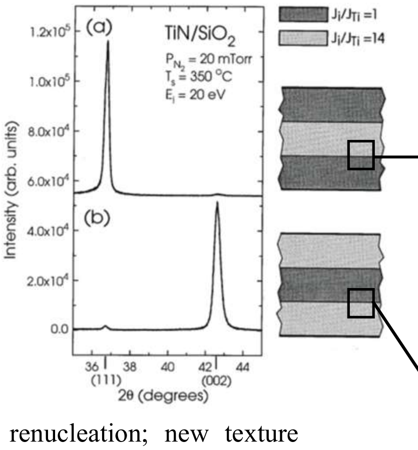

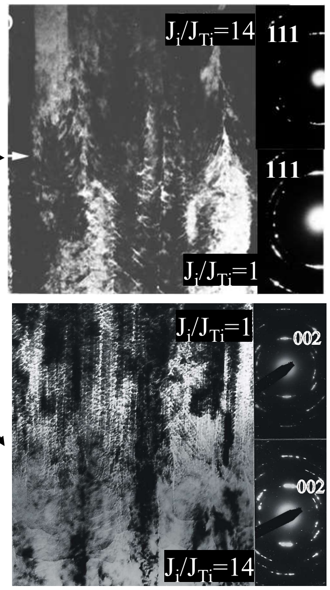

- High ion energy cause renucleation; new texture develops
- In contrast, once texture has developed, low-energy ion irradiation controls film density but preferred orientation persists through **local epitaxy.**

Atomic arrangement in 0002 Ti and polar 111 TiN

TiN(111)
overlayer

d_{TiN} = 0.29995 nm

Ti(0002)
crystallographic
template

d_{Ti} = 0.29053 nm

Ti(0002)/TiN(111)
misfit ≅ 1.6 %

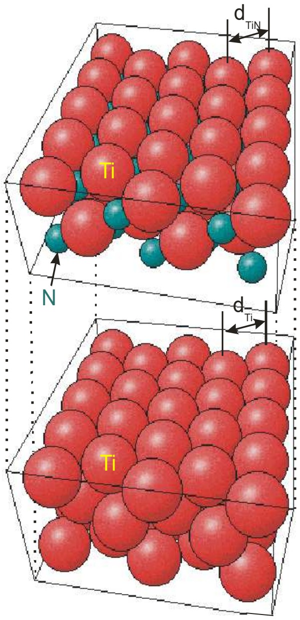

Highly 111-textured TiN/Ti(0002)

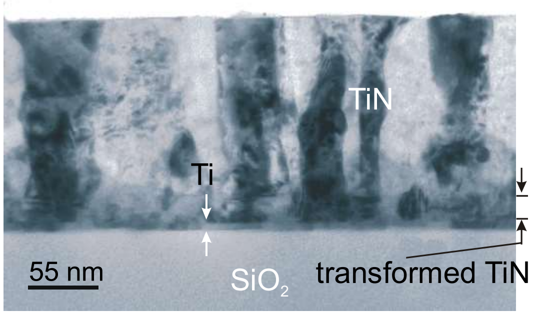

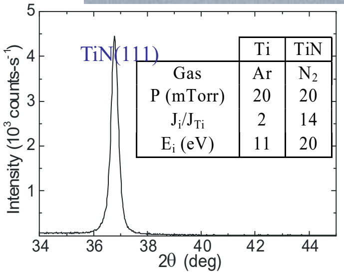

	Ti	TiN
Gas	Ar	N_2
P (mTorr)	20	20
J_i/J_{Ti}	2	14
E_i (eV)	11	20

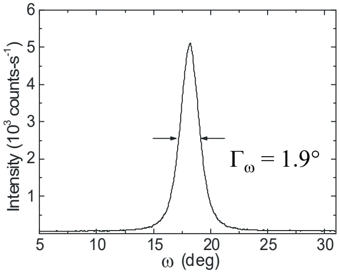

Independent control of density and texture

Density control: $J_i/J_{Ti} = 14$

Texture control: TiN/Ti

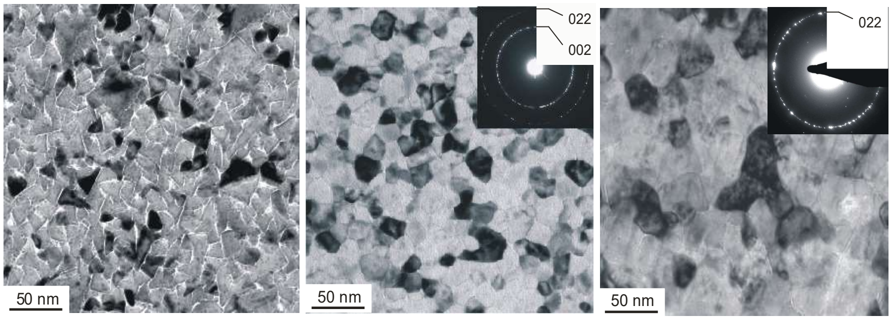

- (111) texture.
- $\langle d \rangle = 20 \pm 14$ nm.
- underdense grain structure.

- (002) texture.
- $\langle d \rangle = 18 \pm 12$ nm.
- dense grain structure.

- (111) texture.
- $\langle d \rangle = 43 \pm 30$ nm.
- dense grain structure.

Texture and density control in δ-TaN

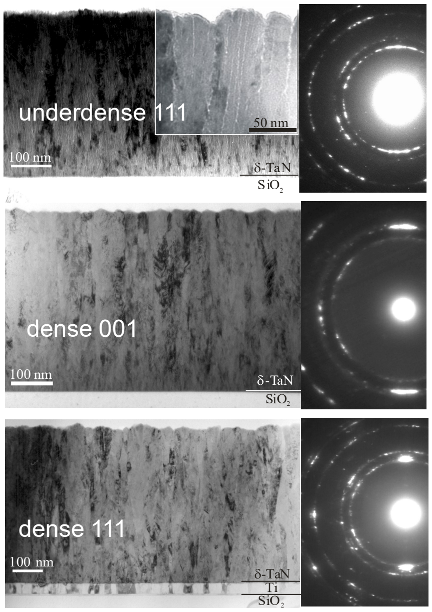

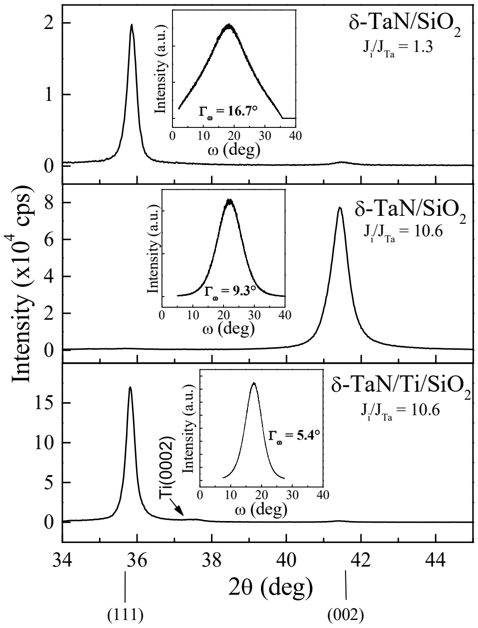

Metal ion etch and local epitaxy to enhance adhesion

The power of epitaxial growth

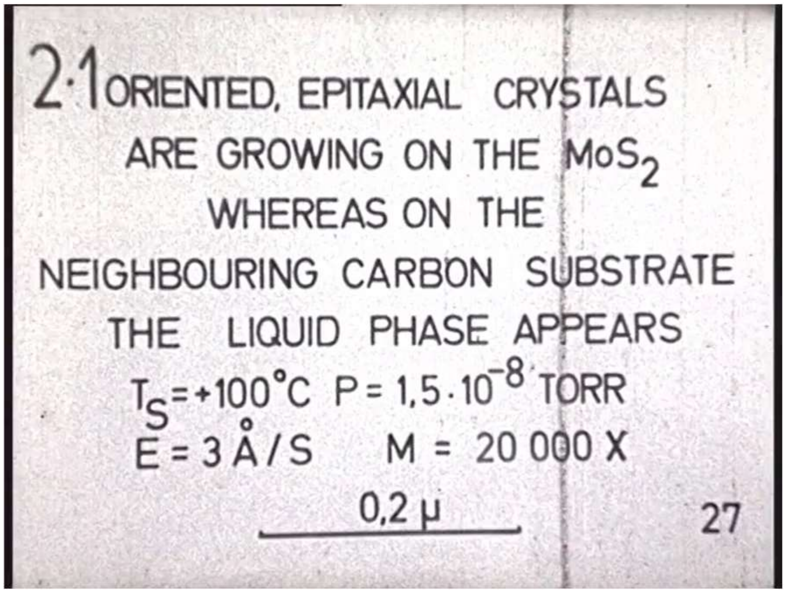

2·1 ORIENTED, EPITAXIAL CRYSTALS
ARE GROWING ON THE MoS_2
WHEREAS ON THE
NEIGHBOURING CARBON SUBSTRATE
THE LIQUID PHASE APPEARS
$T_S = +100^\circ C$ $P = 1{,}5 \cdot 10^{-8}$ TORR
$E = 3$ Å/S M = 20 000 X
0,2 μ
27

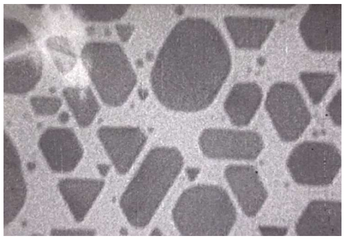

All islands are epitaxial;
Complete coalescence
Shape depends in island size

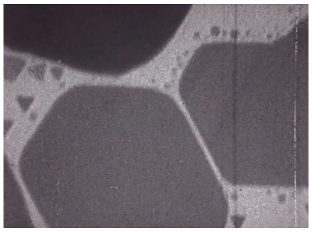

Contamination obstructs island coalescence

The importance of preparing the substrate

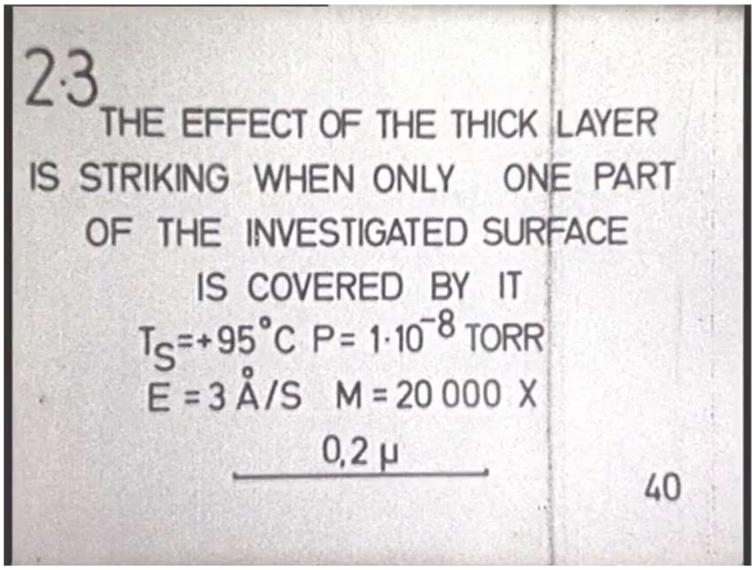

2·3

THE EFFECT OF THE THICK LAYER
IS STRIKING WHEN ONLY ONE PART
OF THE INVESTIGATED SURFACE
IS COVERED BY IT

T_S=+95°C P= $1 \cdot 10^{-8}$ TORR
E = 3 Å/S M = 20 000 X

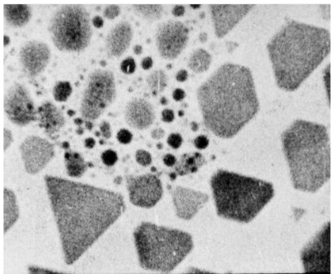

Completely different nucleation mode on contaminated area of the substrate

---

Arc Bond Sputtering (ABS): Cathodic-Arc Metal-Ion Etch/UBM Deposition of Ti0.5Al0.5N/SS

Dieter Münz

Sheffield
Hallam University

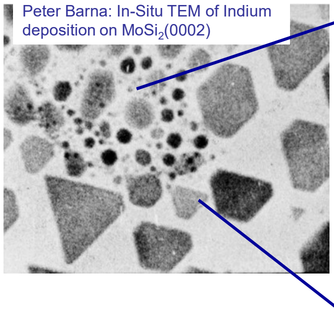

Peter Barna: In-Situ TEM of Indium deposition on $MoSi_2(0002)$

Cathodic arc $Ti_{0.85}Nb_{0.15}$ metal ion etch

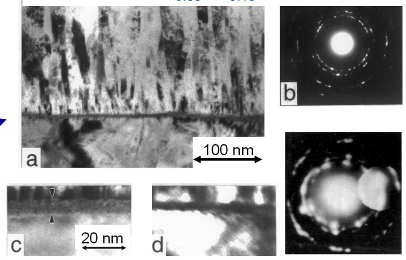

Metal-ion etch with heavy ions amorphized the substrate grains and promotes random nucleation, L_C = 60 N

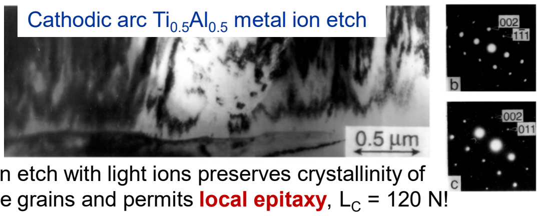

Cathodic arc $Ti_{0.5}Al_{0.5}$ metal ion etch

Metal-ion etch with light ions preserves crystallinity of substrate grains and permits **local epitaxy**, L_C = 120 N!

Ivan Petrov, P. Losbichler, J. E. Greene, W.-D. Münz, T. Hurkmans, and T. Trinh, *Thin Solid Films,* 302 179 (1997).

Microstructure of $Ti_{0.46}Al_{0.54}N$ on SS after cathodic arc Cr etch U_s=1200V

Plan-view TEM of film only (substrate removed)

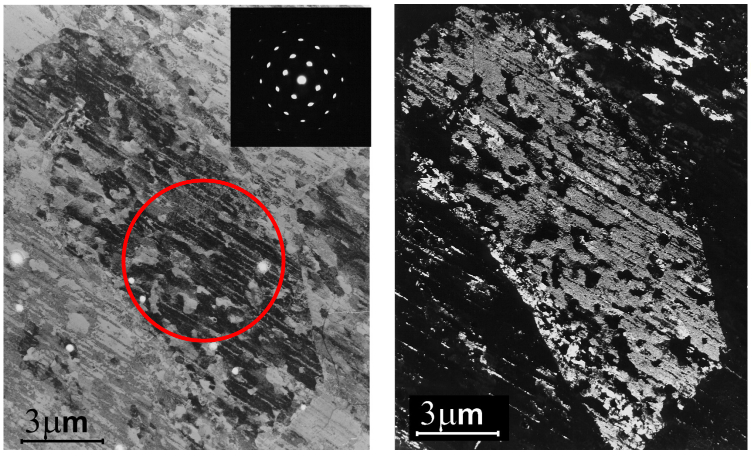

bright field

dark field

IV. CONCLUSION

(1) Ar etching at U_s = 1200 V leads to a low density interface region promoting a competitive columnar growth with small column size and open boundaries resulting in critical load values of 27±3 N.

(2) Cr-ion pretreatment at U_s = 600 V leads either to the formation of a Cr deposit resulting in competitive columnar growth with small column size and open boundaries or partially to local oriented growth. The critical load was 47 ±5 N.

(3) Cr-ion pretreatment at U_s = 1200 V removes at least 100 nm of the steel substrate and Cr is implanted thus providing a clean substrate surface so that local epitaxial growth can occur. In this case the critical load was evaluated to be 63±2 N.

C. Schönjahn, H. Paritong, W.-D. Münz, R. D. Twesten, and I. Petrov, *JVST A,* 19, 1392 (2001).

Sheffield Hallam University

Adhesion & Tool life

3.2 μm TiAlCrYN/TiAlN

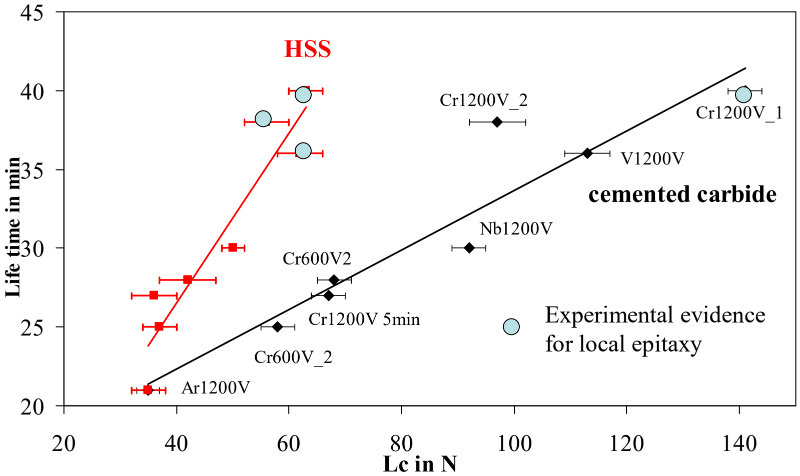

C. Schönjahn, A. P. Ehiasarian, D. B. Lewis, R. New, W.-D. Münz, R. D. Twesten, and I. Petrov *J. Vac. Sci. Technol. A,* **19** 1415 (2001)..

Surface and Coatings Technology 163–164 (2003) 267–272

High power pulsed magnetron sputtered CrN_x films

A.P. Ehiasarian[a,*], W.-D. Münz[a], L. Hultman[b], U. Helmersson[b], I. Petrov[c]

CrN HIPIMS, floating substrate

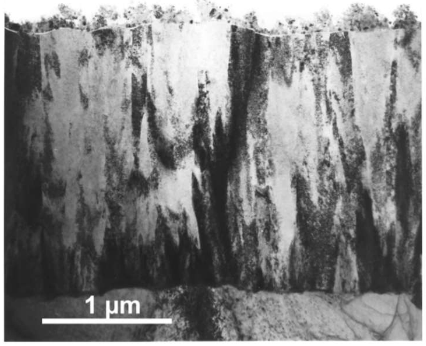

Fig. 6. Cross-sectional TEM view of CrN coating deposited by HIPIMS at $P_{Ar}/P_{N_2}=1{:}4$.

HIPIMS metal ion substrate etch

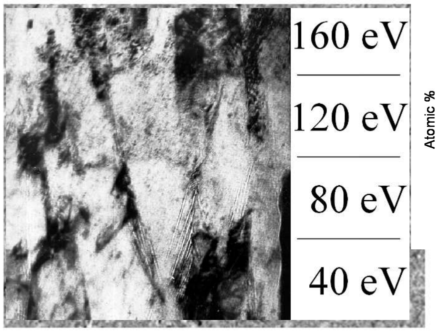

Fig. 4. SEM micrograph of CrN film deposited on HSS after pretreatment by HIPIMS.

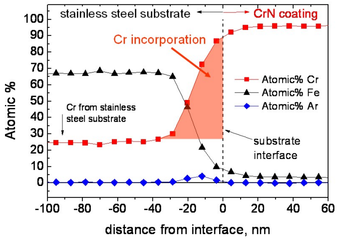

NanoTechnology Centre
for PVD Research
Sheffield Hallam University

Scratch Test Critical Load on HSS = 85 N

Interface microstructure engineering by HIPIMS

CrAlN coating on γ-TiAl
with pretreatment of
HIPIMS of Cr at
U_{bias}=−600 V

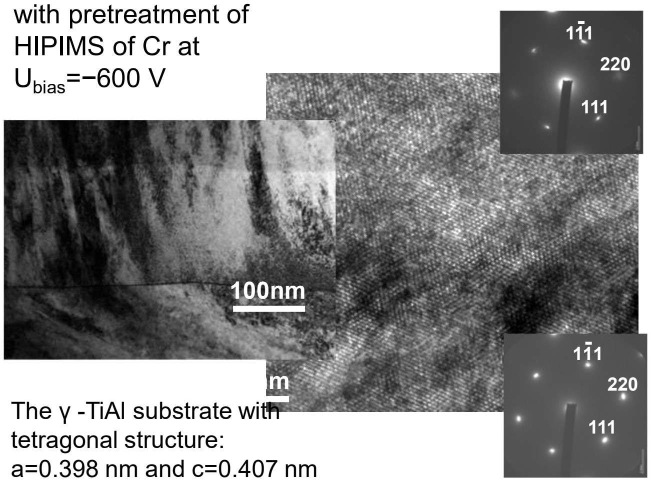

The γ -TiAl substrate with tetragonal structure:
a=0.398 nm and c=0.407 nm
a_{CrN}=0.415 nm.

HIPIMS Vanadium metal ion
etch with 1 kV of SS304

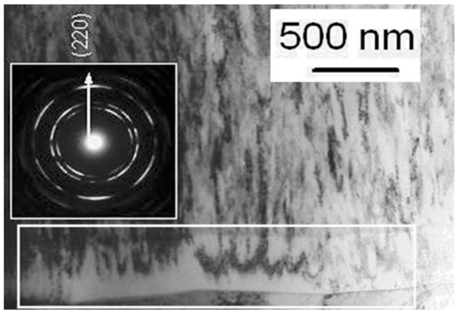

A.P. Ehiasarian, J.G. Wen, I. Petrov , J. Appl. Phys. 101, 054301 (2007)

NanoTechnology Centre
for PVD Research

Nanocomposites via segregation and renucleation

P. Barna: In-situ TEM: indium evaporation on amorphous carbon

T_s = 75 °C
T_s/T_m = 0.81
R = 5 Å/s
p = 5.10^{-6} Torr

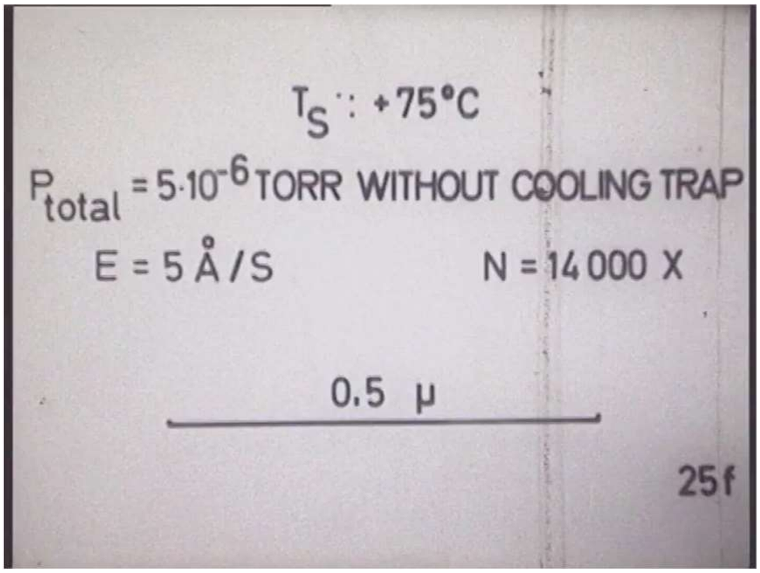

T_S : +75°C

P_{total} = 5·10^{-6} TORR WITHOUT COOLING TRAP

E = 5 Å / S N = 14 000 X

0,5 µ

25f

0.5 µm

Reactive deposition

Effects of additives: *alloying elements; dopants; contaminants*

Indium on a-C; $T_s = 75$ °C, R = 5 Å/s, p = 5.10^{-6} Torr

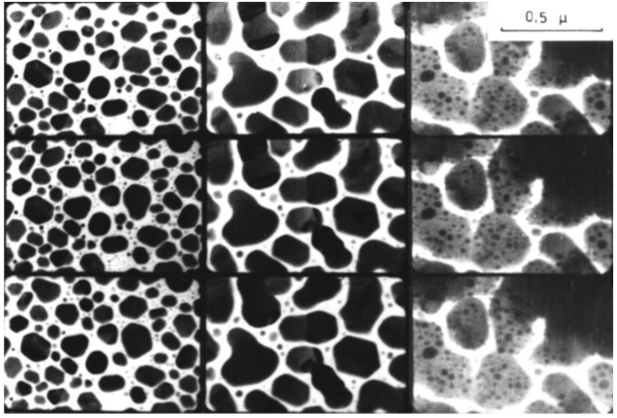

Segregation of co-deposited C results in the formation of a "tissue phase" covering the In crystals, causing renucleation

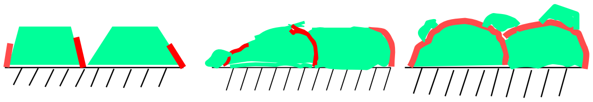

Zone Structure Models

Concept of *Homologuous* Temperature: $T_{substrate}/T_{melting}$

(to account for differences in activation barriers for different materials)

Movchan-Demchishin 1969

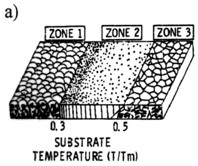

Thornton 1974

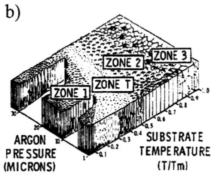

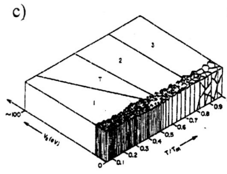

Messier et. al 1984

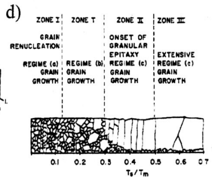

Grovenor et. al 1984

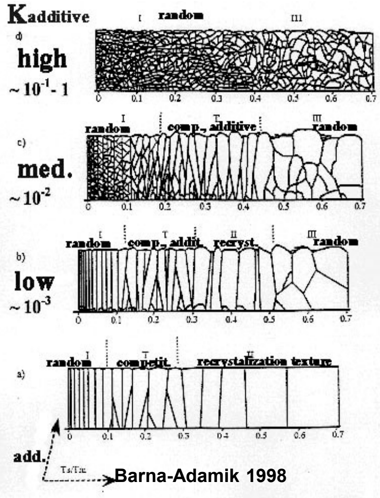

Barna-Adamik 1998

Reactive Deposition

the Al-O system

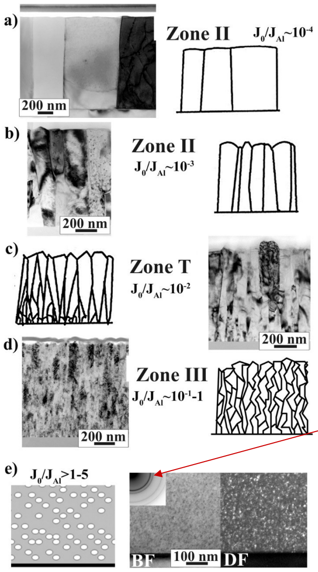

O has low solubility in Al:

- segregates to surfaces and grain boundaries
- forms oxide layers or "tissue phases"
- interrupts the local epitaxial growth
- causes renucleation

⇨ control of grain size.

Equiaxed nanograins with random orientation

P.B.Barna, in J deSegovia (ed) Proc.9th IVC Madrid 1983
P.B.Barna, M.Adamik, Thin Solid Films 317 (1998) 27
J.F.Pocza et al, Jpn J. Appl. Phys. 2 (1974) 525
P.B.Barna et al, Phys. Stat Sol (a) 146 (1994) 31
A.Csanady et al, Surf. Interface Anal., 21 (1994) 546
P.B. Barna et al, Surf. Coat. Technol. 100-1001 (1998) 72.

Superhard and supertough nanocomposites

thermal segregation and renucleation

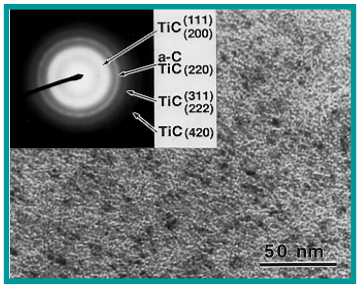

TiC/DLC and YSZ/Au nanocomposites
Voevodin, Zabinski

TiN/SiN_x, W_2N/Si_3N_4, VN/Si3N4, Vepřek et al.
TiC/SiC/aCH, J. Patscheider
ZrN/Cu, AlN/Cu, CrN/Ni, Musil et al.
TiN/TiB_2, TiC/TiB_2, Mitterrer, Mayrhofer et al.
and others

Non-columnar equiaxed structures (e.g., for high-temperature oxidation resistance)

Requires periodic disruption of the columnar structure & renucleation:
- **energetic ion irradiation ⇨ OK, but high stress and defect densities**
- **segregation of incommensurate phase**

Model systems: TiN + YN or CeN

a_{TiN} = 4.24 Å, a_{YN} = 4.89 Å, a_{CeN} = 5.02 Å

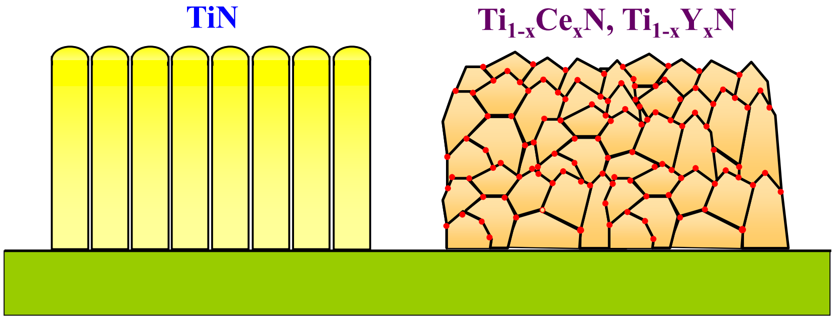

Nanostructured $TiB_{0.8}N_{0.8}$

Non-reactively magnetron sputtering at 300°C; E_i = 25 eV; J_{Ar+}/J_{Ti} ~ 2

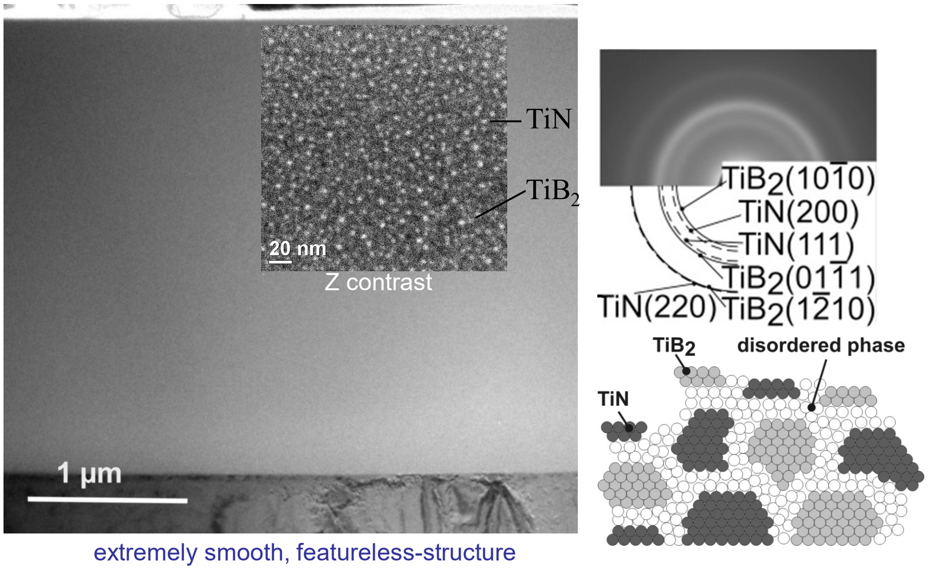

extremely smooth, featureless-structure

P. H. Mayrhofer, C. Mitterer, J. G. Wen, I. Petrov, and J. E. Greene, J. Appl. Phys., 100, 044301 (2006)

Nanostructured $TiB_{0.8}N_{0.8}$

Non-reactively magnetron sputtering at 300°C; E_i = 25 eV; J_{Ar+}/J_{Ti} ~ 2

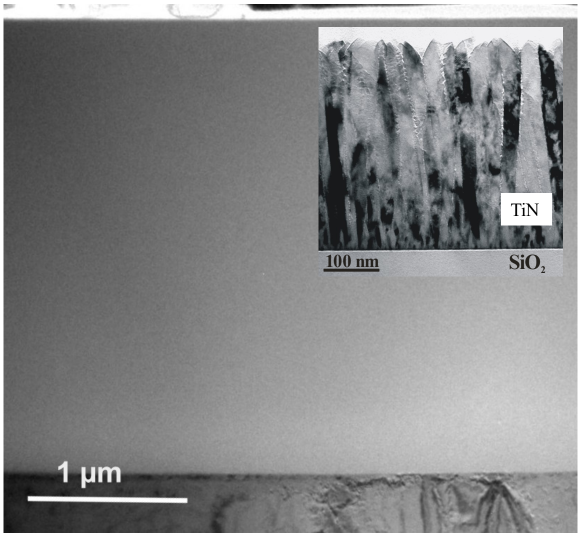

extremely smooth, featureless-structure

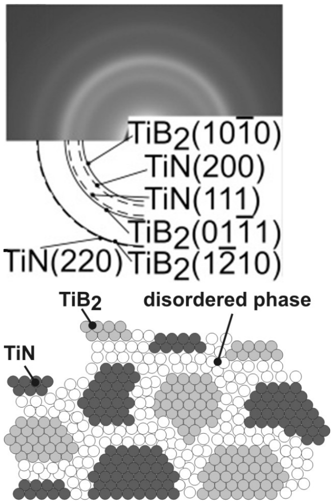

P. H. Mayrhofer, C. Mitterer, J. G. Wen, I. Petrov, and J. E. Greene, J. Appl. Phys., 100, 044301 (2006)

Microstructure of $Ti_{1-x}Ce_xN$

TiN **$Ti_{0.9}Ce_{0.1}N$** **$Ti_{0.8}Ce_{0.2}N$**

$J_i/J_{Me} \approx 5$
T_S= 350 °C

E_i=14 eV

E_i=45 eV

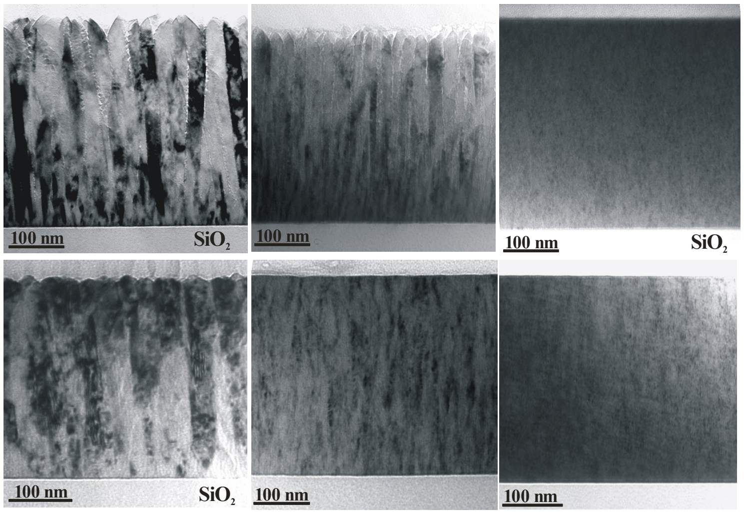

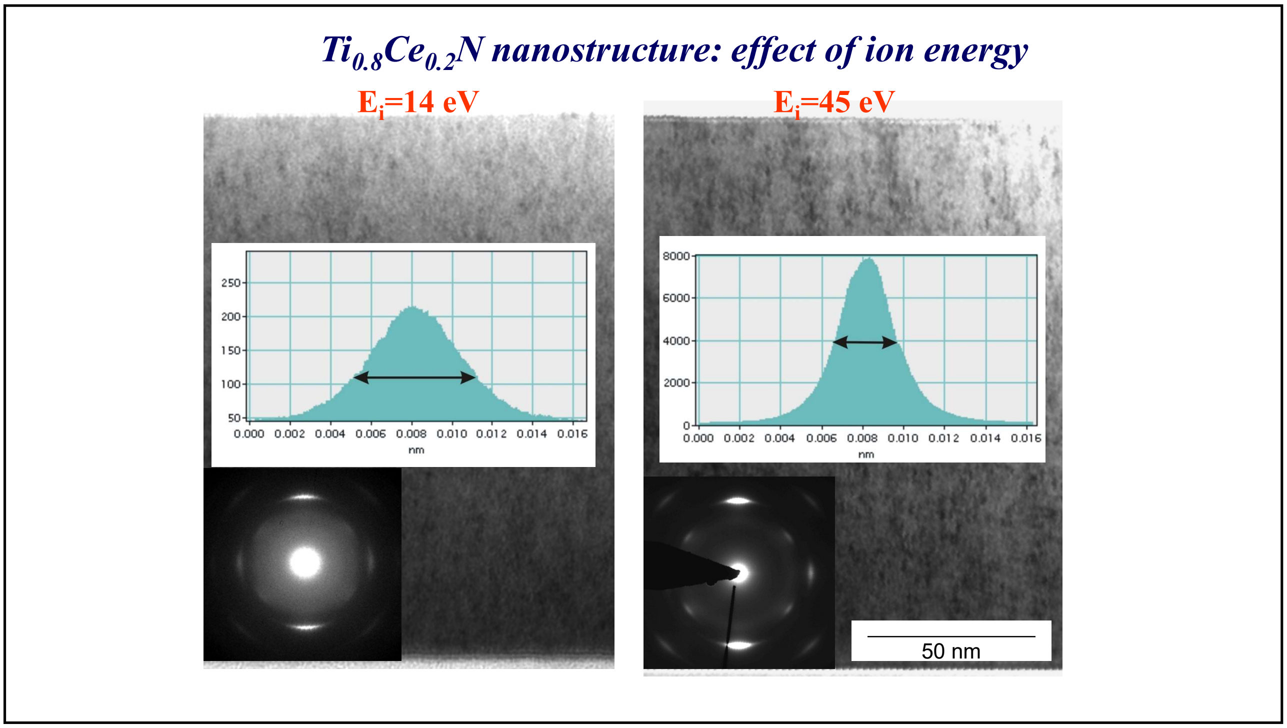

$Ti_{0.8}Ce_{0.2}N$ nanostructure: effect of ion energy

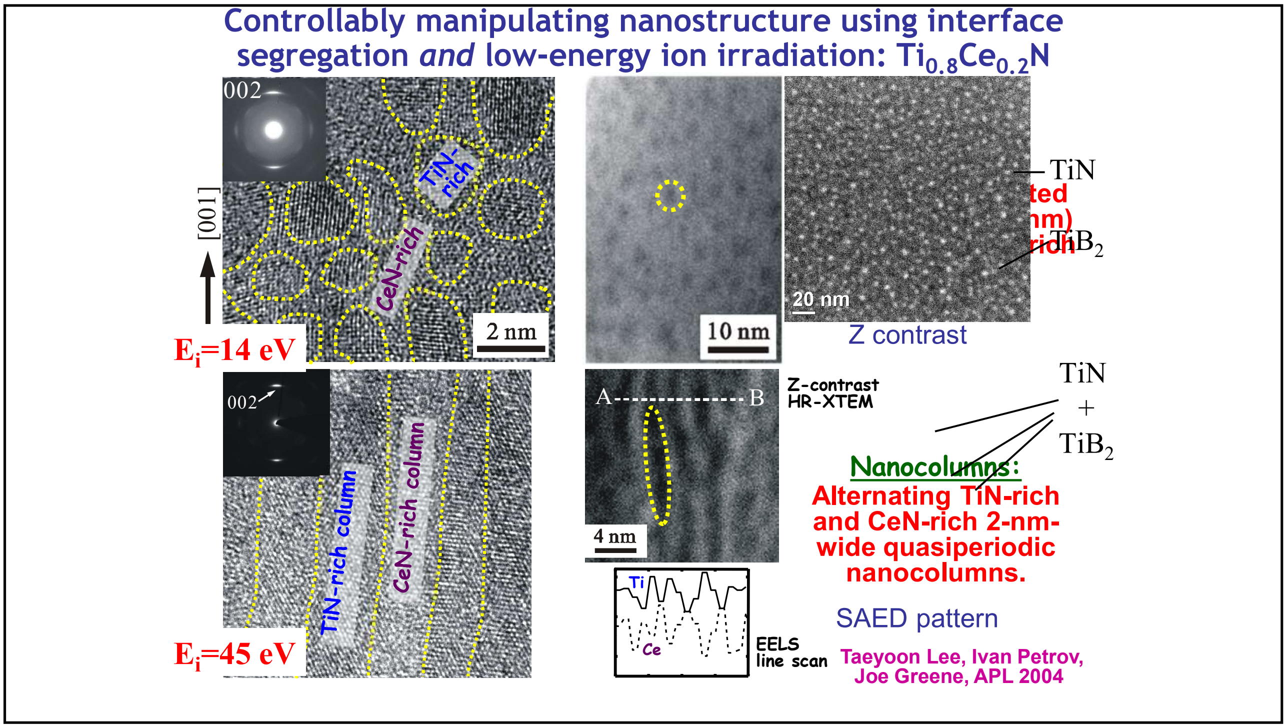

Controllably manipulating nanostructure using interface segregation *and* low-energy ion irradiation: $Ti_{0.8}Ce_{0.2}N$

Z contrast

Nanocolumns:
Alternating TiN-rich and CeN-rich 2-nm-wide quasiperiodic nanocolumns.

SAED pattern

Taeyoon Lee, Ivan Petrov, Joe Greene, APL 2004

DCMS vs HIPIMS

$E_i = e(V_{plasma} - V_{bias})$

Thermal ions (gas)

$E_i = e(V_{plasma} - V_{bias}) + \langle E_{gas\ phase} \rangle$

1. Energetic metal ions
2. Gas and metal ions separated in time

CrN reactive sputter deposition

N_2/Ar=1/1.25; p_{tot} = 2 mTorr

Ehiasarian, Hovsepian, Petrov (unpublished, 2007)

Effects of ion energy

$E_i > 100$ eV, $J_i/J_{Me} = 0.5$

TiN/SiO_2
T_s= 350 °C

XTEM

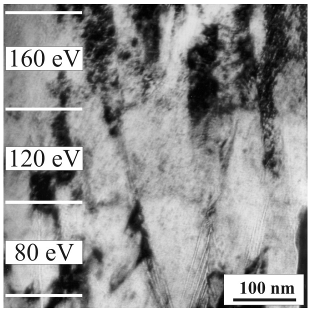

U_{bias}= 0 V

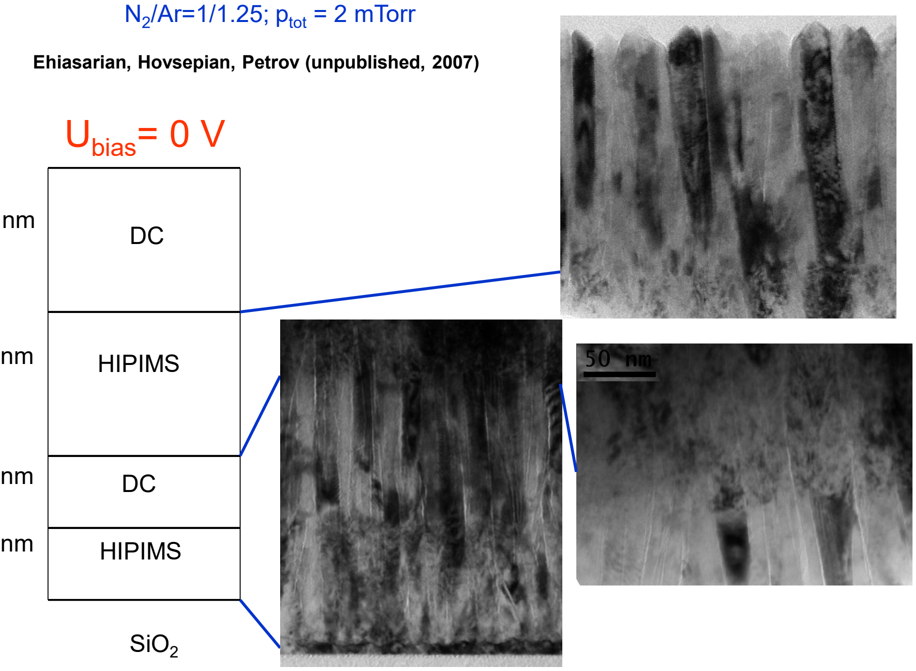

Surface & Coatings Technology 205 (2010) 591–596

Contents lists available at ScienceDirect

Surface & Coatings Technology

journal homepage: www.elsevier.com/locate/surfcoat

On the film density using high power impulse magnetron sputtering

Mattias Samuelsson [a,b,*], Daniel Lundin [a], Jens Jensen [c], Michael A. Raadu [d],
Jon Tomas Gudmundsson [e,f], Ulf Helmersson [a]

Grounded substrates

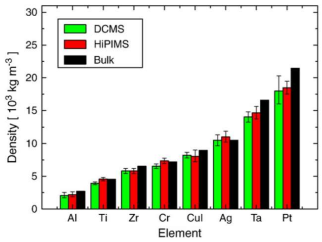

Fig. 3. Thin film density plot for different target materials. The values are calculated for films grown by DCMS and HiPIMS using RBS, SEM and profilometry. The results are compared to the bulk density given in literature.

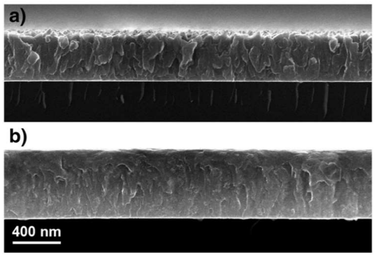

Fig. 4. Cross-sectional SEM image of a Ti sample grown by a) DCMS and b) HiPIMS. The DCMS deposited sample exhibits a porous microstructure and rough surface, whereas the HiPIMS deposited sample exhibits a less pronounced columnar microstructure and a smooth surface. The scale bar applies to both images.

HIPIMS films are denser due to energetic ions

Hybrid HiPIMS/DCMS

V_T ~ 0.3-0.5 kV
P_T ~ 10-50 W/cm^2
p ~ 2-20 mTorr

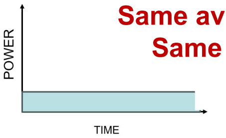

Same average power
Same hardware

peak values
V_T ~ 0.7-2 kV
P_T ~ 500-3000 W/cm^2
p ~ 2-20 mTorr

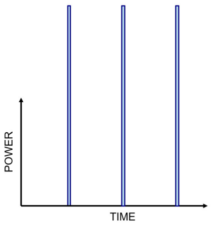

Frequency ~ 100-500 Hz
Duty cycle < 1-4 %

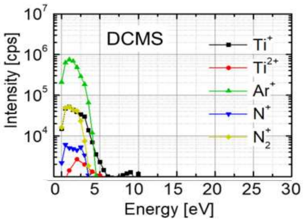

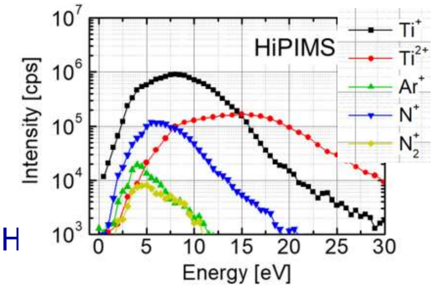

DCMS vs H

1. Thermal gas ions
2. Neutral deposited atoms
3. **High deposition rate**

1. **Energetic metal ions**
2. **Gas and metal ions separated in time**
3. Lower deposition rates

Prof. Greg Greczynski

Hybrid HIPIMS/DCMS co-sputtering: Metal ions and high deposition rate

1. highly supersaturation metastable B1-NaCl TMN coatings using light ion (Al^+, Si^+) irradiation

Model system: Metastable $Ti_{(1-x)}Al_xN$

- AlN, TiN ~ immiscible; 2% solubility at 1000 °C
- Cubic $Ti_{(1-x)}Al_xN$ x<0.67 by PVD at 500 °C
- Cubic $Ti_{(1-x)}Al_xN$: oxidation resistant and wear resistant

cubic $Ti_{(1-x)}Al_xN$

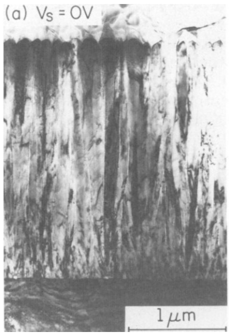

Håkansson, G., Sundgren, J.-E., McIntyre, D., Greene, J.E., Münz, W.-D. TSF 153 (1987) 55

cubic $Ti_{(1-x)}Al_xN$ + wurtzite AlN

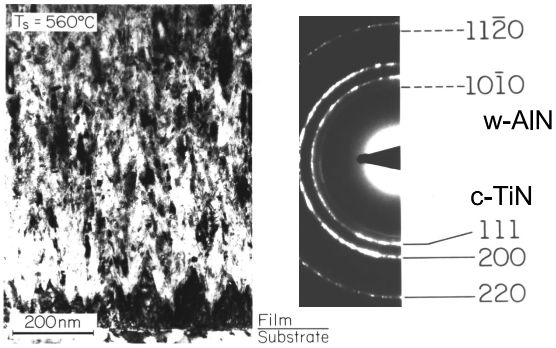

F. Adibi, I. Petrov, L. Hultman, U. Wahlström, T. Shimazu, D. McIntyre, J. E. Greene, J.-E. Sundgren, J. Appl. Phys., 69 6437 (1991).

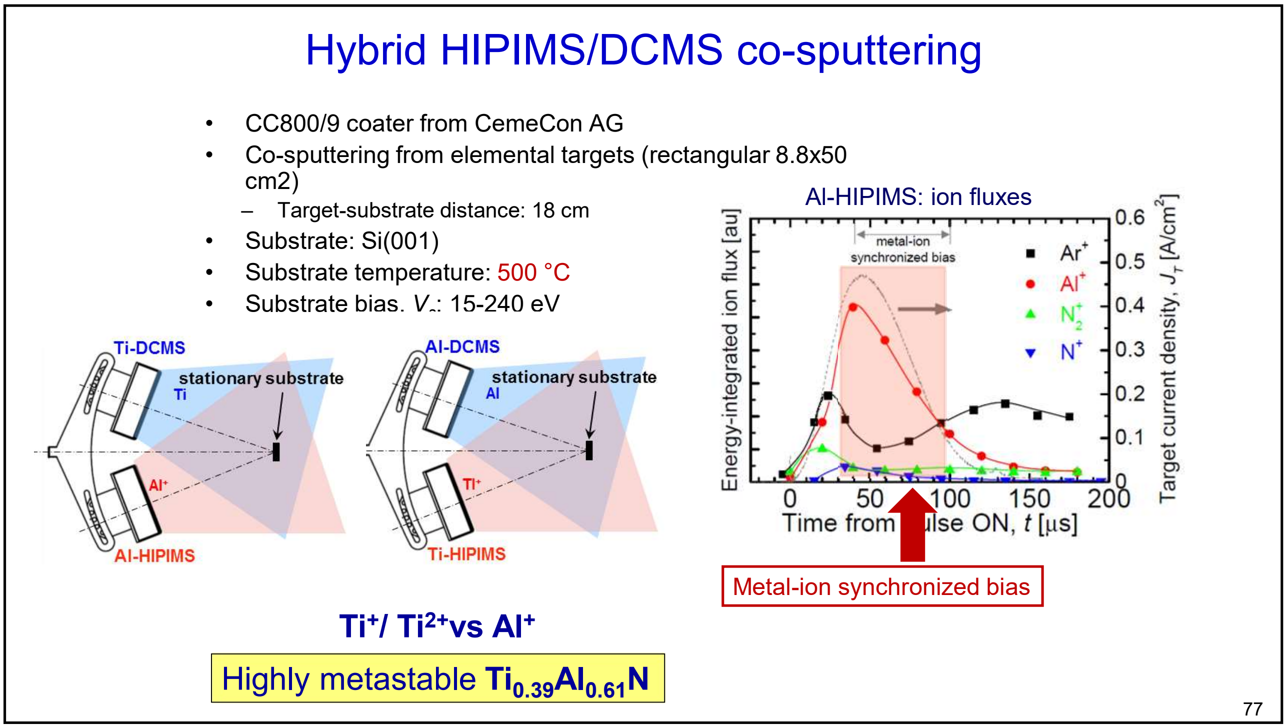

Hybrid HIPIMS/DCMS co-sputtering

- CC800/9 coater from CemeCon AG
- Co-sputtering from elemental targets (rectangular 8.8x50 cm2)
  - Target-substrate distance: 18 cm
- Substrate: Si(001)
- Substrate temperature: 500 °C
- Substrate bias, V: 15-240 eV

Metal-ion synchronized bias

Ti^+/ Ti^{2+}vs Al^+

Highly metastable $\mathbf{Ti_{0.39}Al_{0.61}N}$

77

77

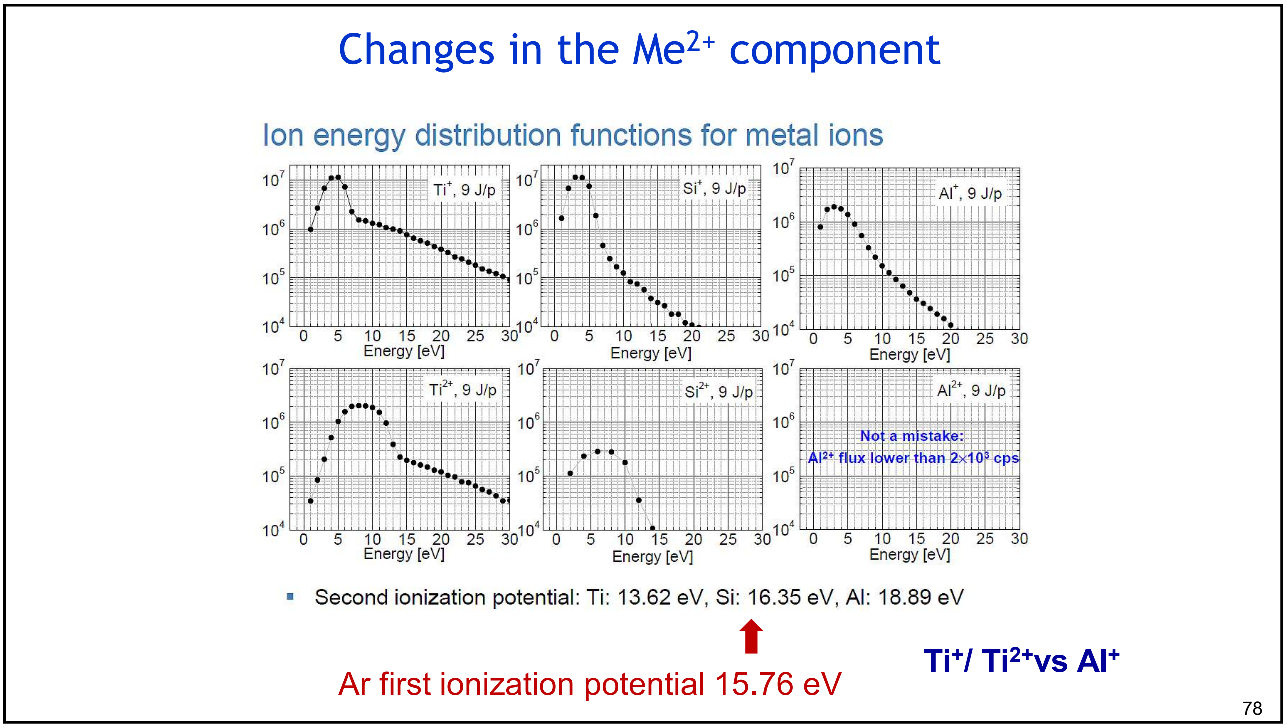

Changes in the Me^{2+} component

Ion energy distribution functions for metal ions

Not a mistake:
Al^{2+} flux lower than 2×10³ cps

- Second ionization potential: Ti: 13.62 eV, Si: 16.35 eV, Al: 18.89 eV

Ar first ionization potential 15.76 eV

Ti^+/ Ti^{2+}vs Al^+

78

78

$Ti_{0.39}Al_{0.61}N$

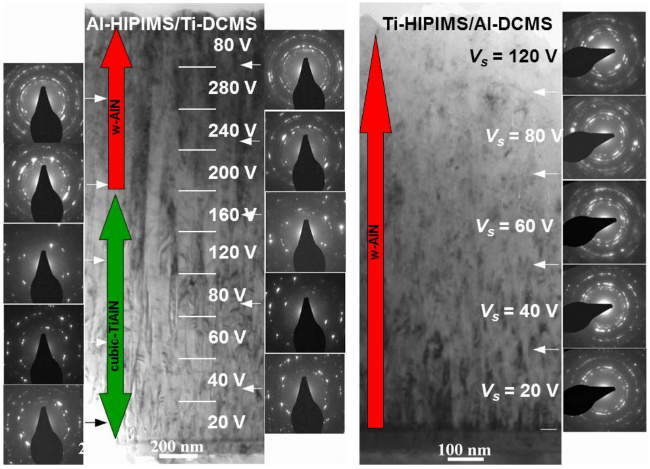

T_S = 500 °C

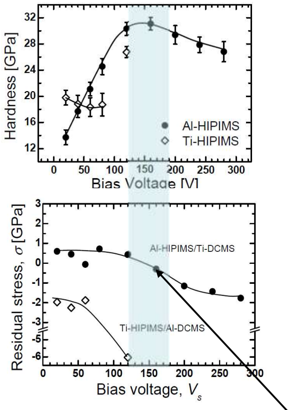

hard stress-free films

Al^+ vs Ti^+/ Ti^{2+}

G. Greczynski, J. Lu, J. Jensen, I. Petrov, J.E. Greene, S. Bolz, W. Kölker, Ch. Schiffers, O. Lemmer, and L. Hultman,
Thin Solid Films 556 (2014) 87–98

$Ti_{1-x}Si_xN$

Ti-HiPIMS/Si-DCMS

$Ti_{0.74}Si_{0.26}N$

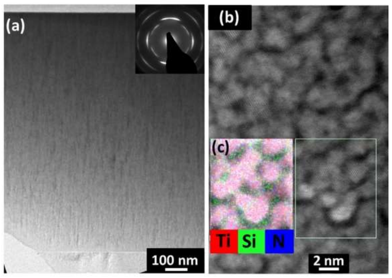

T_S = 500 °C

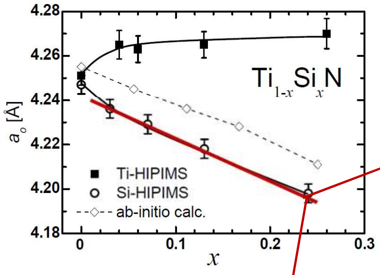

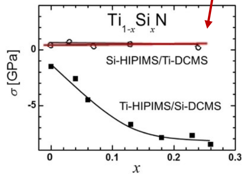

Si-HiPIMS/Ti-DCMS

$Ti_{0.76}Si_{0.24}N$

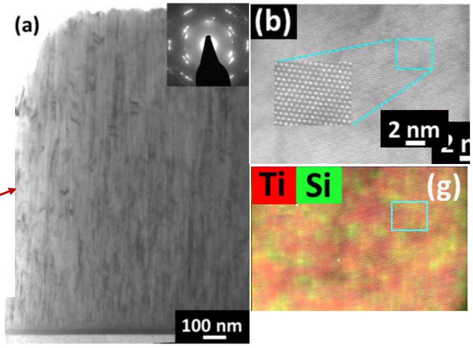

Single-phase, metastable alloys with B1-NaCl structure, stress free

G. Greczynski, J. Patscheider, J. Lu, B. Alling, A. Ektarawong, J. Jensen, I. Petrov, J.E. Greene, L. Hultman,
Surface & Coatings Technology 280 (2015) 174–184

JOURNAL OF APPLIED PHYSICS **121**, 171907 (2017)

Unprecedented Al supersaturation in single-phase rock salt structure VAlN films by Al$^+$ subplantation

G. Greczynski,[1,2,a)] S. Mráz,[2] M. Hans,[2] D. Primetzhofer,[3] J. Lu,[1] L. Hultman,[1]
and J. M. Schneider[2]

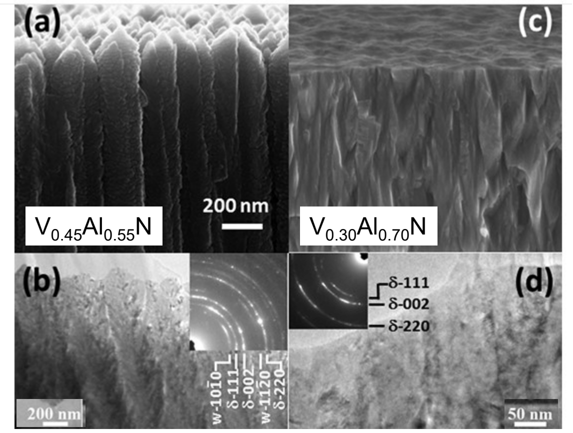

$V_{1-x}Al_xN$

T_S = 500 °C

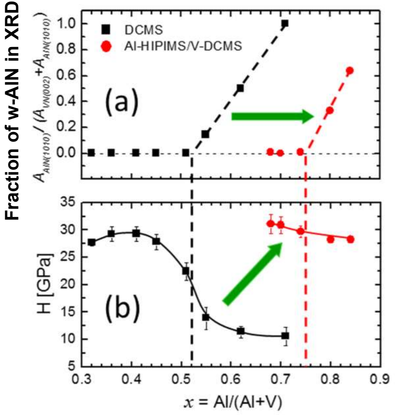

(a) continuous-bias DCMS growth of $V_{1-x}Al_xN$

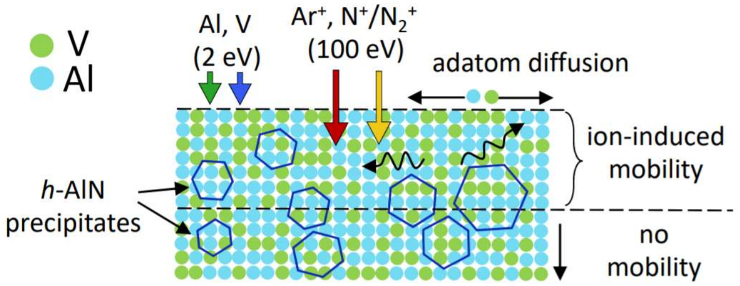

Similar picture applies for Ti-HiPIMS/Al-DCMS deposition under Ti$^+$/Ti^{2+} irradiation

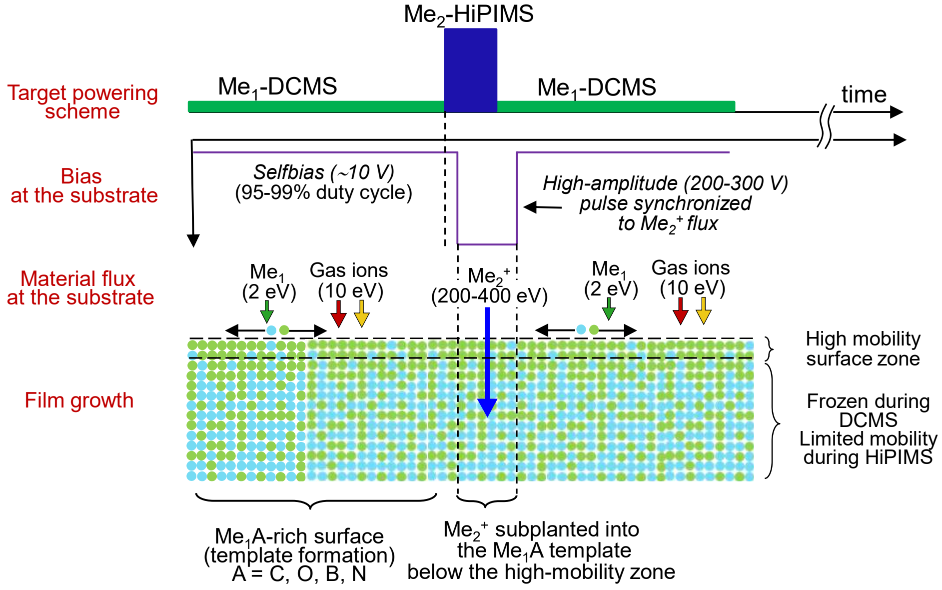

Me$_2$-HiPIMS

Target powering scheme

Me$_1$-DCMS

Me$_1$-DCMS

time

Bias at the substrate

Selfbias (~10 V)
(95-99% duty cycle)

High-amplitude (200-300 V) pulse synchronized to Me$_2^+$ flux

Material flux at the substrate

Me$_1$ (2 eV)

Gas ions (10 eV)

Me$_2^+$ (200-400 eV)

Me$_1$ (2 eV)

Gas ions (10 eV)

High mobility surface zone

Film growth

Frozen during DCMS
Limited mobility during HiPIMS

Me$_1$A-rich surface
(template formation)
A = C, O, B, N

Me$_2^+$ subplanted into
the Me$_1$A template
below the high-mobility zone

G. Greczynski, S. Mráz, J. M. Schneider; L. Hultman, J. Appl. Phys. 127, 180901 (2020)

Summary – drastically different pathways to achieve highly supersaturation metastable B1-NaCl TMN coatings using light ion (Al$^+$, Si$^+$) irradiation

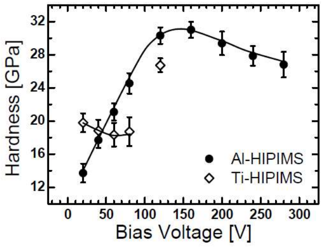

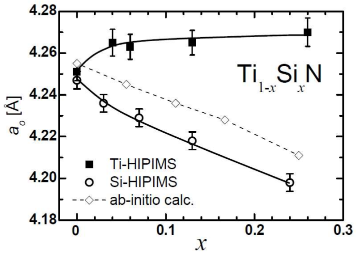

T$_S$ = 500 °C

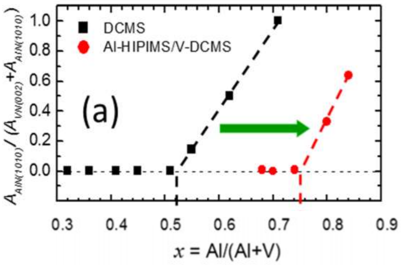

Hybrid HIPIMS/DCMS co-sputtering: Metal ions and high deposition rate

2. **Low-temperature growth** of dense, hard, and low-stress refractory ceramic thin films via heavy metal (Ta, W) ion irradiation

$T_s < 150$ °C

Heavy Metal Ions

- Large number of low energy recoils
- Nearly straight path
- Incorporated into the matrix – low stresses

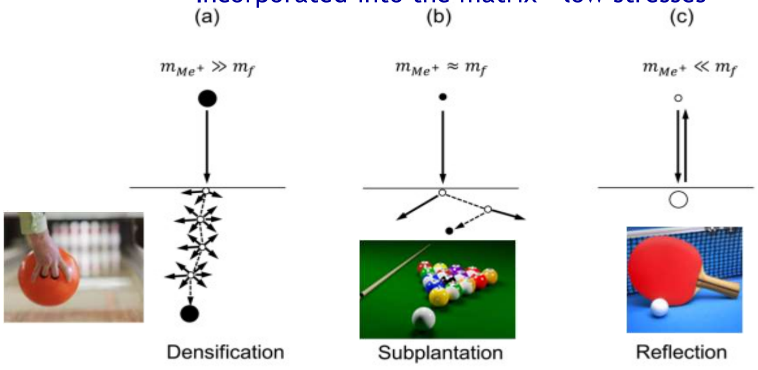

Densification by large number of low energy recoils at $T_S < 150$ °C to substitute the thermally-driven adatom mobility at $T_S > 450$ °C

Novel strategy for low-temperature, high-rate growth of dense, hard, and stress-free refractory ceramic thin films

JVST A 32 (2014) 041515

Grzegorz Greczynski, Jun Lu, Stephan Bolz, Werner Kölker, Christoph Schiffers, Oliver Lemmer, Ivan Petrov, Joseph E. Greene, and Lars Hultman

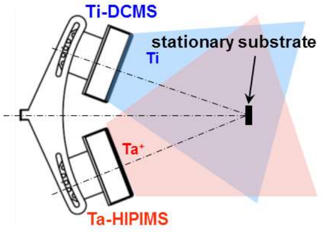

or
Ti-HIPIMS

Ti^+ vs Ta^+

$Ti_{0.92}Ta_{0.08}N$

No external heating

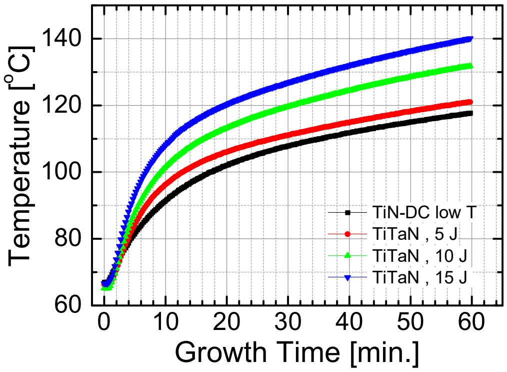

T_s < 120 °C

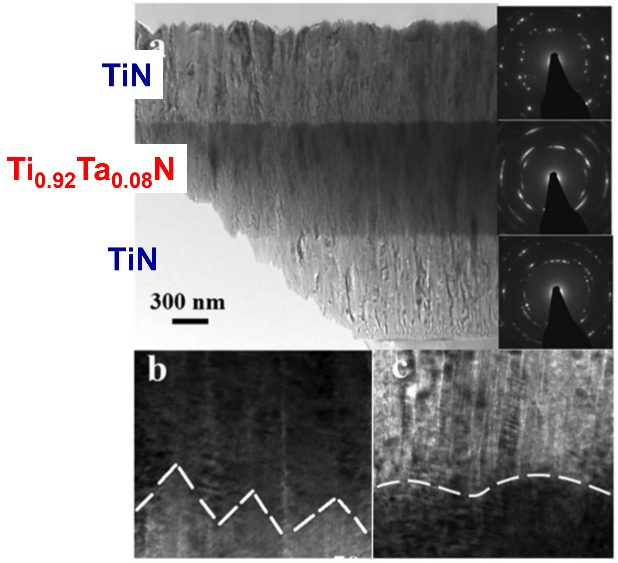

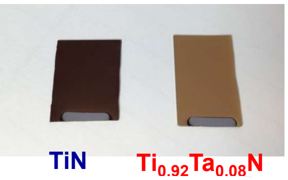

TiN **$Ti_{0.92}Ta_{0.08}N$**

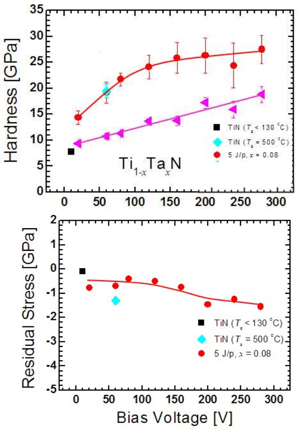

G. Greczynski, J. Lu, J. Jensen, I. Petrov,J.E. Greene,S. Bolz, W. Kölker, Ch. Schiffers, O. Lemmer, and L. Hultman, JVST A 32 (2014) 041515

TRIM for 160 eV ion bombardment

Ta^+

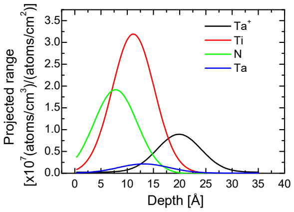

Ti^+

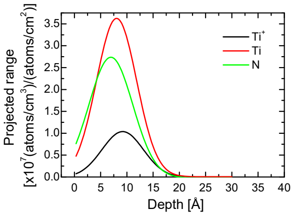

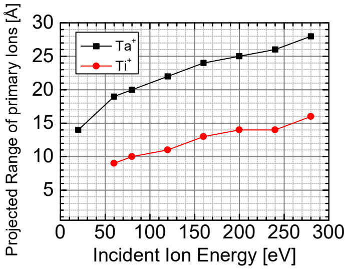

Ta^+ goes beyond the intense cascade region and gets incorporated in the films: additional densification

JOURNAL OF APPLIED PHYSICS **121**, 171902 (2017)

Low-temperature growth of dense and hard $Ti_{0.41}Al_{0.51}Ta_{0.08}N$ films via hybrid HIPIMS/DC magnetron co-sputtering with synchronized metal-ion irradiation

H. Fager,[1] O. Tengstrand,[1,a)] J. Lu,[1] S. Bolz,[2] B. Mesic,[2] W. Kölker,[2] Ch. Schiffers,[2]
O. Lemmer,[2] J. E. Greene,[1,3] L. Hultman,[1] I. Petrov,[1,3] and G. Greczynski[1]

T_s < 150 °C

H = 15 GPa

H = 28 GPa

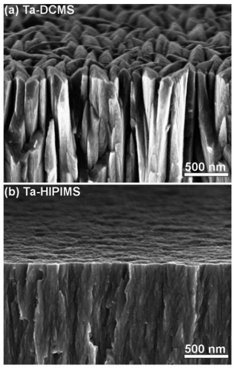

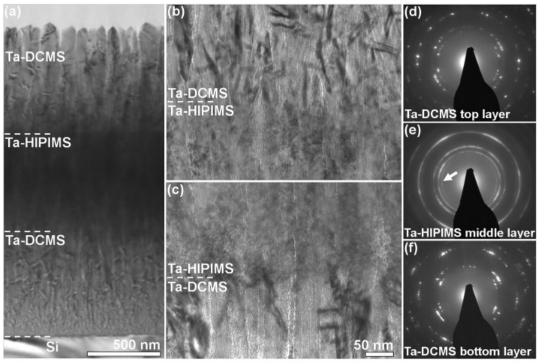

The crucial role of metal ion mass

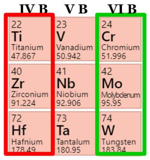

(Cr, Mo, or W)-HiPIMS/$Ti_{0.5}Al_{0.5}$-DCMS
Metal ion synchronized bias of 120 V

Hybrid HiPIMS/DCMS setup

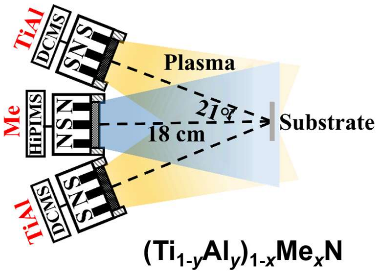

$(Ti_{1-y}Al_{y})_{1-x}Me_{x}N$

XPS measured O content
C_O – 3.8 at%
H = 8 GPa
σ = 0 GPa

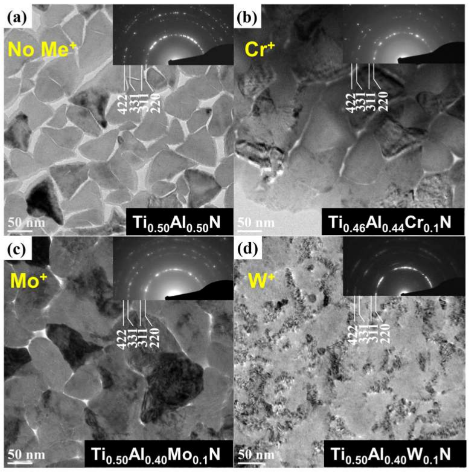

C_O = 2.7 at%
H = 14 GPa
σ = 0 GPa

C_O = 2.3 at%
H = 22.5 GPa
σ = 0 GPa

C_O = 0.4 at%
H = 32 GPa
σ = 1 GPa

X. Li, B. Bakhit, M.P. Johansson Joesaar, L. Hultman, I. Petrov, G. Greczynski, Surf. Coat. Techn. 415 (2021)127120

The crucial role of metal ion mass

Monte Carlo TRIM simulations of collision cascades upon irradiation of $Ti0_{.50}Al_{0.50}N$ surfaces with 120 eV metal ions.

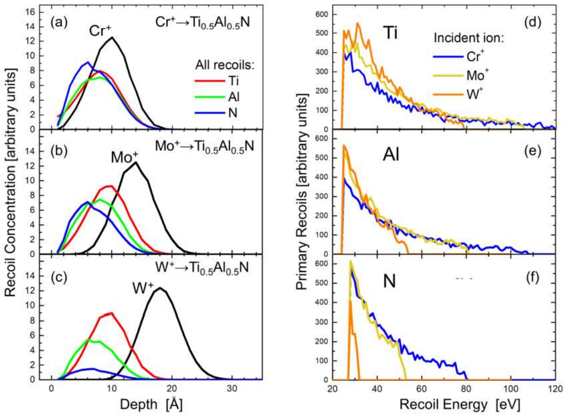

FIG. 12. Monte Carlo TRIM simulations of collision cascades upon irradiation of $Ti_{0.50}Al_{0.50}N$ surfaces with 120 eV metal ions. Me^+ ion and primary recoil (Ti, Al, and N) distribution functions are shown for Me = (a) Cr, (b) Mo, and (c) W. Corresponding Ti, Al, and N primary recoil energy distributions are shown in panels (d)–(f). [From Li *et al.*, Surf. Coat. Technol. **415**, 127120 (2021). Copyright 2021 Author(s), licensed under a Creative Commons Attribution (CC BY) license.]

W irradiation:
- Large number of low energy recoils
- N sublattice almost intact
- Larger penetration depth – additional densification

X. Li, B. Bakhit, M.P. Johansson Joesaar, L. Hultman, I. Petrov, G. Greczynski, Surf. Coat. Techn. 415 (2021)127120

Effects of Heavy Metal Ion Dose, Energy, Momentum
$(Ti_{1-y}Al_y)_{1-x}W_xN$

W fraction, $x = W/(W+Ti+Al)$
Ionized fraction W, α
Ion dose ~ αx
Ion energy ~ xV
Ion momentum ~$xV^{0.5}$

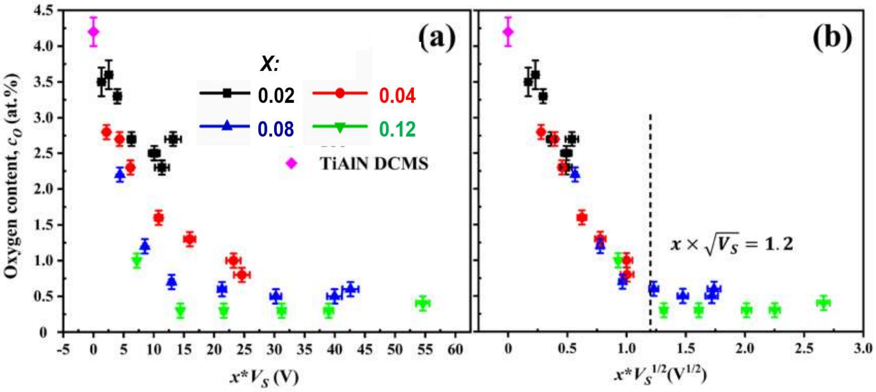

Figure 1. The ToF-ERDA-derived oxygen concentrations c_o for $(Ti_{1-y}Al_y)_{1-x}W_xN$ films grown with the HiPIMS pulse length τ_{ON} = 20 (x = 0.02), 30 (x = 0.04), 50 (x = 0.07), and 100 μs (x = 0.12) as a function of (**a**) $x \times V_s$ and (**b**) $x \times \sqrt{V_s}$.

Xiao Li, B. Bakhit, M.P. Johansson Joesaar, I. Petrov, L. Hultman, G. Greczynski, Scientific Reports 12 (2022) 2166

Thermal stability of the TiAlWN coatings deposited at T_S < 150 °C

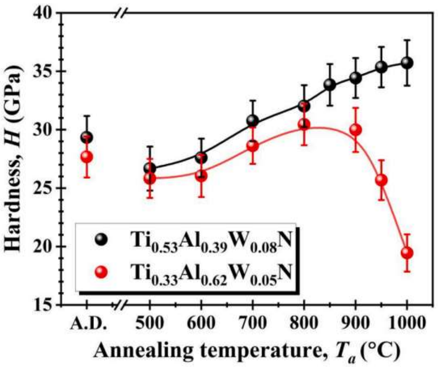

$Ti_{0.33}Al_{0.62}W_{0.05}N$

- 600-800 °C, $H\uparrow$ by spinodal decomposition of coherent **c-AlN**
- T_a > 800 ° C, $H\downarrow$ by **h-AlN** incoherent precipitation

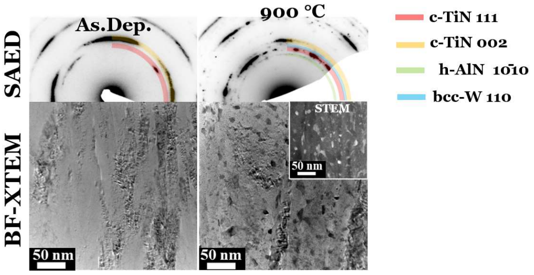

$T_a \geq$ 900 ° C: also bcc-W precipitation!

O. V. Pshyk, X. Li, I.Petrov, D.G. Sangiovanni, J. Palisaitis, L. Hultman, G. Greczynski, Acta Mater. 255 (2023) 119105

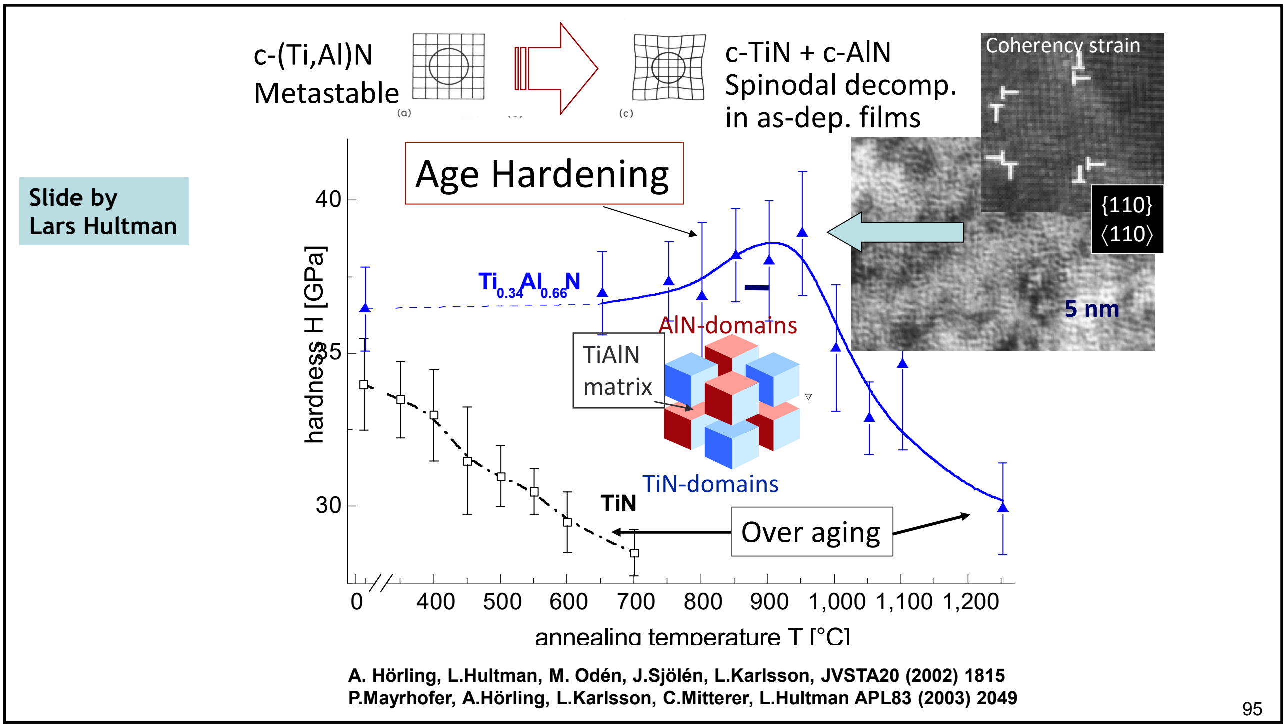

Slide by Lars Hultman

A. Hörling, L.Hultman, M. Odén, J.Sjölén, L.Karlsson, JVSTA20 (2002) 1815
P.Mayrhofer, A.Hörling, L.Karlsson, C.Mitterer, L.Hultman APL83 (2003) 2049

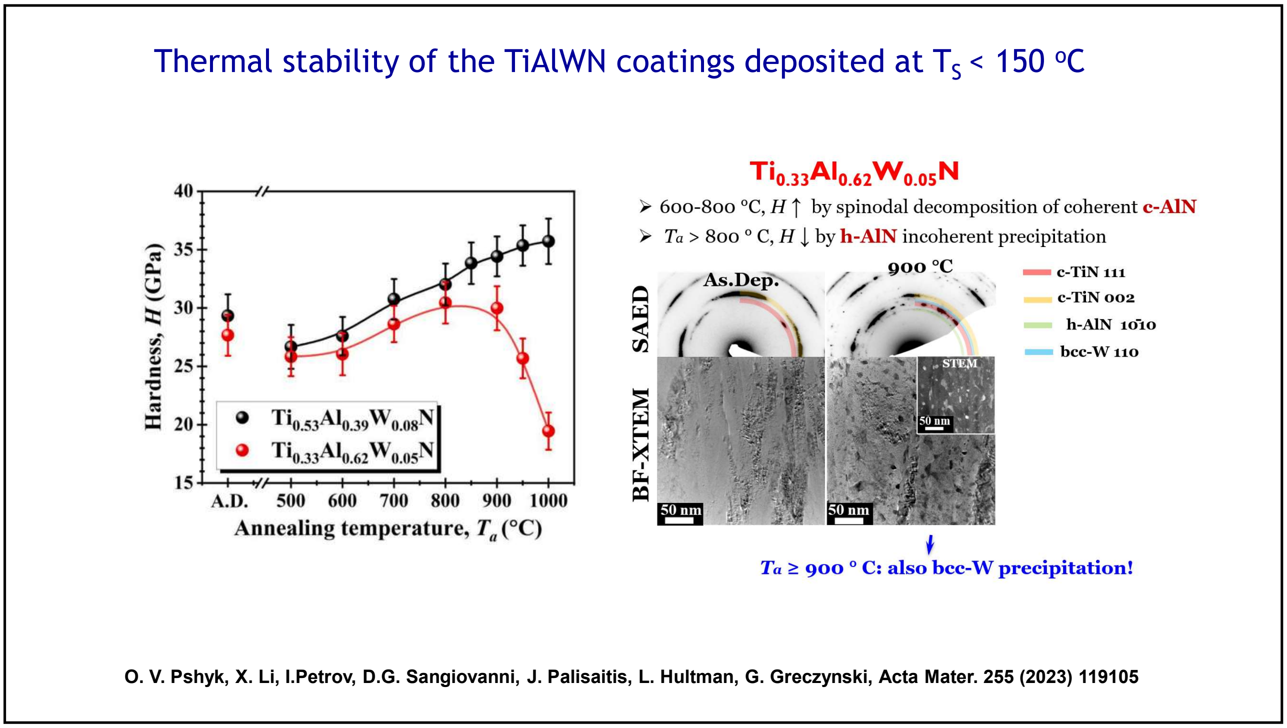

Thermal stability of the TiAlWN coatings deposited at T_S < 150 °C

$Ti_{0.33}Al_{0.62}W_{0.05}N$

- 600-800 °C, H ↑ by spinodal decomposition of coherent **c-AlN**
- T_a > 800 ° C, H ↓ by **h-AlN** incoherent precipitation

T_a ≥ 900 ° C: also bcc-W precipitation!

O. V. Pshyk, X. Li, I.Petrov, D.G. Sangiovanni, J. Palisaitis, L. Hultman, G. Greczynski, Acta Mater. 255 (2023) 119105

Discovery of Guinier-Preston zone hardening in refractory nitride ceramics

O.V. Pshyk[a,1,*], X. Li[a], I. Petrov[a,b], D.G. Sangiovanni[a], J. Palisaitis[a], L. Hultman[a], G. Greczynski[a]

Acta Materialia 255 (2023) 119105

In analogy to the age hardening mechanism in Al(Cu) alloys, e.g.

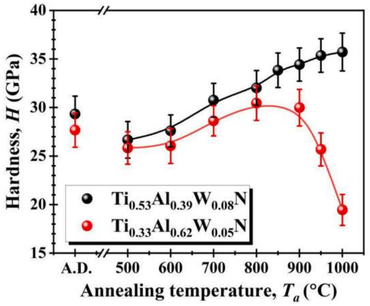

900 °C - $Ti_{0.53}Al_{0.39}W_{0.08}N$

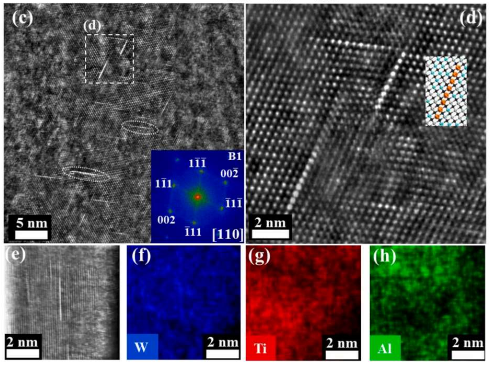

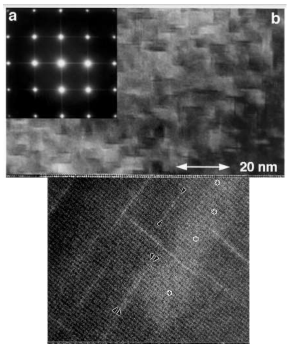

Konno TJ et al J.Electr.Microsc. 50(2001)105

Key is the preservations of the cubic lattice

Atom-thick W discs on {111}

Atom-thick Cu discs on {001}

Epitaxial $V_{0.6}W_{0.4}N$/MgO(001): Evidence for ordering on the cation sublattice

H. Kindlund,[a)] J. Lu, and J. Jenser I. Petrov and J. E. Greene L. Hultman

J. Vac. Sci. Technol. A 31(4), Jul/Aug 2013

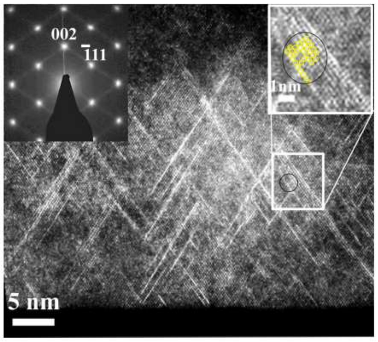

Other possibilities:
Combinations of B1-NaCl TMN, e.g. TiN, ZrN, HfN, VN with Ta, Mo, W
How about in TMB_2?

Effects of metal-ion irradiation in hybrid HiPIMS/DCMS:

light ions (Al^+, Si^+)
subplantation
supersaturated cubic films
Examples:
Ti**Al**N
V**Al**N
Zr**Al**N
Ti**Si**N
$Ti_{0.68}\mathbf{Al}_{0.32}B_{1.35}$

heavy ions (Ta^+, W^+, Hf^+)
low-energy recoil creation
effective densification at **T_S<150°C**
Examples:
$Ti_{0.92}\mathbf{Ta}_{0.08}N$
$Ti_{0.41}Al_{0.51}\mathbf{Ta}_{0.08}N$
$Ti_{0.50}Al_{0.40}\mathbf{W}_{0.10}N$
$Ti_{0.67}\mathbf{Hf}_{0.33}B_{1.7}$
$Zr_{0.7}\mathbf{Ta}_{0.3}B_{1.5}$

G. Greczynski, L. Hultman, I. Petrov, *J. Appl. Phys. 134* (2023) 140901
40+ references therein

$Hf_{1-x}Al_xN$ / MgO(001)

Brandon Howe

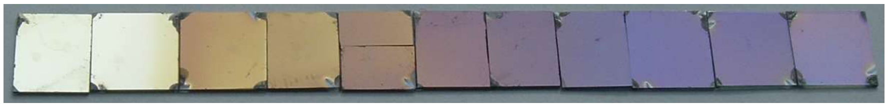

x* = 0** ***$Hf_{1-x}Al_xN$/MgO(001) increasing x → ***x* = 0.54**

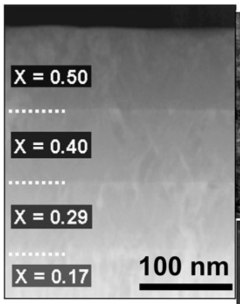

Z-Contrast

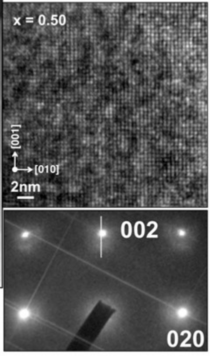

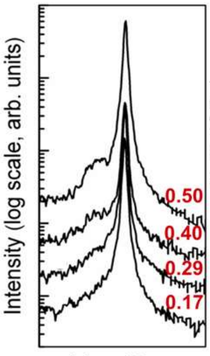

Line Scan

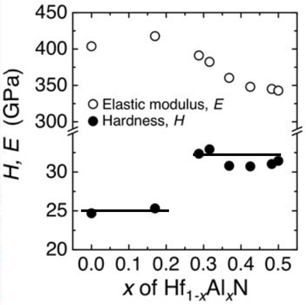

Howe, B., Sardela, M., Wen, J.-G., Voevodin, A., Greene, J., Hultman, L., and Petrov, I., "Growth and Physical Properties of Epitaxial $Hf_{1-x}Al_xN$ Alloys Grown on MgO(001)", Surface & Coatings Technology, 202, 809–814 (2007).

Manipulating [AlN] in $Hf_{1-x}Al_xN$ using E_i

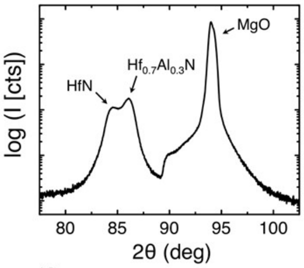

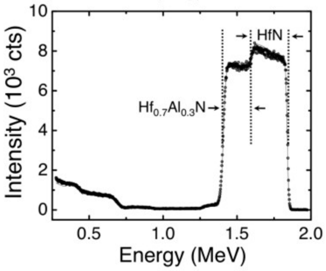

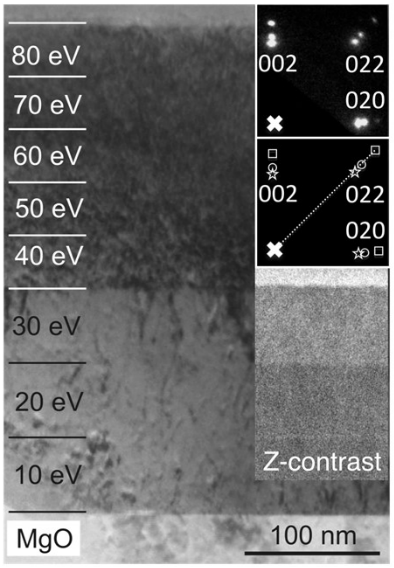

Manipulating [AlN] in $Hf_{1-x}Al_xN$ using E_i

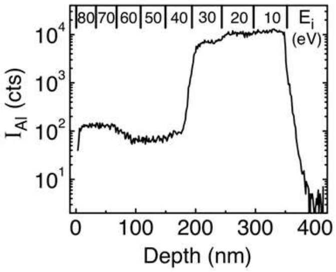

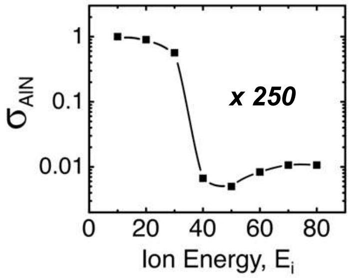

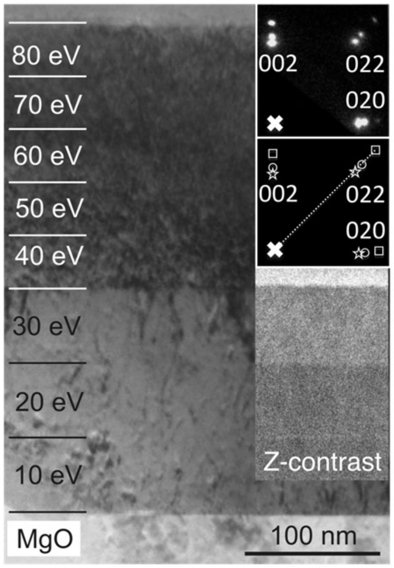

Sputter Yield Amplification

	TRIM	180° hard collision	
Collision pairs	$P_{reflection}$	$E_{transfer}$	$E_{backscatter}$
Ar → Hf	~0.25	$0.60E_i$	$0.40E_i$
Ar → Al	~0.0007	$0.97E_i$	$0.03E_i$

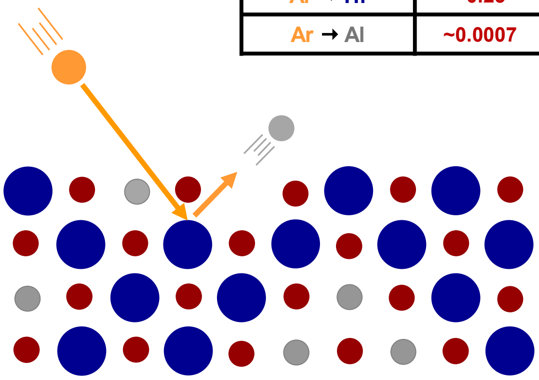

m_{Ar} = 39.9 amu

m_{Hf} = 178.5 amu

m_{Al} = 27.0 amu

$Hf_{0.7}Al_{0.3}N$

Superlattices by E_i modulation 10-40 eV

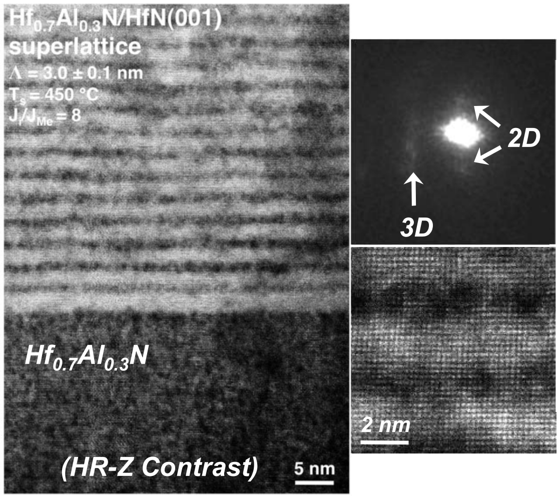

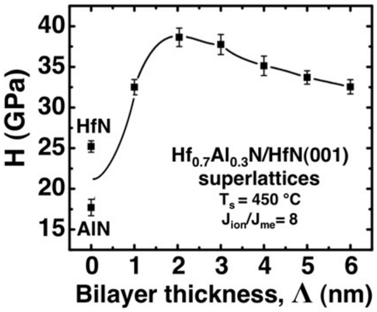

Superposition of a 3D self-organized and 2D engineered nanostructure

Transition metal diborides

Transition metal diborides with AlB_2 structure

M=Ti, V, Cr, Mg, Y, Sc, Al, Nb, Ta, Hf, Zr,…

Formidable research has been invested over the past three decades in TM nitride, carbide, oxide, and oxinitride thin films.

Borides exhibit exceptional properties, from superhardness to superconductivity and thermal and chemical stability.

MB_2 coatings are emerging as the next generation of hard, wear-, oxidation- and corrosion-resistant coatings.

Melting point:
TiN - 3,200 K, ZrN - 3,225 K
TiB_2 - 3,500 K, ZrB_2 - 3,520 K

However, they much less studied because of challenges with their synthesis.

Challenges in diboride PVD synthesis

TM nitrides - a cubic B1-NaCl structure with wide single-phase field

TM diborides have – a hexagonal AlB_2-type structure with a narrow single-phase field
phase separation upon overstoichiometry:

Sputter-deposited TMB_x contain excess boron with x ranging from 3.5 to 2.4

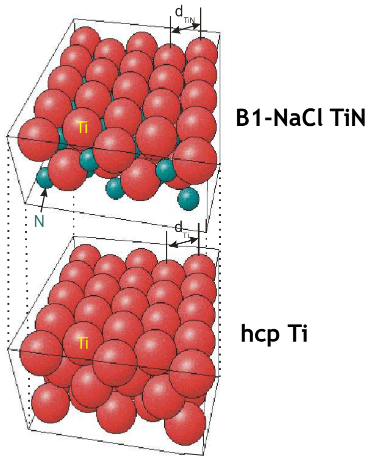

- **Metal plains essentially unchanged**
- **N occupies interstitial - ~40 % vacancies**

Challenges in diboride PVD synthesis

TM nitrides – a cubic B1-NaCl structure with wide single-phase field

TM diborides have – a hexagonal AlB_2-type structure with a narrow single-phase field
phase separation upon overstoichiometry:

Sputter-deposited TMB_x contain excess boron with x ranging from 3.5 to 2.4

Interesting nanostructures ⇨ P. Mayrhofer et at APL 86 (2005)

- Control of B/TM ratio is a challenge
- Synthesis of stoichiometric epitaxial MB_2
- Synthesis of metastable $M1_{(1-x)}M2_xB_2$
- Determine fundamental properties.

AlB -type structure

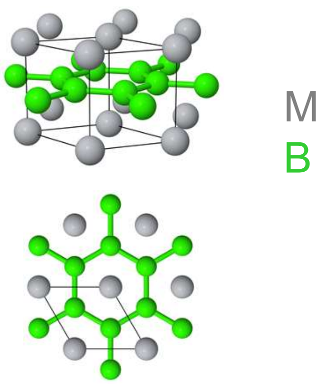

B atoms form strongly-bonded graphene-like sheets between layers of close-packed metal atoms
Metal atoms held on-top positions

JOURNAL OF APPLIED PHYSICS 104, 063304 (2008)

Experiment and simulation of the compositional evolution of Ti–B thin films deposited by sputtering of a compound target

Jörg Neidhardt,[1] Stanislav Mráz,[2,a)] Jochen M. Schneider,[2] Erik Strub,[3] Wolfgang Bohne,[3]
Bartosz Liedke,[4] Wolfhard Möller,[4] and Christian Mitterer[1]

TiB_x targets sputtered in Ar

Experiment

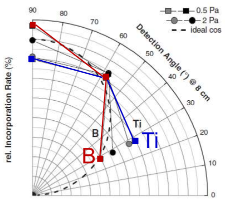

TRIM simulation

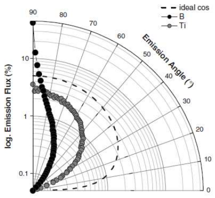

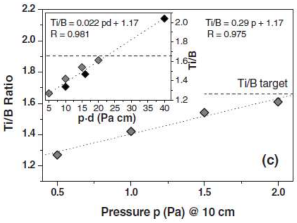

- mass mismatch between Ar (m_{Ar}=39.9 amu) and B and Ti (m_B=10.8 and m_{Ti}=47.9 amu)
- sputtered B atoms are preferentially ejected along the target normal, while the Ti angular ejection distribution extends toward lower angles
- increasing pressure → diffusive transport: B/Ti ratio closer to the target composition
- bias sputtering preferentially sputters B.

APPLIED PHYSICS LETTERS 86, 131909 (2005)

Self-organized nanocolumnar structure in superhard TiB_2 thin films

P. H. Mayrhofer[a)] and C. Mitterer
Department of Physical Metallurgy and Materials Testing, University of Leoben, A-8700 Leoben, Austria
J. G. Wen, J. E. Greene, and I. Petrov
Frederick Seitz Materials Research Laboratory and Department of Materials Science,
University of Illinois, Urbana, Illinois 61801

Overstoichiometric films $TiB_{2.4}$

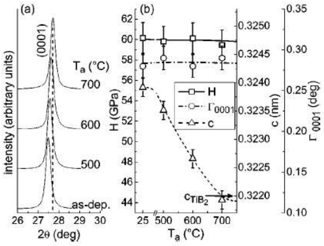

FIG. 1. (a) XRD patterns from an as-deposited $TiB_{2.4}$ film and samples which have been annealed for 1 h at temperatures T_a. (b) Hardness H, lattice constant c, and full width at half maximum Γ of the (0001) XRD reflection as a function of T_a. For comparison, the lattice constant c of TiB_2 is indicated by an arrow.

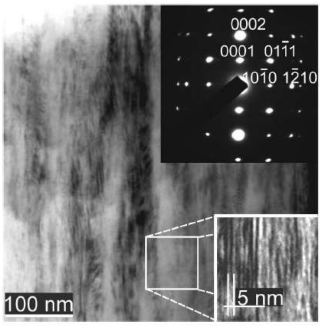

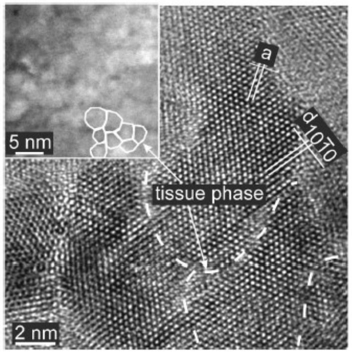

Stoichiometric and substoichiometric MB_2 – determine fundamental properties

Challenges

TM nitrides – a cubic B1-NaCl structure with wide single-phase field

TM diborides have – a hexagonal AlB_2-type structure with a narrow single-phase field
phase separation upon overstoichiometry:

Sputter-deposited TMB_x contain excess boron with x ranging from 3.5 to 2.4

- **Control of B/TM ratio is a challenge**
- **Synthesis of stoichiometric epitaxial MB_2**
- **Synthesis of metastable $M1_{(1-x)}M2_xB_2$**
- **Synthesis of diboride superlattices**
- **Determine fundamental properties.**

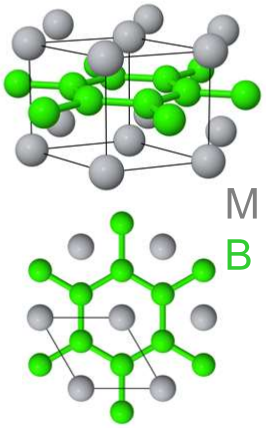

B atoms form strongly-bonded graphene-like sheets between layers of close-packed metal atoms
Metal atoms held on-top positions

Controlling the B/Ti ratio in magnetron-sputter-deposited TiB_x thin films
effects of Ar pressure and external B field

Unbalanced DCMS of TiB_2 target at 100 W; T_s = 700 °C

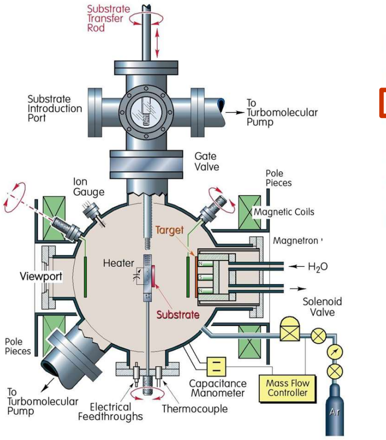

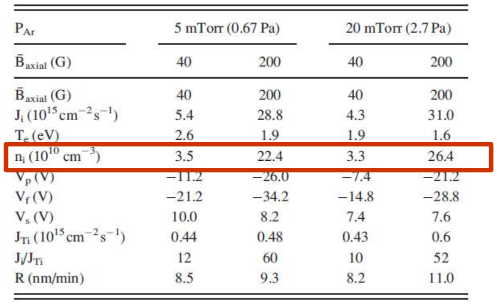

P_{Ar}	5 mTorr (0.67 Pa)		20 mTorr (2.7 Pa)	
$\bar{B}_{axial}$ (G)	40	200	40	200
$\bar{B}_{axial}$ (G)	40	200	40	200
J_i (10^{15} $cm^{-2}s^{-1}$)	5.4	28.8	4.3	31.0
T_e (eV)	2.6	1.9	1.9	1.6
n_i (10^{10} cm^{-3})	3.5	22.4	3.3	26.4
V_p (V)	−11.2	−26.0	−7.4	−21.2
V_f (V)	−21.2	−34.2	−14.8	−28.8
V_s (V)	10.0	8.2	7.4	7.6
J_{Ti} (10^{15} $cm^{-2}s^{-1}$)	0.44	0.48	0.43	0.6
J_i/J_{Ti}	12	60	10	52
R (nm/min)	8.5	9.3	8.2	11.0

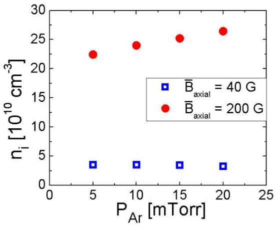

n_i > 2.5 x 10^{11} cm-3

I Petrov, A Hall, A Mei, N Nedfors, I Zhirkov, J Rosen, A Reed, B Howe, G Greczynski, J Birch, L Hultman, J.E. Greene, JVSTA, Vol. 35 (2017) 050601

Controlling the B/Ti ratio in magnetron-sputter-deposited TiB_x thin films

Unbalanced DCMS of TiB_2 target at 100 W; T_s = 700 °C

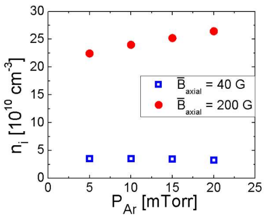

First ionization potentials

Ti: 6.8 eV   B: 8.3 eV

TABLE I. Electron-impact ionization cross-sections $\sigma(E_e)$ for Ti, B, and Ar as a function of electron energy E_e (Ref. 35).

	$\sigma(E_e)$ ($\times 10^{-16}$ cm^2)			
	$E_e = 10$ eV	$E_e = 25$ eV	$E_e = 50$ eV	$E_e = 100$ eV
Ti^+	5.93	7.46	5.52	3.63
B^+	0.11	2.15	2.46	2.04
Ar^+	—	2.12	2.93	2.49

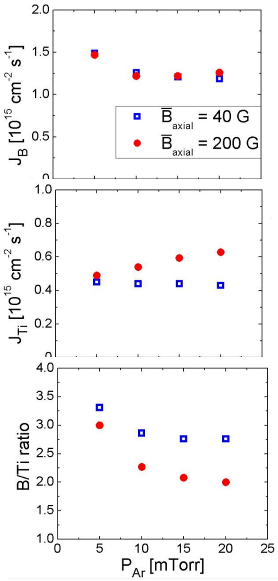

B flux unaffected

Ti flux increases ~ 40%
(ion fraction)

Stoichiometric composition

I Petrov, A Hall, A Mei, N Nedfors, I Zhirkov, J Rosen, A Reed, B Howe, G Greczynski, J Birch, L Hultman, J.E. Greene, JVSTA, Vol. 35, Sep/Oct 2017, 050601

Controlling the B/Ti ratio of TiB_X thin films grown by high-power impulse magnetron sputtering

Babak Bakhit, Ivan Petrov, J. E. Greene, Lars Hultman, Johanna Rosén, and Grzegorz Greczynski

030604-1 J. Vac. Sci. Technol. A 36(3), May/Jun 2018

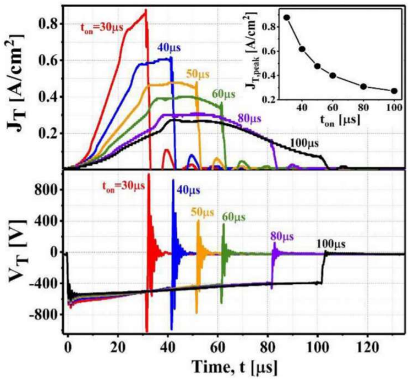

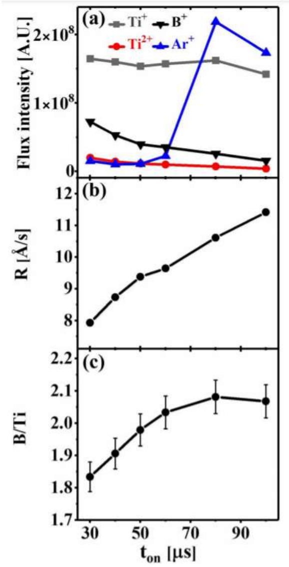

- **Gas rarefaction favors Ti transport to the substrate**
- **The metal ionizes at higher rate than B when plasma density increases**
- **Ions are led to the substrate by the plasma**

Contents lists available at ScienceDirect

Acta Materialia

journal homepage: www.elsevier.com/locate/actamat

Where is the unpaired transition metal in substoichiometric diboride line compounds?

Justinas Palisaitis[a,*], Martin Dahlqvist[a], Allen J. Hall[b], Jimmy Thörnberg[a], Ingemar Persson[a], Nils Nedfors[a], Lars Hultman[a], J.E. Greene[a,b,c], Ivan Petrov[a,b,c], Johanna Rosen[a], Per O.Å. Persson[a]

Epitaxial $TiB_{1.9}/Al_2O_3(0001)$

H = 43 GPa, ρ = 19 μΩ.cm.

DCMS
Ta = 900 °C
J_i/J_{Ti} = 52
E_i = 8 eV

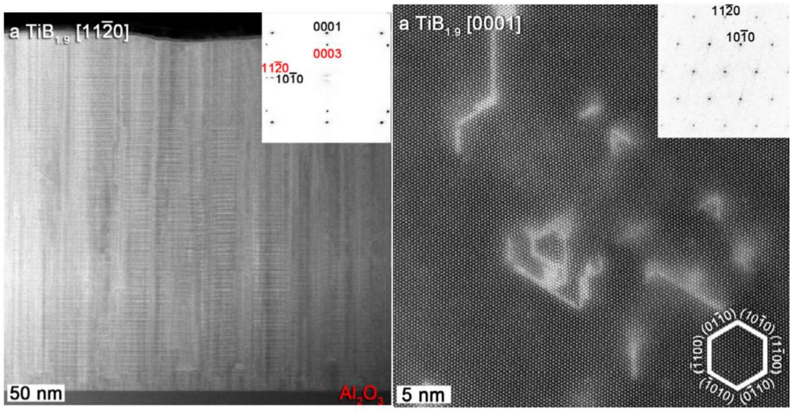

J. Palisaitis, M. Dahlqvist, Allen J. Hall et al.
Acta Materialia 204 (2021) 116510

Epitaxial $TiB_{1.9}/Al_2O_3(0001)$

H = 43 GPa, ρ = 19 μΩ.cm.

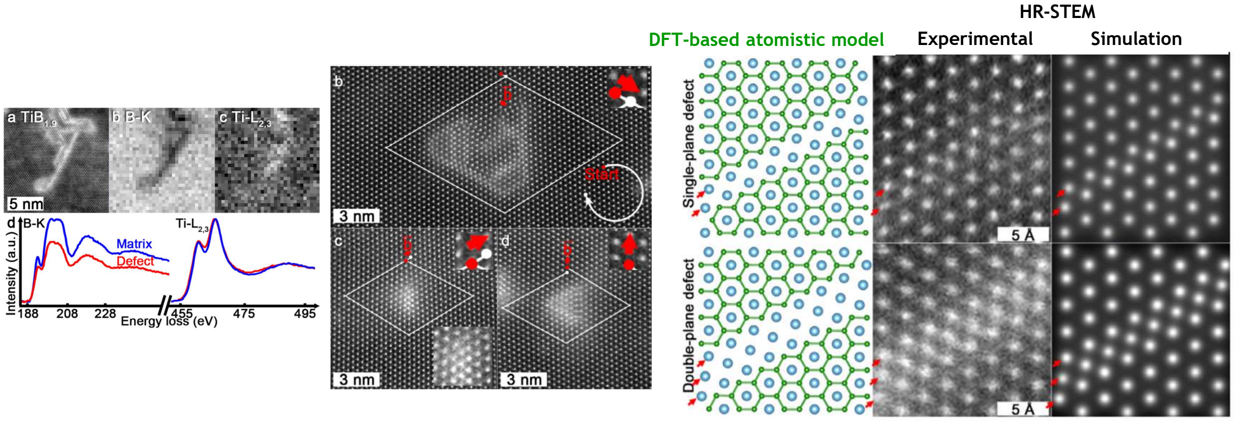

B vacancies order to form Ti-based stacking faults within the diboride structure which terminates the {1$\bar{1}$00} prismatic planes

Synthesis and characterization of CrB_2 thin films grown by DC magnetron sputtering

Scripta Materialia 200 (2021) 113915

Megan M. Dorri[a,*], Jimmy Thörnberg[a], Niklas Hellgren[b], Justinas Palisaitis[a],
Andrejs Petruhins[a], Fedor F. Klimashin[a], Lars Hultman[a], Ivan Petrov[a,c,d], Per O.Å. Persson[a],
Johanna Rosen[a,*]

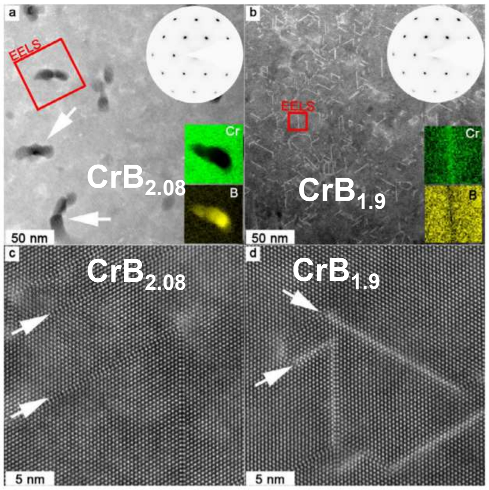

Cr stacking faults on {1100} prismatic planes

Microstructure and materials properties of understoichiometric TiB_x thin films grown by HiPIMS

Jimmy Thörnberg[a,*], Justinas Palisaitis[a], Niklas Hellgren[b], Fedor F. Klimashin[a],
Naureen Ghafoor[a], Igor Zhirkov[a], Clio Azina[a], Jean-Luc Battaglia[c], Andrzej Kusiak[c],
Maurico A. Sortica[d], J.E. Greene[a,e,f], Lars Hultman[a], Ivan Petrov[a,e,f], Per O.Å. Persson[a],
Johanna Rosen[a]

Surface & Coatings Technology 404 (2020) 126537

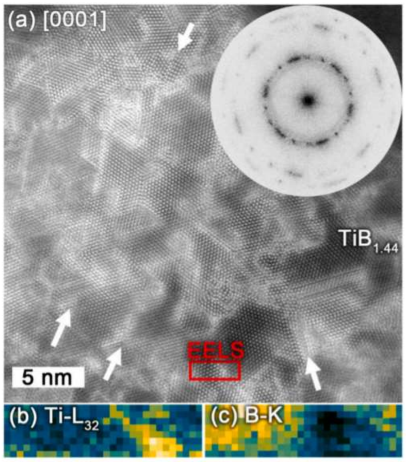

T_s = 900 °C

Ti stacking faults on {1100} prismatic planes

J. Thörnberg et al

Surface & Coatings Technology 404 (2020) 126537

Improved oxidation properties from a reduced B content in sputter-deposited TiB_x thin films

Jimmy Thörnberg[a], Babak Bakhit[a], Justinas Palisaitis[a], Niklas Hellgren[b], Lars Hultman[a], Grzegorz Greczynski[a], Per O.Å. Persson[a], Ivan Petrov[a,c,d], Johanna Rosen[a,*]

Surface & Coatings Technology 420 (2021) 127353

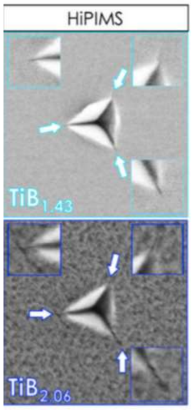

H = 44 GPa
K_C = 4.2 MPa√m

H = 41 GPa
K_C = 3.2 MPa√m

T_a = 400 °C in air

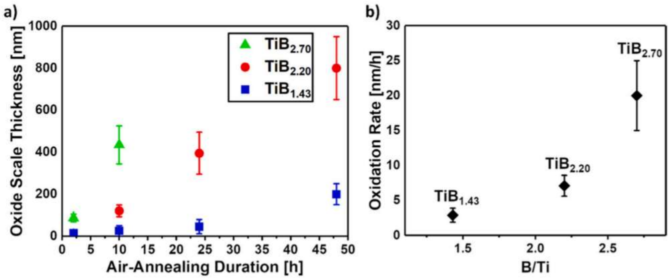

Light metal irradiation in diboride films

Hybrid HIPIMS/DCMS co-sputtering with synchronized metal-ion bias

Babak Bakhit

Improving the high-temperature oxidation resistance of TiB_2 thin films by alloying with Al

Acta Mater. 196, 677-689 (2020)

Babak Bakhit[a,*], Justinas Palisaitis[a], Jimmy Thörnberg[a], Johanna Rosen[a], Per O.Å. Persson[a], Lars Hultman[a], Ivan Petrov[a,b,c], J.E. Greene[a,b,c], Grzegorz Greczynski[a]

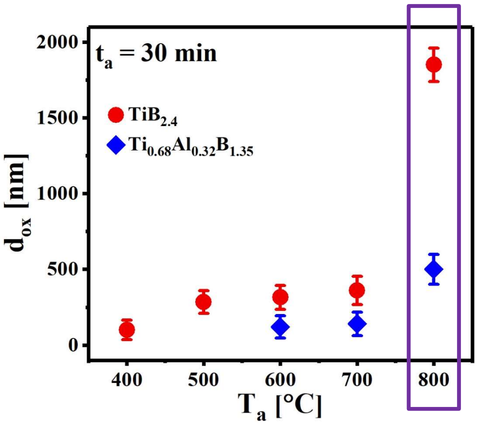

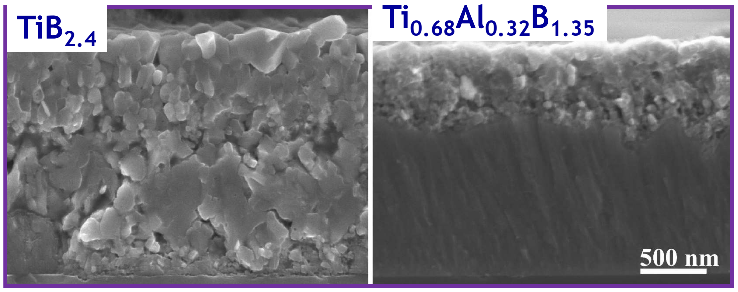

- Onset temperature for oxide-scale formation is 400 °C for $TiB_{2.4}$, 600 °C for $Ti_{0.68}Al_{0.32}B_{1.35}$.
- Scale thickness increases after 700 °C for both films, but it more significant for $TiB_{2.4}$.

STEM, EDX, and B-EELS results of as-dep. $TiB_{2.4}$ and $Ti_{0.68}Al_{0.32}B_{1.35}$:

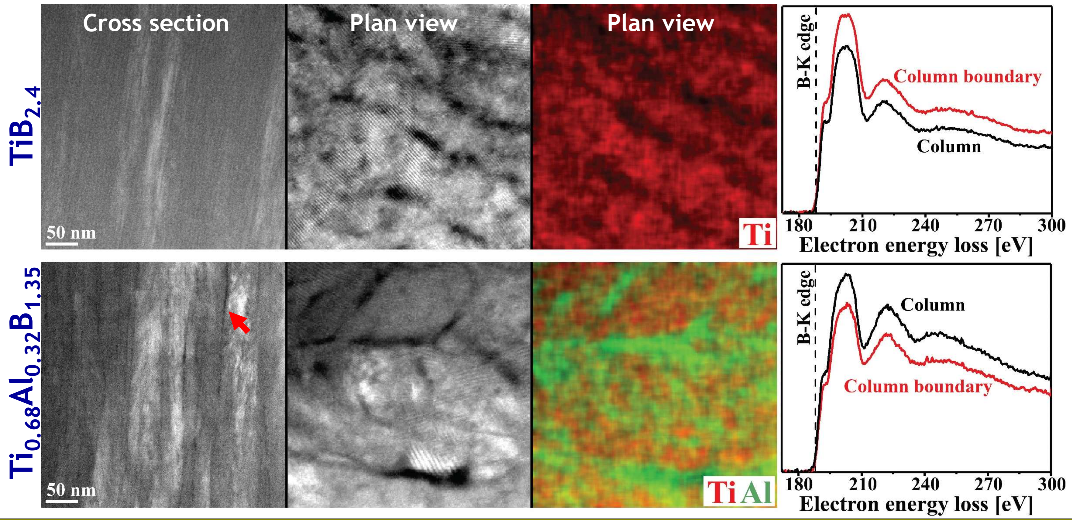

- Cross-sectional STEMs: $TiB_{2.4}$ has fine columns - $Ti_{0.68}Al_{0.32}B_{1.35}$ has wider columns with dark boundaries.
- Plan-view STEMs, EDX and EELS: $TiB_{2.4}$ has B-rich column boundaries - $Ti_{0.68}Al_{0.32}B_{1.35}$ has Al-rich boundaries.

B. Bakhit, et al., Acta Mater. 196, 677-689 (2020)

Possible oxidation mechanisms (schematic illustrations):

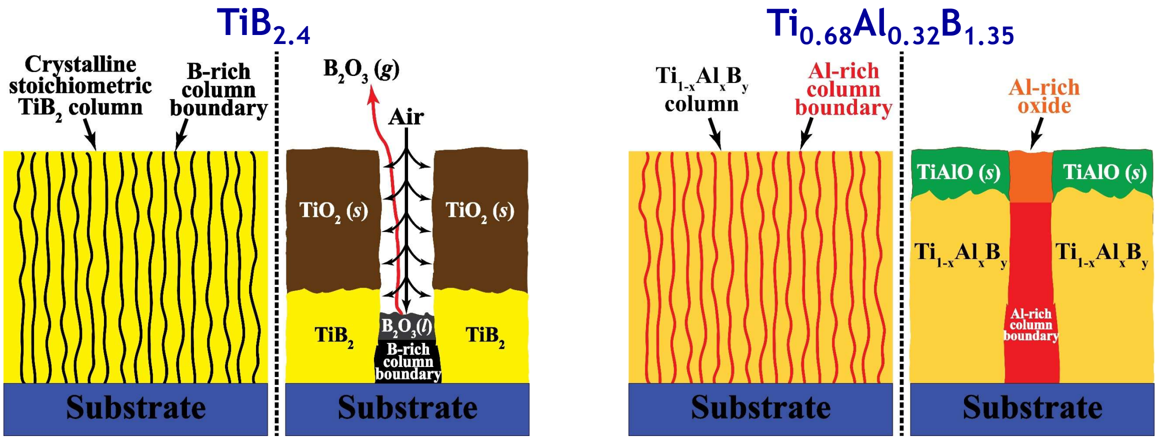

Al-rich column boundaries avoid the rapid oxidation along the boundaries and enhance oxidation resistance.

B. Bakhit, et al., Acta Mater. 196, 677-689 (2020).

Heavy metal irradiation in diboride films

Hybrid HiPIMS/magnetron co-sputtering

ZrB_2 DCMS P= 5000 W

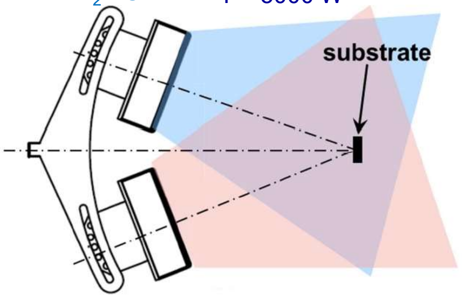

Ta HiPIMS P = 0, 600, 1200, 1800 W

synchronized metal-ion irradiation

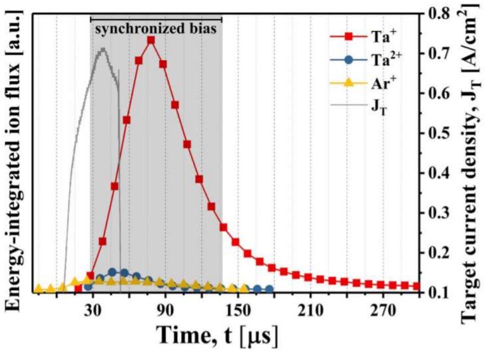

Strategy for simultaneously increasing both hardness and toughness in ZrB_2-rich $Zr_{1-x}Ta_xB_y$ thin films

Babak Bakhit, David L. J. Engberg, Jun Lu, Johanna Rosen, Hans Högberg, Lars Hultman, Ivan Petrov, J. E. Greene, and Grzegorz Greczynski

Journal of Vacuum Science & Technology A **37**, 031401 (2019)

123

Strategy for simultaneously increasing both hardness and toughness in ZrB_2-rich $Zr_{1-x}Ta_xB_y$ thin films

Journal of Vacuum Science & Technology A **37**, 031401 (2019)

Babak Bakhit, David L. J. Engberg, Jun Lu, Johanna Rosen, Hans Högberg, Lars Hultman, Ivan Petrov, J. E. Greene, and Grzegorz Greczynski

Plan-view Z-contrast STEM images of $Zr_{1-x}Ta_xB_y$ films:

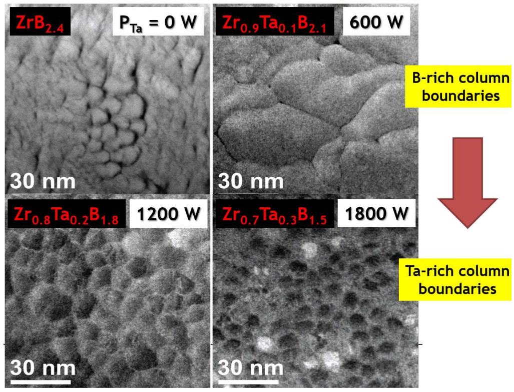

B-rich column boundaries

Ta-rich column boundaries

STEM, EDX, and B-EELS results of $ZrB_{2.4}$ and $Zr_{0.8}Ta_{0.2}B_{1.8}$ films:

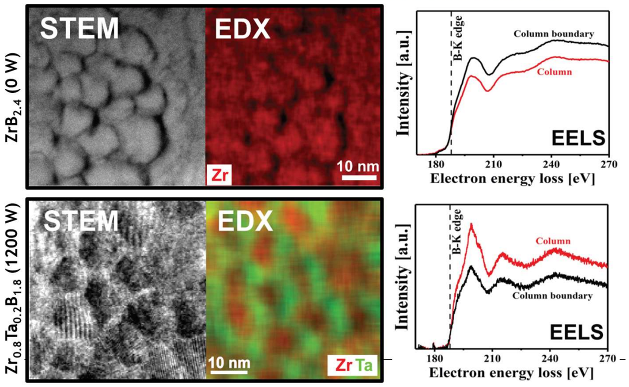

124

STEMs of (0001)-textured $Zr_{0.7}Ta_{0.3}B_{1.5}$ films

Plan-views

Cross-section

along the fiber-texture axis

off the fiber-texture axis

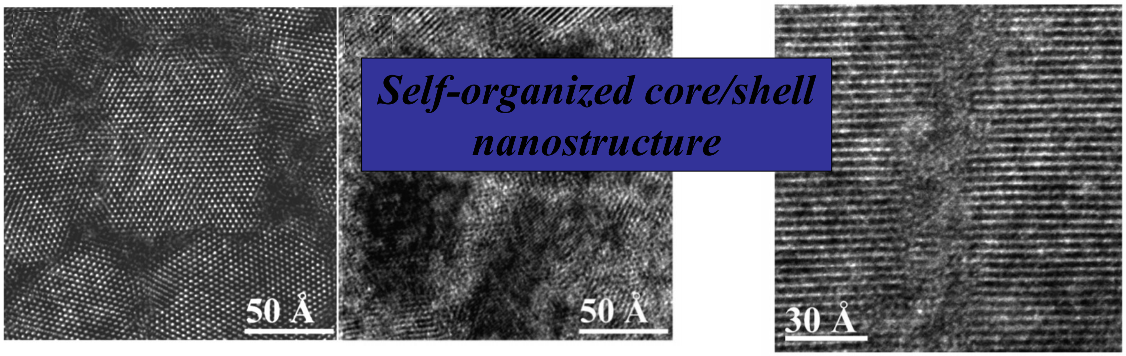

Self-organized core/shell nanostructure

Electron channeling highlights the crystalline core

Z-contrast highlights the Ta-rich disordered shell

B. Bakhit, J Palisaitis, P. Persson, B Alling, J Rosen, L Hultman, I Petrov, J.E. Greene, G Greczynski
Surf. Coat. Technol. 401, 126237 (2020)

Nanoindentation hardness, H and fracture toughness, K_c $Zr_{1-x}Ta_xB_y$ films

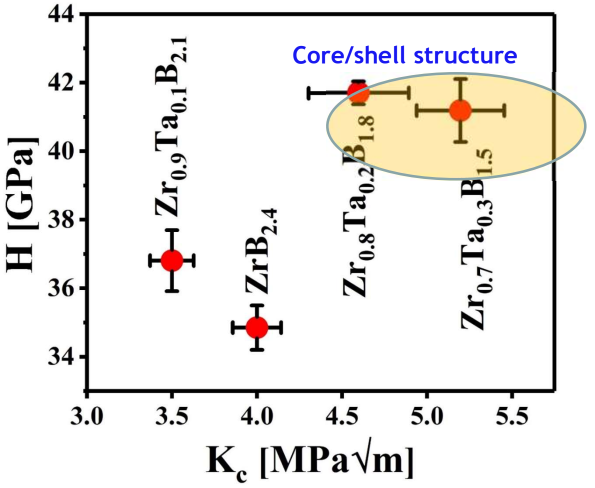

Increase in H is due to:
- solid-solution hardening + column width decrease

Increase in K_c is due to:
- dense metallic-glass-like shells

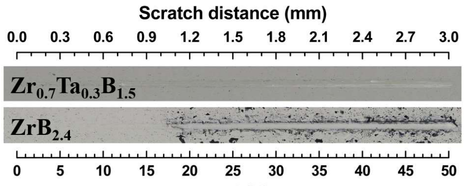

Results by Zhengtao Wu

B. Bakhit, D. Engberg, J. Lu, J. Rosen, H. Högberg, L. Hultman, I. Petrov, JE Greene, G. Greczynski
J Vac. Sci. Technol. A 37, 031506 (2019).

Nanoindentation H of $Zr_{1-x}Ta_xB_y$ films as a function of T_a:

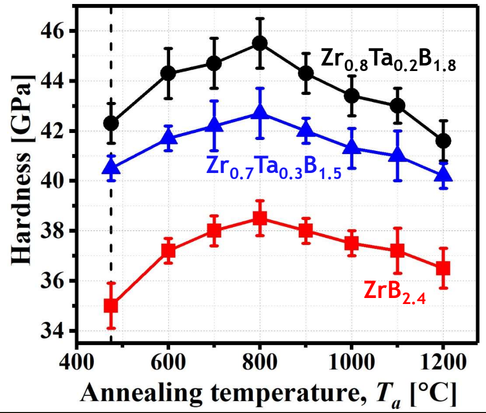

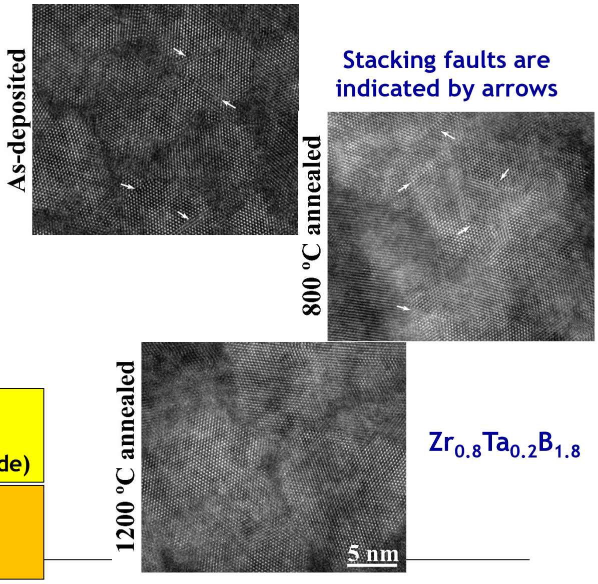

Stacking faults are indicated by arrows

$Zr_{0.8}Ta_{0.2}B_{1.8}$

Increase in H (≤800°C) is due to:
- **Point-defect recovery, increasing chemical-bond density**
- **Preserving stacking faults (barriers against dislocation glide)**

Decrease in H (>800°C) is due to:
- **Stacking fault annihilation, recrystallization, and column coarsening**

B Bakhit, J Palisaitis, Z Wu, M Sortica, D Primetzhofer, P Persson, J Rosen, L Hultman, I Petrov, J.E. Greene, G Greczynski, Scripta

---

Samira Dorri

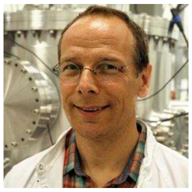

Prof. Jens Birch

A recent example of superb interface engineering by sputter epitaxy

Artificial superlattices with abrupt interfaces by monolayer-controlled growth kinetics during magnetron sputter epitaxy, case of hexagonal CrB_2/TiB_2 heterostructures

Materials & Design 251 (2025) 113661

Samira Dorri [a,*], Olle Nyqvist [a], Justinas Palisaitis [a], Alexei Vorobiev [b,c], Anton Devishvili [c], Per Sandström [a], Per O.Å. Persson [a], Naureen Ghafoor [a], Fredrik Eriksson [a], Jens Birch [a]

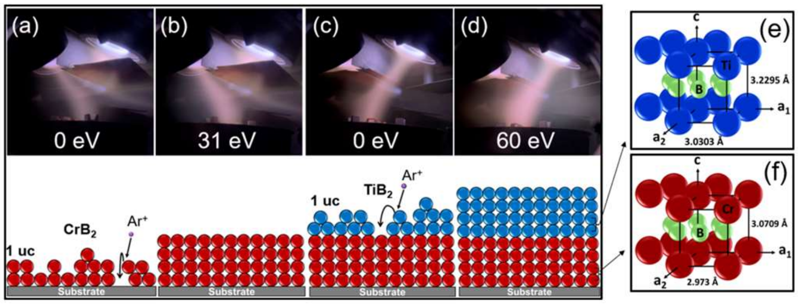

The first unit cell with 0 V bias then bias applied at an optimized value

Fig. 1. Plasma discharge appearance with corresponding schematics, illustrating different growth stages, where different ion-energies are applied for different stages of the individual CrB_2 and TiB_2 layers during modulated ion-assisted magnetron sputter epitaxy. (a) and (c) show growth of the first uc for CrB_2 and TiB_2 layers, respectively, when the applied substrate bias is 0 to protect the formed interfaces from intermixing. (b) and (d) show 2D epitaxy and layer densification thanks to increased adatom mobility and sub-surface atomic displacements in CrB_2 and TiB_2 layers, respectively. (e) and (f) show the atomic arrangements in the hexagonal unit cell of TiB_2 and CrB_2, respectively.

Samira Dorri et al

Materials & Design 251 (2025) 113661

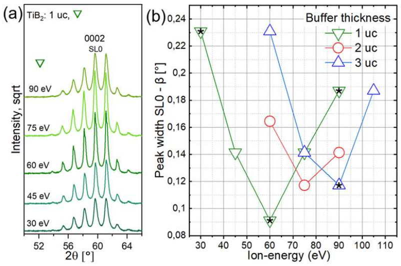

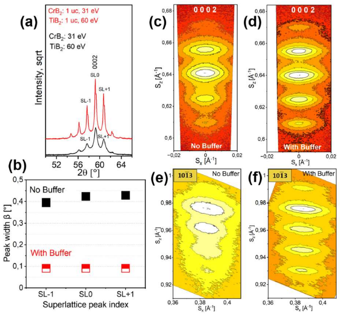

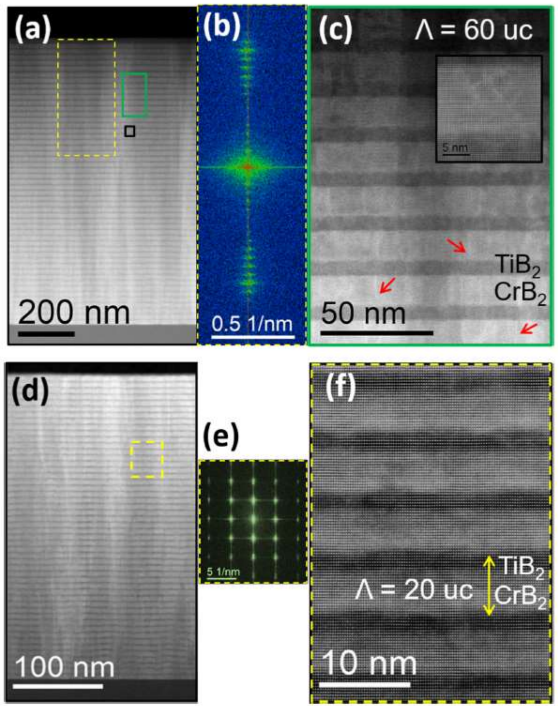

Main points on TMB$_2$:

HIPIMS synthesis of a range understoichiometric TMB$_2$

Metal-rich stacking faults to accommodate B deficiency

Enhanced hardness, ductility, oxidation resistance, age hardening

Modeling TiN(001) Film Growth by Classical Molecular Dynamics

Ab-inito and Classical Molecular Dynamics Simulations

1. D.G. Sangiovanni, D. Edström, L. Hultman, V. Chirita, I. Petrov, and J.E. Greene, "The Dynamics of Ti, N, and TiN_x (x = 1 - 3) Admolecule Transport on TiN(001) Surfaces," *Phys. Rev. B* 86, 155443 (2012).
2. D.G. Sangiovanni, D. Edström, L. Hultman, I. Petrov, J.E. Greene, and V. Chirita, "Ab-inito and Classical Molecular Dynamics Simulations of N_2 Desorption from TiN(001) Surfaces," *Surf. Sci.* 624, 25 (2014).
3. D. Edström, D. G. Sangiovanni, L. Hultman, V. Chirita, I. Petrov, and J. E. Greene, "Ti and N Adatom Descent Pathways to the Terrace from Atop Two-dimensional TiN/TiN(001) Islands," *Thin Solid Films* 558, 37 (2014).
4. D.G. Sangiovanni, D. Edström, L. Hultman, I. Petrov, J.E. Greene, and V. Chirita, "Ti Adatom Diffusion on TiN(001): Ab-initio and Classical Molecular Dynamics Simulations," *Surf Sci.* 627, 34 (2014).
5. Daniel Edström; Davide G Sangiovanni, L. Hultman, Ivan Petrov, J.E. Greene, and V. Chirita "The Dynamics of TiN_x (x = 1-3) Admolecule Interlayer and Intralayer Transport on TiN/TiN(001) Islands," *Thin Solid Films* 589, 133 (2015).
6. D.G. Sangiovanni, F. Tasnádi, L. Hultman, I. Petrov, J.E. Greene, and V. Chirita, "N and Ti Adatom Dynamics on Stoichiometric Polar TiN(111) Surfaces," *Surf. Sci.* 649,72 (2016).
7. D. Edström, D.G. Sangiovanni, L. Hultman, I. Petrov, J.E. Greene, and V. Chirita, "Large-scale Molecular Dynamics Simulations of TiN/TiN(001) Epitaxial Film Growth," *J. Vac. Sci. Technol. A* 34, 041509 (2016).
8. D.G. Sangiovanni, A.B. Mei, L. Hultman, V. Chirita, I. Petrov, J.E. Greene. "*Ab initio* Molecular Dynamics Simulations of N/VN(001) Surface Reactions: N_2 Dissociative Chemisorption, N Adatom Migration, and N_2 Desorption," *J. Phys. Chem. C* 120, 12503 (2016).
9. D. Edström, D.G. Sangiovanni, L. Hultman, I. Petrov, J.E. Greene, and V. Chirita, "Effects of Incident N Atom Kinetic Energy on TiN/TiN(001) Film Growth Dynamics: A Molecular Dynamics Investigation," *J. Appl. Phys.* 121, 025302 (2017).
10. D. Edström, D.G. Sangiovanni, L. Hultman, I. Petrov, J.E. Greene, V. Chirita, TSF (2019)

Understanding microstructure evolution in TM nitrides

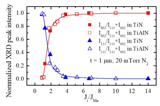

Film growth experiment XTEM

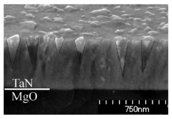

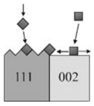

Thought experiments

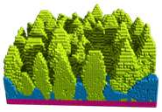

Kinetic Monte-Carlo

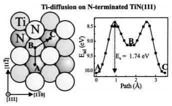

DFT

Atomistic studies LEEM, HT-STM

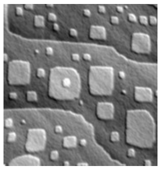

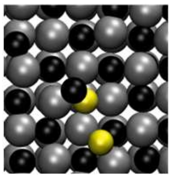

Ab-initio MD

Classical Molecular dynamic

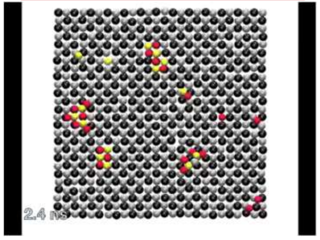

1990s 2000s 2010s 2020

TiN(111) and (001): LEEM / STM Complementary Study

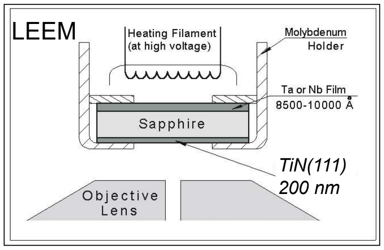

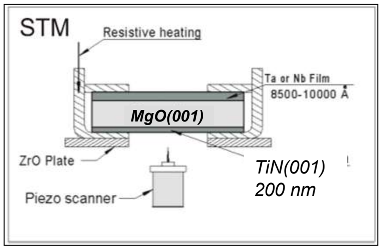

T_s = 1688 K t_{real} = 4 min
t_{movie} = 9 sec
3x3μm

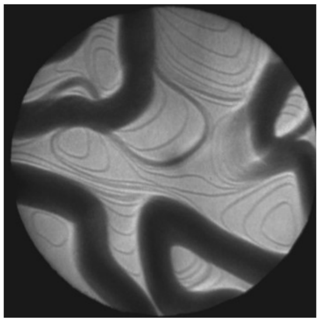

Wacek Swiech
S. Kodambaka

T_s = 1125 K t_{real} = 145 min
t_{movie} = 19 sec
0.1x0.1μm

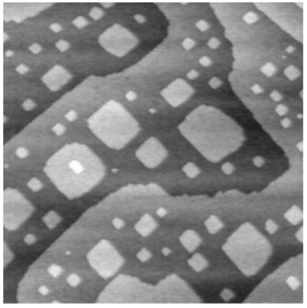

Vania Petrova
S. Kodambaka

S. Kodambaka, S.V. Khare, W. Święch, K. Ohmori, I. Petrov, J.E. Greene, Nature 429, 49 (2004).

Molecular dynamics (MD):
ab-initio (AIMD) and classical (CMD)

AIMD:

•density functional theory (DFT)

- Accurate
- Limited supercell sizes (~10^2 atoms) and simulated times (~ns)
- Benchmark CMD predictions for small systems and high temperatures

CMD:

•Semi-empirical models, modified embedded atom method (MEAM)

•Validated parameterization for TiN surfaces (LEEM.STM) and AIMD

•Large supercells (~10^6 atoms), long simulations (~μs)

D.G. Sangiovanni, D. Edström, L. Hultman, I. Petrov, J.E. Greene, V. Chirita, Surface Science **627**, 34 (2014)

Texture in TiN and $Ti_{0.5}Al_{0.5}N/SiO_2$

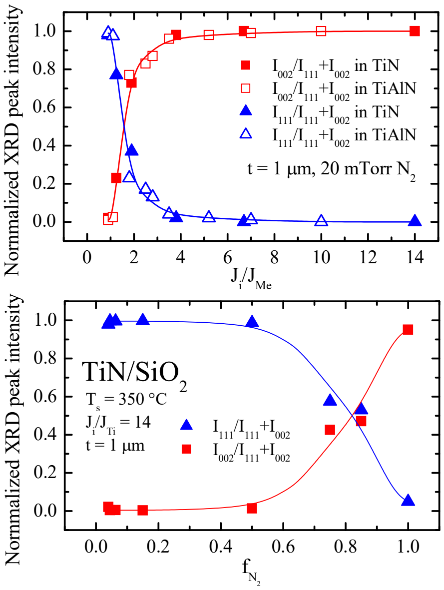

Texture in TaN/SiO$_2$

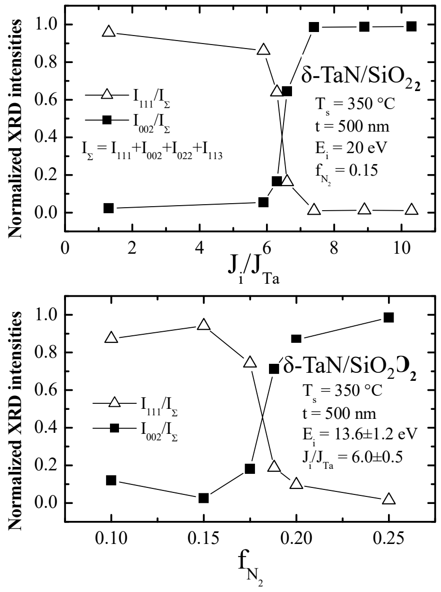

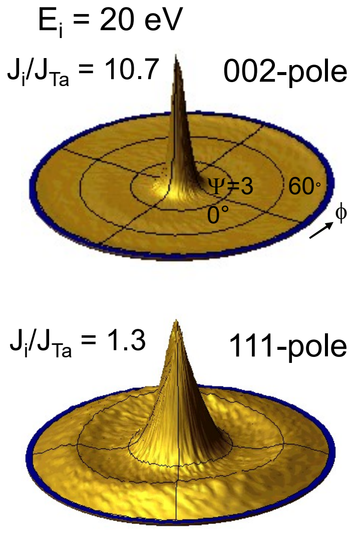

Competitive grain growth

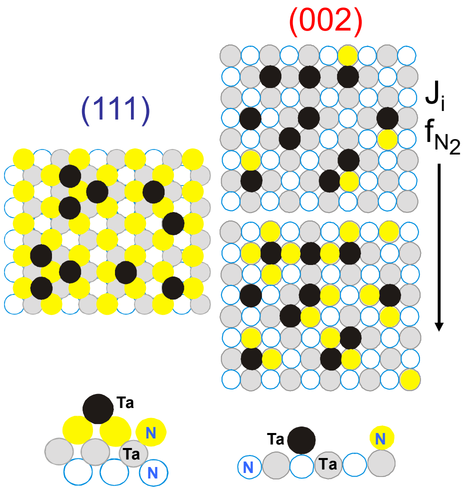

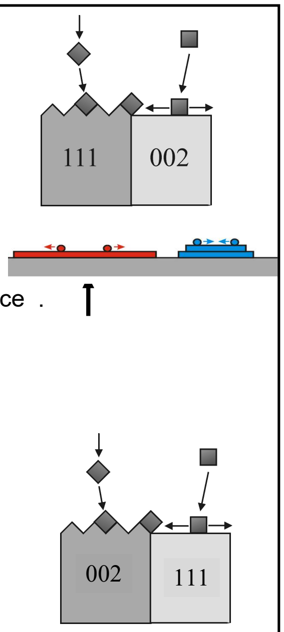

Low J_i/J_{Ta} ⟶ high J_i/J_{Ta}:

- Momentum transfer to surface .
- θ_N on (002) ↑ due to collisionally-induced dissociative chemisorption of N_2^+.

- Low J_i/J_{Ta} or f_{N2}: $D_{111} < D_{002}$ ⟶ 111 texture
- High J_i/J_{Ta} or f_{N2}: $D_{111} > D_{002}$ ⟶ 002 texture

Atomic-Scale Surface Processes Controlling the Growth of Cubic Transition-metal Nitrides: TiN, CrN, ScN, and TaN

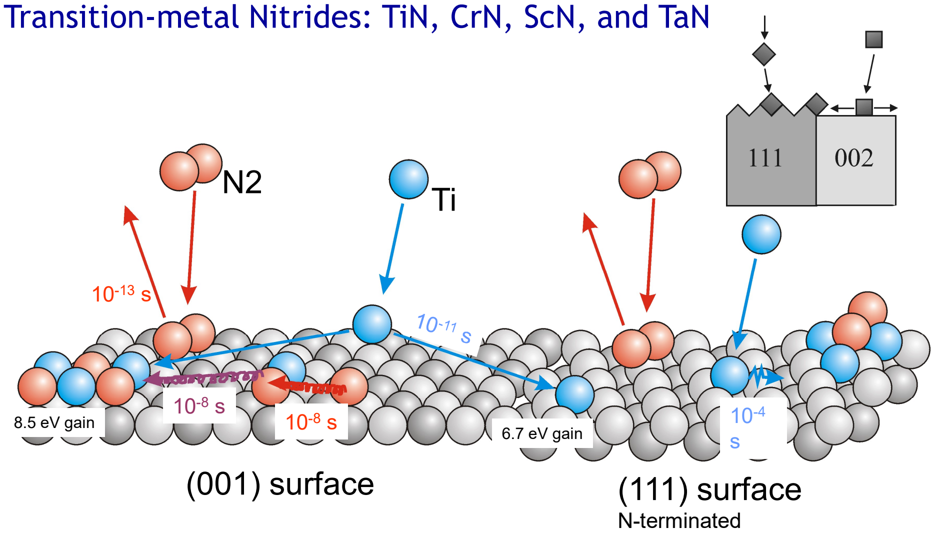

Density functional calculations & scanning tunneling microscopy

D. Gall, S. Kodambaka, M.A. Wall, I. Petrov, and J. E. Greene, *Physical Review B* (2003)

139

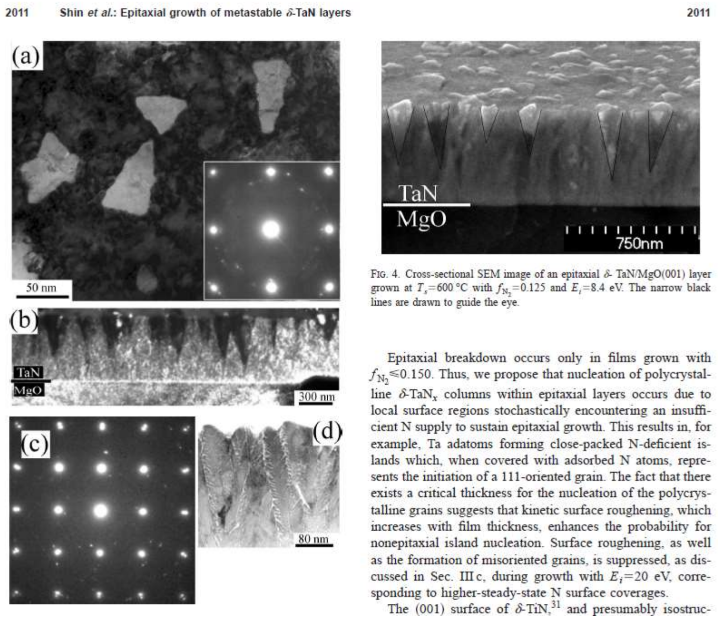

FIG. 4. Cross-sectional SEM image of an epitaxial δ- TaN/MgO(001) layer grown at T_s=600 °C with f_{N_2}=0.125 and E_i=8.4 eV. The narrow black lines are drawn to guide the eye.

Epitaxial breakdown occurs only in films grown with $f_{N_2} \leqslant 0.150$. Thus, we propose that nucleation of polycrystalline δ-TaN_x columns within epitaxial layers occurs due to local surface regions stochastically encountering an insufficient N supply to sustain epitaxial growth. This results in, for example, Ta adatoms forming close-packed N-deficient islands which, when covered with adsorbed N atoms, represents the initiation of a 111-oriented grain. The fact that there exists a critical thickness for the nucleation of the polycrystalline grains suggests that kinetic surface roughening, which increases with film thickness, enhances the probability for nonepitaxial island nucleation. Surface roughening, as well as the formation of misoriented grains, is suppressed, as discussed in Sec. III c, during growth with E_i=20 eV, corresponding to higher-steady-state N surface coverages.

The (001) surface of δ-TiN,[31] and presumably isostruc-

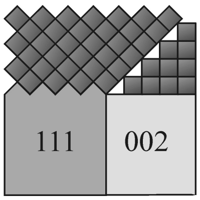

111 nucleation on 001 under nitrogen deficiency

140

Modeling TiN(001) Film Growth by Classical Molecular Dynamics

- **Modified Embedded Atom Method**
- **Calculations performed with LAMMPS – Large-scale Atomic & Molecular Massively Parallell Simulator – open source code from Sandia.**
- **Paramters optimized to reproduce bulk[1] and surface[2] properties of TiN**

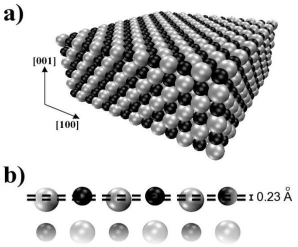

- Monitor dynamics of N, Ti and TiN_x with x=1,2,3 on TiN(001) islands at 1000 K.
- **6 layers of 18*18 atoms**
- **1 fs time step**
- **Statistically independent 10 ns runs, for a total of 0.25 µs per species.**

[1] Kim et al. Acta Materialia 56 (2008)

[2] D. G. Sangiovanni, D. Edstrom, L. Hultman, V. Chirita, I. Petrov, and J. E. Greene. PHYS. REV. B 86, 155443 (2012)

N adatom adsorption on TiN(001)

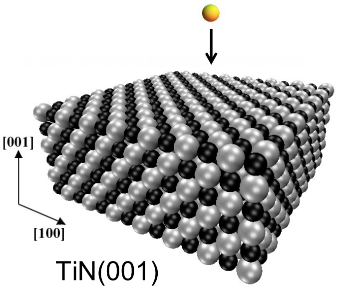

TiN(001) substrate

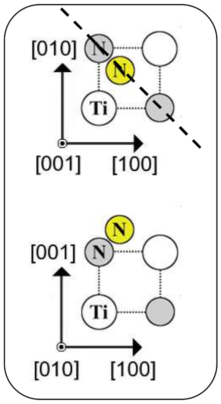

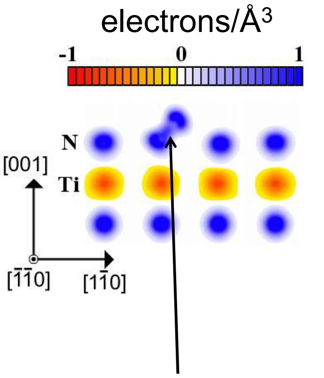

Strong bonding with surface N-atom (N_{surf})

Considerably less mobile than Ti adatoms!

N adatom (N_{ad}) diffusion on TiN(001)

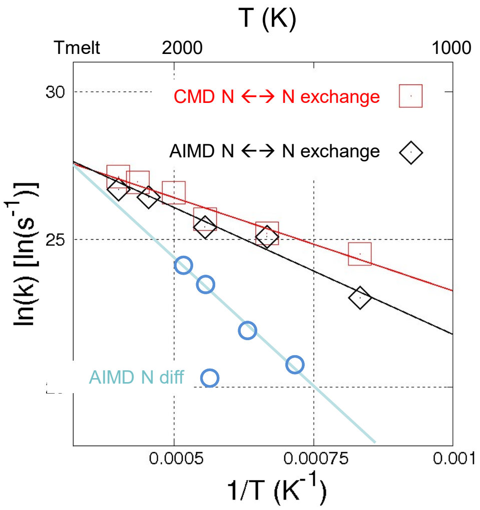

AIMD run, 2500 K, duration: 5 ps

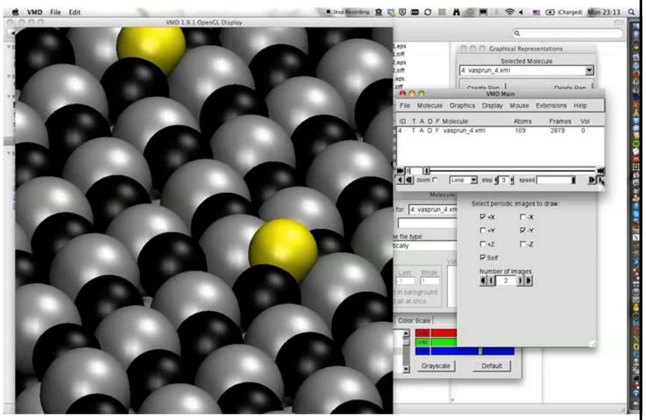

N-adatom <-> surface N-atom exchange: $E_a \approx 0.65$ eV, $A \approx 1.0 \times 10^{13}$ s^{-1}

N adatom surface diffusion: $E_a \approx 1.43$ eV, $A \approx 12.8 \times 10^{13}$ s^{-1}

N loss during TiN(001) growth

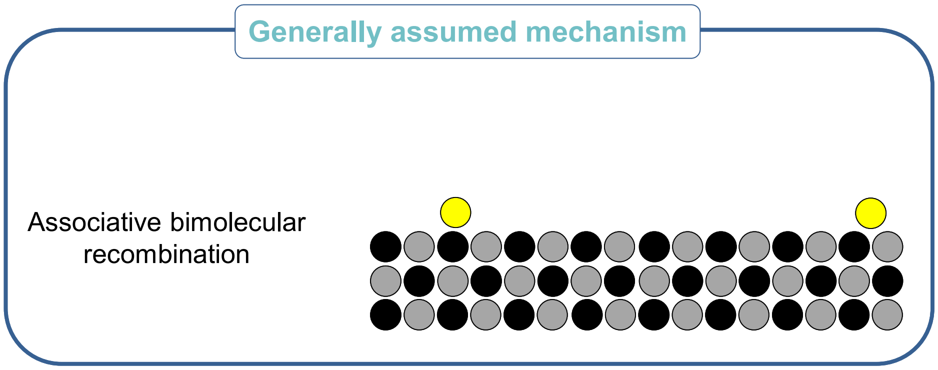

Generally assumed mechanism

Associative bimolecular recombination

N_{ad}/N_{ad} long-range interactions

AIMD runs, 2500 K

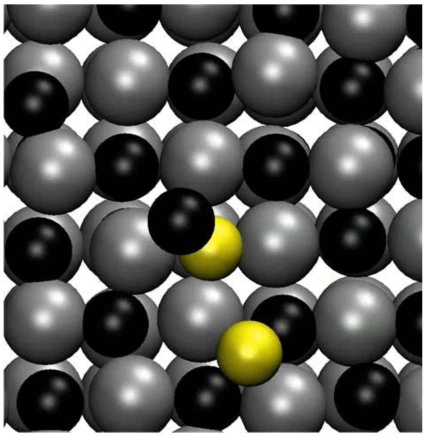

D.G. Sangiovanni, D. Edström, L. Hultman, I. Petrov, J.E. Greene, V. Chirita
Surface Science **624**, 25 (2014)

N loss during TiN(001) growth

Present calculations

N_{ad}/N_{ad} long-range repulsive interactions

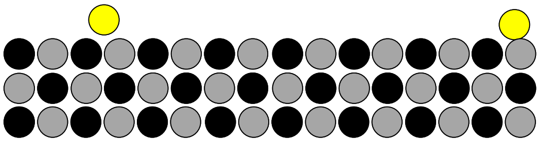

Sangiovanni et al., SS **624**, 25 (2014)

N adatom (N_{ad}) removes surface N atom (N_{surf})

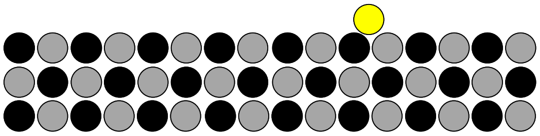

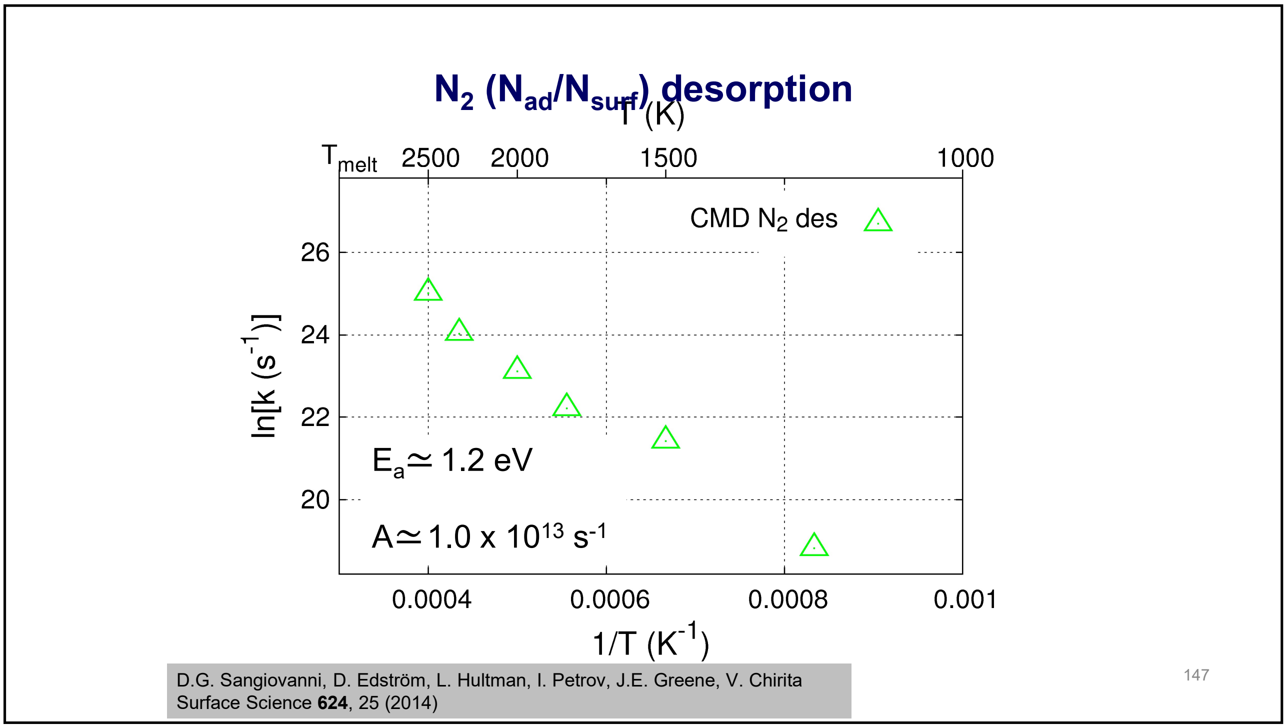

N_2 (N_{ad}/N_{surf}) desorption

D.G. Sangiovanni, D. Edström, L. Hultman, I. Petrov, J.E. Greene, V. Chirita
Surface Science **624**, 25 (2014)

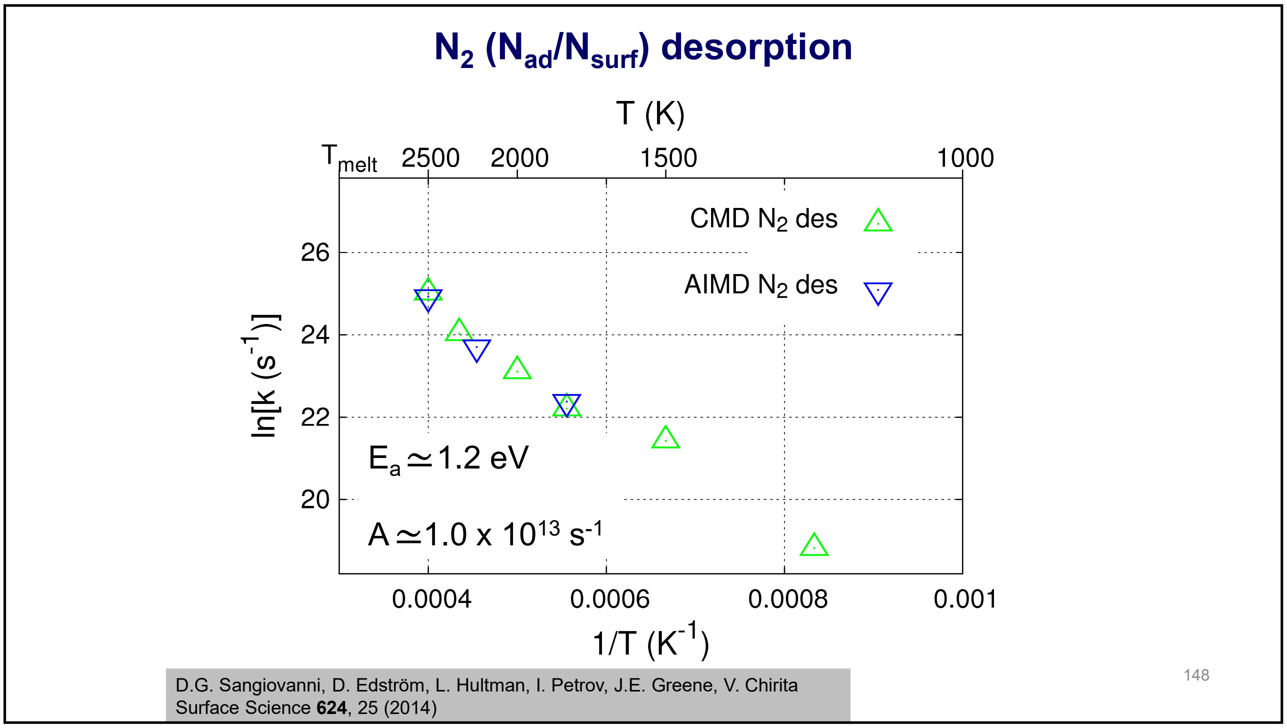

N_2 (N_{ad}/N_{surf}) desorption

D.G. Sangiovanni, D. Edström, L. Hultman, I. Petrov, J.E. Greene, V. Chirita
Surface Science **624**, 25 (2014)

Consistent AIMD and CMD results for Ti and N/TiN(001)

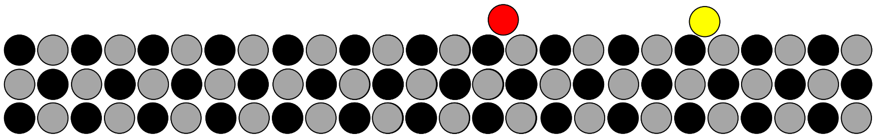

- Ti adatoms highly mobile on TiN(001)
- N adatoms essentially stationary
- Desorbing N_{ad}/N_{surf} pairs leave anion vacancies in the surface

---

Position and dynamics of Ti, N and TiN_x (x = 1, 2, and 3) at 1000 K on TiN(001)

Diffusion on a terrace

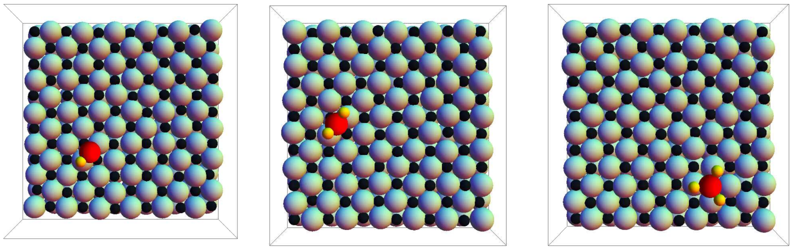

		Net Diffusion events	Net migration (d_{NN})	Net velocity (Å/ns)	Diffusion coefficient (cm²/s)
non-epi Ti	Ti	2082	2195	18.62	$0.52*10^{-6}$
	TiN	723	682	5.79	$0.21*10^{-6}$
	TiN_2	915	1060	8.99	$0.28*10^{-6}$
epi-Ti	TiN_3	4	6	0.05	$0.13*10^{-8}$

D. G. Sangiovanni, D. Edstrom, L. Hultman, V. Chirita, I. Petrov, and J. E. Greene.
PHYS. REV. B 86, 155443 (2012)

Charge transfer maps

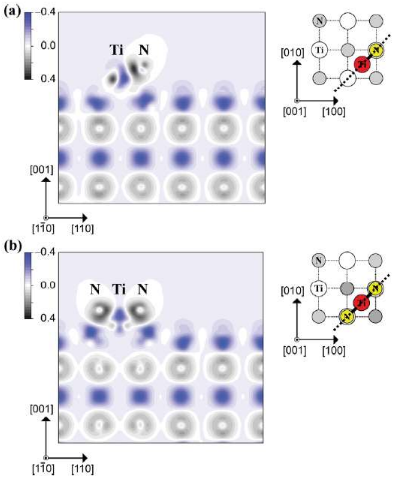

differences in the charge density distributions
in gas phase N and Ti atoms and
chemisorbed atoms
on relaxed TiNx/TiN(001)
black denotes increased electron density
blue – decreased electron density

D. G. Sangiovanni, D. Edstrom, L. Hultman, V. Chirita, I. Petrov, and J. E. Greene.
PHYS. REV. B 86, 155443 (2012)

Results on TiN(111)

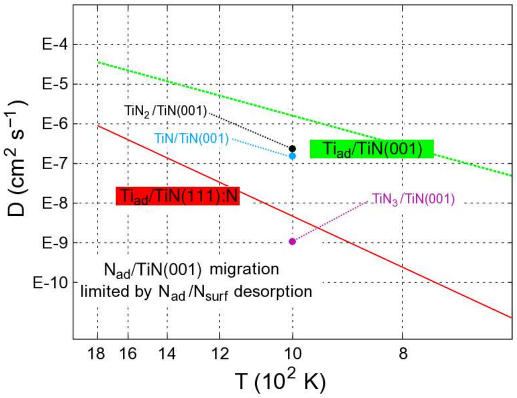

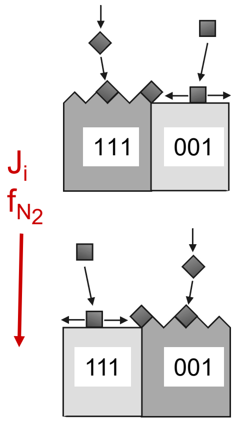

D. G. Sangiovanni, D. Edstrom, L. Hultman, V. Chirita, I. Petrov, and J. E. Greene.
Surface Sciencee 649(2016) 72-79

Diffusion on an island

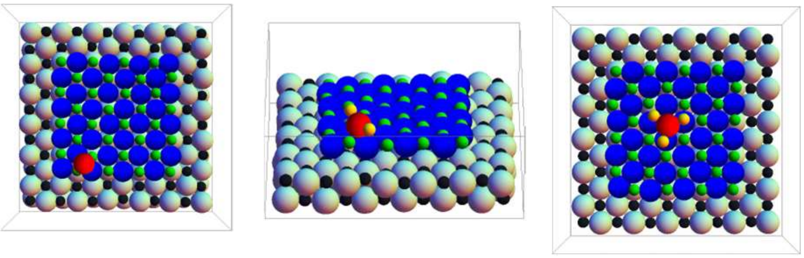

	Descent mechanisms				Residence time (ns)
	No descent	Direct hop	Single push-out	Double push-out	
Ti adatom	14%	0%	72%	14%	1.15
N adatom	92%	4%	4%	0%	1.96
TiN dimer	22%	36%	36%	6%	0.99
TiN_2 trimer	14%	86%	0%	0%	0.72

D Edström, DG Sangiovanni, L Hultman, I Petrov, JE Greene, V Chirita, Thin Solid Films 589 (2015) 133

Modeling TiN(001) Film Growth by Classical Molecular Dynamics

Growth simulation setup

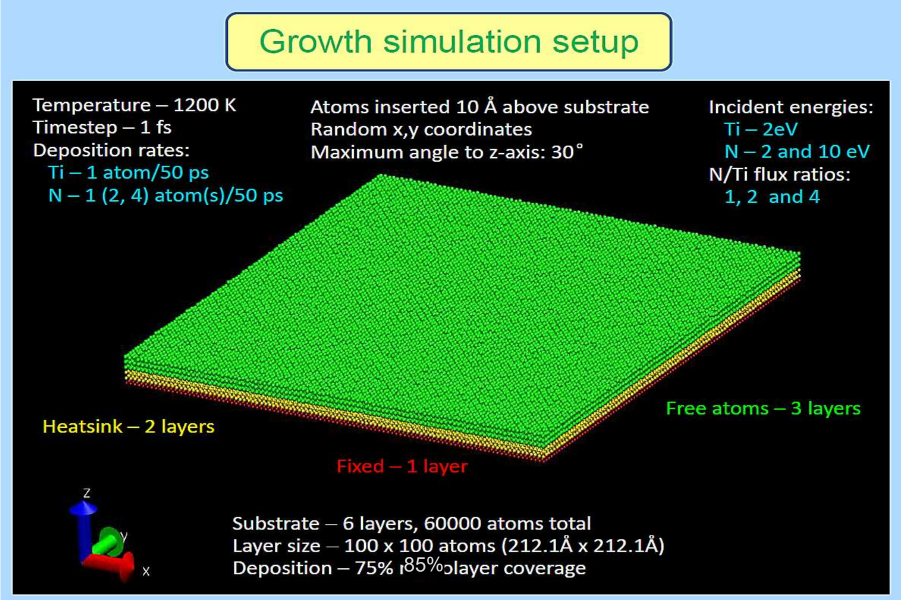

Temperature – 1200 K
Timestep – 1 fs
Deposition rates:
Ti – 1 atom/50 ps
N – 1 (2, 4) atom(s)/50 ps

Atoms inserted 10 Å above substrate
Random x,y coordinates
Maximum angle to z-axis: 30°

Incident energies:
Ti – 2eV
N – 2 and 10 eV
N/Ti flux ratios:
1, 2 and 4

Substrate – 6 layers, 60000 atoms total
Layer size – 100 x 100 atoms (212.1Å x 212.1Å)
Deposition – 75% r85%olayer coverage

CMD: Modeling TiN(001) Film Growth

2 eV fluxes at 1200 K, N/Ti = 1

100x100x6 atoms of TiN(001); a total of 60 000 atoms

0.85 monolayers deposited

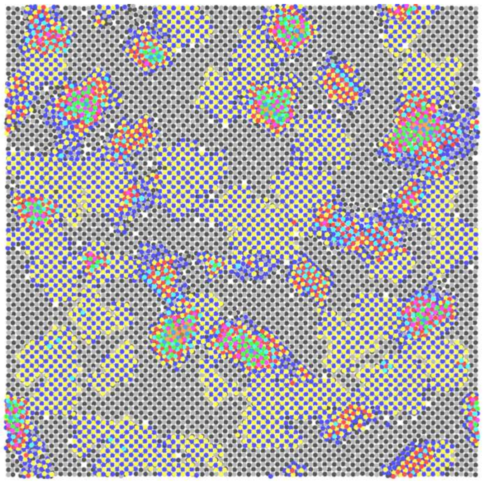

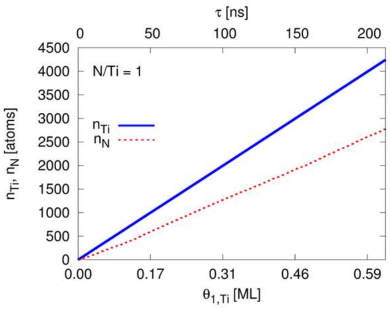

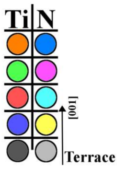

D Edström, DG Sangiovanni, L Hultman, I Petrov, JE Greene, V Chirita, JVST A 34 (2016) 041509

CMD: Modeling TiN(001) Film Growth

2 eV fluxes at 1200 K, N/Ti = 4

100x100x6 atoms of TiN(001); a total of 60 000 atoms

0.85 monolayers deposited

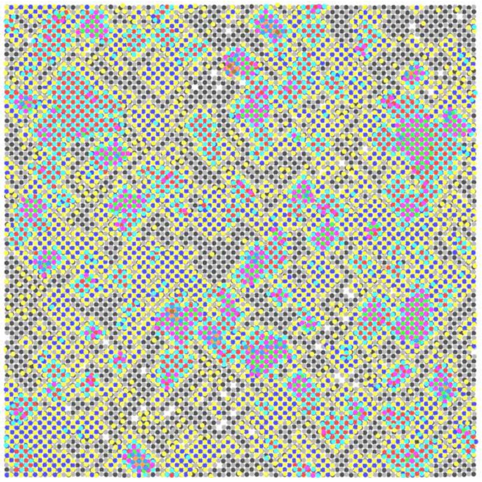

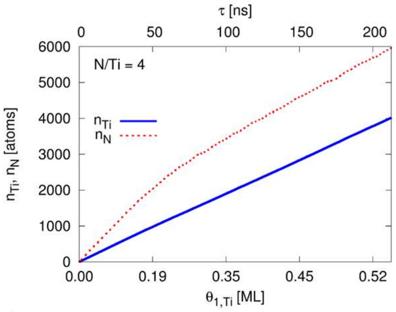

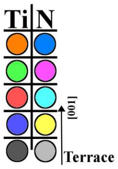

D Edström, DG Sangiovanni, L Hultman, I Petrov, JE Greene, V Chirita, JVST A 34 (2016) 041509

CMD: Modeling TiN(001) Film Growth

2 and 10 eV N at 1200 K, N/Ti = 4

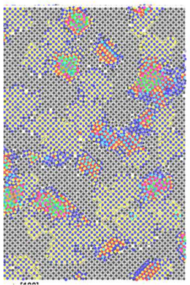

2 eV N
2 eV Ti
N/Ti = 1

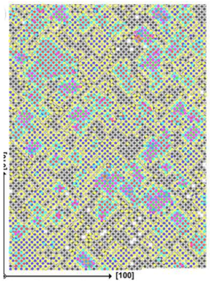

2 eV N
2 eV Ti
N/Ti = 4

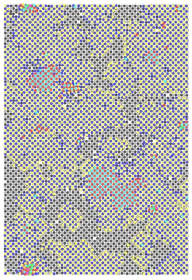

10 eV N
2 eV Ti
N/Ti = 4

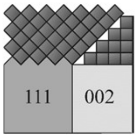

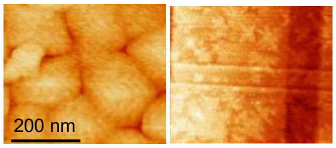

D Edström, DG Sangiovanni, L Hultman, I Petrov, JE Greene, V Chirita, J.Appl.Phys 121 (2017) 025302

Low-energy bombardment: restructuring leading to epitaxy

10 eV N
2 eV Ti
N/Ti = 6

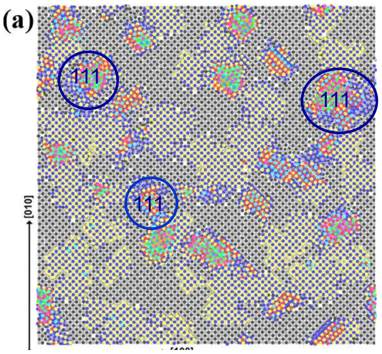

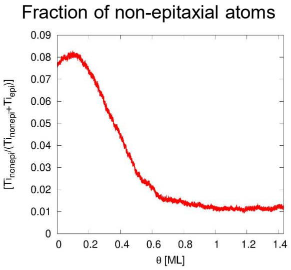

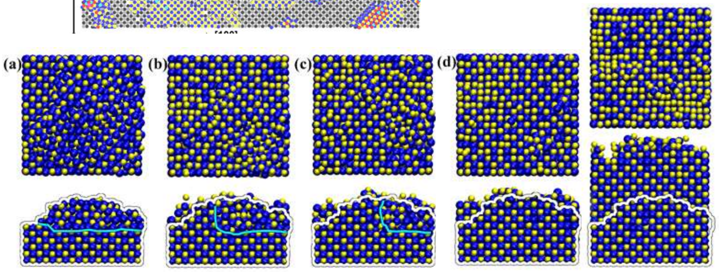

0 ML 0.6 ML 0.8 ML 1.1 ML 9.8 ML

D. Edström, D.G. Sangiovanni, L. Hultman, I. Petrov, J.E. Greene, V. Chirita, TSF (2019) submitted

Low-energy bombardment: restructuring leading to epitaxy

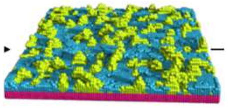

10 eV N
2 eV Ti
N/Ti = 6

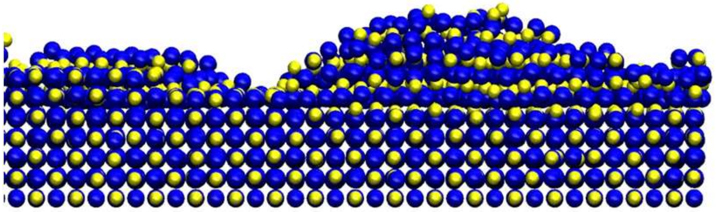

Movie by Davide G. Sangiovanni

Fraction of non-epitaxial atoms

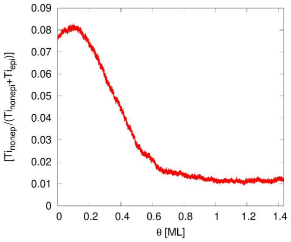

D. Edström, D.G. Sangiovanni, L. Hultman, I. Petrov, J.E. Greene, V. Chirita, Thin Solid Film 688 (2019) 137380